EUROPEAN COMMISSION
DIRECTORATE-GENERAL
Joint Research Centre

Institute for Environment and Sustainability

Selected UV photochemical and photobiological impacts on marine ecosystems: general characteristics and sensitivity analyses

Vantrepotte, V. and Mélin, F.

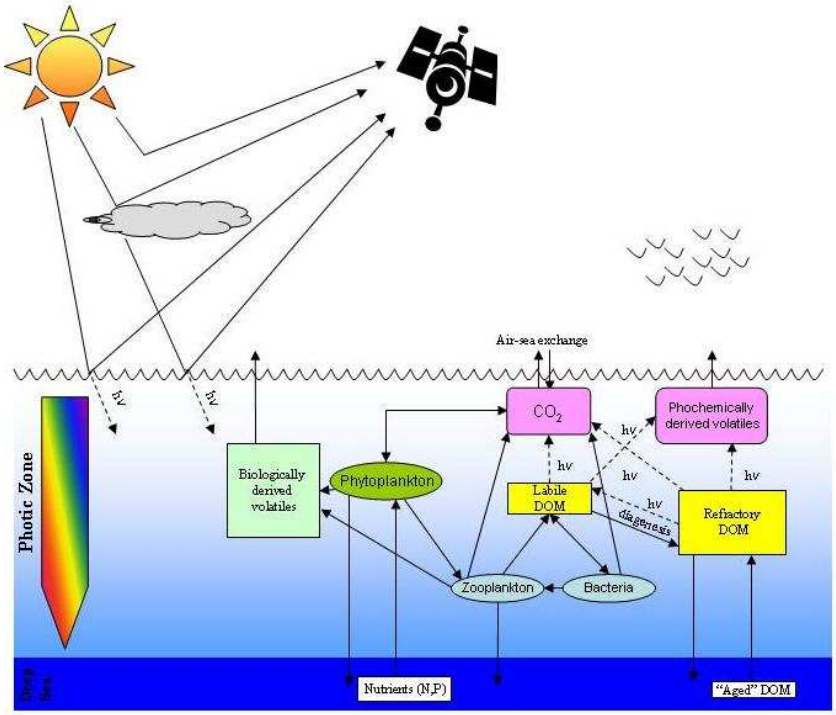

Institute for Environment and Sustainability

2007

EUR 22720 EN

The mission of the Institute for Environment and Sustainability is to provide scientific-technical support to the European Union's Policies for the protection and sustainable development of the European and global environment.

European Commission
Directorate-General Joint Research Centre
Institute for Environment and Sustainability

Contact information
Address:I-21020 Ispra (Va)
E-mail: vincent.vantrepotte@jrc.it
Tel.: +39 0332 786563
Fax: +39 0332 789034

http://ies.jrc.ec.europa.eu
http://www.jrc.ec.europa.eu

EUR 22720 EN

ISSN 1018-5593

Luxembourg: Office for Official Publications of the European Communities

Printed in Italy

Abstract

In the recent years, numerous efforts have been performed in order to characterize the impacts of UVR on marine photobiology and photochemistry. The quantification of these UV-dependent processes through modelling approaches requires (i) an accurate description of UV underwater light field (ii) an adapted parameterization of the response of marine water compounds and/or organisms to spatio-temporal changes in solar radiations. The spatial and temporal variability of the absorption coefficient of the colored detrital material, which is a key element for studying undersea UV climate, has been characterized in the two basins selected for this study (the Mediterranean Sea and the Norwegian Seas) using the SeaWiFS products archive for the period 1998-2006. Moreover, the various models currently available for the description of selected optical (CDOM photobleaching), photochemical (CO and DIC production) and photobiological (primary production inhibition) effects of UVR on marine waters have been described. Further, the general characteristics of these UV-dependent processes have been presented focusing, in particularly, on their variability along the daily, vertical and spectral dimensions. Several sensitivity analyses have been performed in order to define the relative importance of the various inputs of the spectral and depth resolved model on the final estimations. Finally, some of the straightforward models recently proposed in order to estimate some of the UV impacts at large temporal and or spatial scales have been tested and their limits of application have been discussed.

Table of Contents

Introduction

The detection of a significant depletion of stratospheric ozone in Antarctica in the 1980's has induced a significant increase in the attention of scientists about exposure of terrestrial and aquatic ecosystems to damaging UV radiation (UVR). Starting from the studies dedicated to the southern and northern hemispheres, UV photobiology and photochemistry have become integral parts of biogeochemical studies at the global scale. As a matter of fact, UVR effects on marine ecosystems were relatively unknown until the past 20 years and numerous efforts have been developed to elucidate the specific UV photoprocesses in natural waters. In particular, recent years have brought a wealth of information on the interactions between the field of ultraviolet and visible radiation in the water column and the various forms of life that inhabit it, from zooplankton (Rhode et al. 2001), phytoplankton (Cullen et al. 1992; Boucher and Prézelin 1996; Neale et al. 1998a; Neale et al. 1998b; Vernet 2000; Banaszak and Neale 2001), bacterioplankton (Herndl et al. 1993) to viruses (Wilhelm et al. 1998). The effects of UVR on marine organisms are highly variable from one trophic level to the other and take place at different physiological and structural levels (Häder et al. 1998). However, the chronic alteration of key physiological processes induced by UVR can affect the whole ecosystem productivity and therefore have an influence on the whole marine community structure (Vernet et al. 1994; Sinha and Häder 2002). Moreover, the fact that shortwave radiation is efficient for photosensitizing dissolved organic compounds opens the door to all sorts of photochemical processes (see the review by Häder et al. 1998 and Whitehead and De Mora 2000). These photobiological and photochemical processes are often intertwined in complex ways (Figure 1, Zepp et al. 1998; Mopper and Kieber 2000) and therefore it appears important to consider these various effects in an integrated way.

From the biological point of view, the first contribution of light in the water column is photosynthesis. Marine primary productivity is at the base of the marine food chain and represents a fundamental element of Earth's carbon cycle (Field et al. 1998). The radiation regime, and in particular its ultraviolet component, can have a negative impact on phytoplankton growth and productivity by inducing a possible bleaching of the photosynthetic pigments related to the light harvesting processes (Donkor and Häder 1996), or a damage of DNA structure (Boelen et al. 2000; Helbling et al. 2001). The influence of UVR on these organisms is however complex since it depends on the balance between the damaging effects of these radiations and the protective and/or repair processes developed by the algal cells to limit the stress induced by UVR (Vernet 2000; Roy 2000). Conversely, the effect of UVR should not be considered as necessarily detrimental but depends on the spectral character of light, the community composition and the environmental forcing (Boucher and Prézelin 1996; Barbieri et al. 2002).

From the photochemical point of view, several studies have been performed to characterize the numerous processes resulting of the interactions between UVR and the colored fraction of the dissolved organic matter, i.e. the Chromophoric Dissolved Organic Matter (CDOM). These photodependent processes are complex since UVR might act directly on dissolved material or indirectly by modifying its availability for microbial degradation (Miller and Moran 1997; Moran and Zepp 1997).

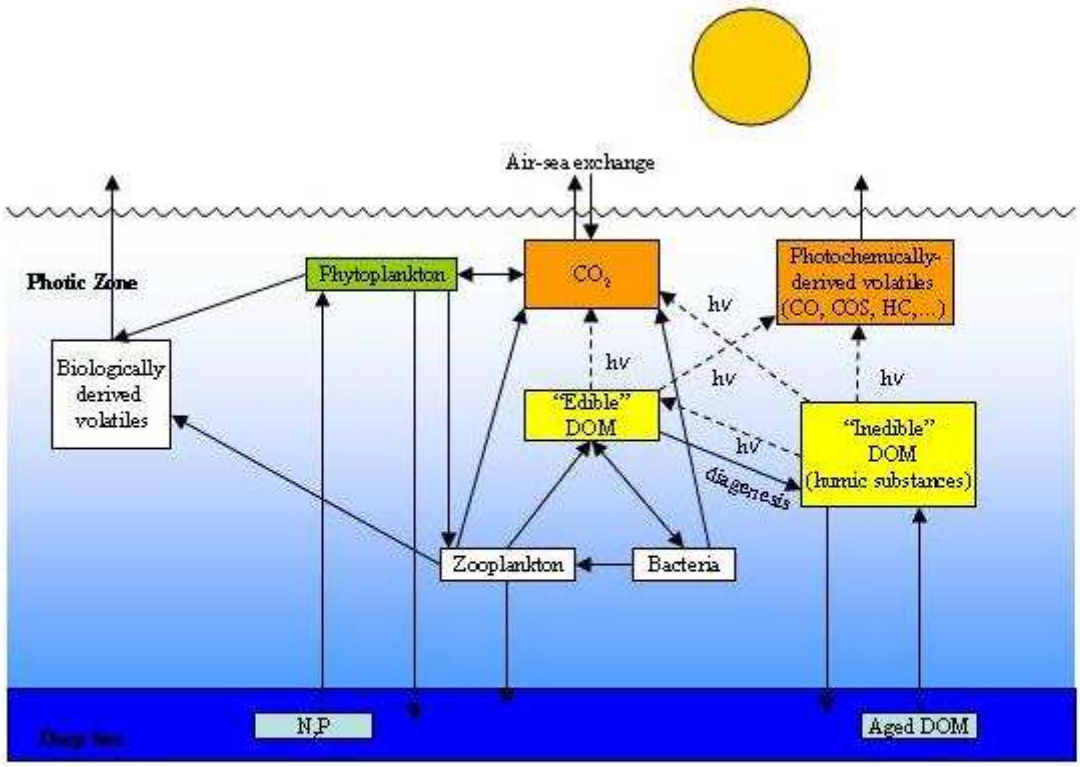

Figure 1: Conceptual model of the interactions of UV-B radiation with biogeochemical cycles in aquatic ecosystems redrawn from Mopper and Kieber (2000). The penetration of UVB is controlled by the optically active components of marine water and mainly by CDOM. Photoreactions driven by UVB are multiple and can lead to enhance the biological availability of the CDOM producing various labile compounds and chemically reactive trace gases.

The exposure of marine dissolved matter to solar radiations modifies the chemical structure of CDOM resulting in an alteration of its optical properties through photobleaching processes (Whitehead and De Mora 2000 and references therein). The photosensibilization of CDOM by UVR can also lead to the production of a variety of organic and inorganic compounds acting significantly on marine biological productivity (Kieber et al. 1989), oceanic carbon cycle (Miller and Zepp 1995; Miller et al. 2002; Johannessen and Miller 2001) and/or sea-air gases exchanges (Miller and Zepp 1995; Gallegos et al. 1998; Whitehead and De Mora 2000). The chemically reactive species formed through photodegradation processes include biologically labile photoproducts, e.g., ammonium, amino acids and low molecular weight organic compounds (Kieber et al. 1989; Bushaw et al. 1996; Moran and Zepp 1997), hydroxyl radicals (Zepp et al. 1992), oxygen radicals (Blough and Del Vecchio 1995), free radicals (Whitehead and De Mora 2000), hydroxen peroxide (Moore et al. 1993) or reduced iron (Whitehead and De Mora 2000). CDOM photomineralisation can also result in the direct formation of inorganic gases such as carbon monoxide (CO, Miller and Zepp 1995, Zafiriou et al. 2003) as well

as to the production of dissolved inorganic carbon (DIC, Granéli et al. 1996; Miller and Moran 1997, Gallegos et al. 1998; Vähätalo et al. 2000; Johannessen and Miller 2001). In addition, UVR have been shown to have a significant influence on the ocean sulfur cycling by acting on the dimethyl sulfide (DMS, Toole et al. 2003, Bouillon and Miller 2004) and carbonyl sulfide (COS, Zepp and Andreae 1994, Weiss et al. 1995) dynamics.

The quantitative estimation of the UV phochemical and photobiological effects on marine ecosystems at large scale has to face two major challenges. The first one concerns the accurate description of the UV underwater light field which still represents an open field of study (e.g. Vantrepotte and Mélin 2006). The second one is related to the prediction, through adapted parameterizations, of how the marine chemical components and/or organisms respond to environmental changes in UV exposure. The latter feature has been shown to be technically complex to achieve due to the current limited ability to reproduce precisely both the intensity and spectral composition of sunlight in the laboratory and to quantify with a sufficient precision some of the UV photoproducts. The complexity of modelling the UV photobiological (and photochemical) effects is further increased by the needs to consider several environmental forcings, such as the vertical mixing regime, which have been shown to significantly modulate the UV impacts on natural waters (Neale et al. 1998b).

However, numerous "quantum yields" representing the ratio between the moles of photoproducts formed per moles of photons absorbed by CDOM (also called Apparent Quantum Yieds: AQY) have been recently documented in the literature. In particularly, various AQYs parametrizations are currently available for estimating the rate of photobleaching (Whitehead et al. 2000; Osburn et al. 2001; Del Vecchio and Blough 2002), DIC (Moran and Zepp 1997; Vähätalo et al. 2000; Osburn et al. 2001), CO (Ziolkowski 2000; Zafiriou et al. 2003) and biologically labile compounds photoproductions (Miller et al. 2002) or the rate of DMS photolysis (e.g. Toole et al. 2003). Although all these functions present a strong spectral dependence with photons in the UVB region having a greater photosensitizing efficiency than photons in the near visible band AQYs have also been shown to exhibit a strong spatio-temporal variability reflecting changes in CDOM photolability according to its origin (terrestrial and/or marine) and/or light history (Johannessen and Miller 2001; Bélanger et al. 2006; White et al. 2006). Similarly, several functional relationships, based on experimental studies on phytoplankton culture or natural assemblages, have been recently developed to quantify the UV (and visble) photoinhibition of primary production (Cullen et al. 1992; Boucher and Prézelin 1996, Neale et al. 1998b; Neale 2001). These relationships, called Biological Weighting Functions (BWFs), have been show to depend on the phytoplankton community composition and environmental conditions even though they globally present a conservative shape with a decrease of biological weighting from the UVB to the UVA and visible domain. In addition to the BWFs description, the quantification of UV photobiological effects also requires information on the Exposure-Response Curve which determines the kinetic of the phytoplankton response to a defined exposure to UVR. More precisely, the ERC definition is related to the need to establish whether the effect of the UVR is a function of the instantaneous exposure or cumulated dose. This distinction, which refers to the reciprocity principle, depends on the balance between damage and repair processes as well as on the time scale considered (Neale et al. 1998b; Neale 2001).

The long-term objective of this project is to derive a distribution of visible and ultraviolet radiation in marine waters and to quantify, for selected basins, some of its impacts of relevance for the functioning of the ecosystems and the elemental cycles. More specifically, a first goal is to derive a distribution of the ultraviolet and visible radiation spectrum at the ocean surface and interior, map the depth of its penetration, and calculate the levels of exposure in the water column. Subsequently, this distribution will be used to quantify the photoinhibition experienced by phytoplankton, the dynamics of photobleaching affecting CDOM, and the photoproduction of DIC (and CO) from

the dissolved organic pool, and to make tentative synoptic estimates of these rates for selected regions, using optical remote sensing information and appropriate models. The ocean module, simple enough to allow calculations at basin scale, uses up-to-date bio-optical relationships to represent the water optical properties. The other inherent optical properties (IOPs) account for phytoplankton, non-algal particles and chromophoric dissolved organic matter (CDOM). To obtain basin-scale assessments, satellite-derived distributions of IOPs based on SeaWiFS/MODIS are produced with a quasi-analytical bio-optical algorithm (Lee et al. 2002), and include absorption by phytoplankton and the sum of absorption by CDOM and non algal particles. Two test basins were chosen for this exercise: the Mediterranean and the Norwegian seas. The former has the advantage of representing a miniature ocean with a highly diversified biological and physical regime receiving large fluxes of solar radiations. The Norwegian Sea is an example of subarctic to arctic basin, having a pronounced solar flux seasonal cycle, as well as very transparent waters for short wavelengths (Højerslev and Aas 1991). Moreover, its geographical position can serve as a test basin for ozone-related analyses.

The first part of this report deals with the description of the spatial distribution of satellite derived colored dissolved and detrital organic materials absorption coefficient ($a_{dg}(\lambda)$, m^{-1}) and its relative importance for the absorption budget in the selected basins. The second part of this report is related to the description of the different parameterizations and models currently available for the estimation of the selected photochemical and photobiological effects of UVR, with a peculiar attention given to the modelling of photobleaching, DIC (and CO) photoproduction and primary production inhibition rates. The third part of the document concerns the characterization of the general patterns of the UVR-dependent photobiological and photochemical processes. For instance, the dependence of these processes on the water masses (biological and/or optical) and atmosphere (i.e. ozone concentration) characteristics have been estimated. Moreover, the variations in DIC, CO and/or primary production inhibition rates along the vertical, temporal and spectral dimensions have been illustrated. In the fourth part, the results of several sensitivity analyses, performed in order to appreciate the relative importance of the model definition (in terms of AQYs and BWF or ERC), the choice of the spatio-temporal resolution (vertical and/or spectral), the description of the water column vertical structure (for CDOM and phytoplankton biomass) and mixing regime for the estimation of both UV photochemical and photobiological effects, are presented. Finally, the last part of the document illustrates various straightforward models recently developed to quantify some of the UV-related effects on marine ecosystems at large temporal and/or spatial scales and a discussion on their limits of application.

Chapter 1

Satellite derived colored dissolved and detrital organic materials absorption

1.1 $a_{dg}(\lambda)$ spatial distribution and relative contribution to the absorption budget

During the last 20 years, several algorithms have been developed to derive some inherent optical properties (IOPs) from satellite remote sensing reflectance spectra (e.g. Carder et al. 1999; Lee et al. 2002). The various models currently available for partitioning the Visible Spectral Sea Reflectance (VSSR) signal measured by the satellite-borne sensors into various IOPs are however designed to derive the absorption coefficient of detrital material as a whole, without an explicit distinction of its particulate (or non-algal particles, NAP) and dissolved (CDOM) components. Indeed, the high similarity in CDOM and NAP absorption spectral shapes makes them very difficult to separate using classical analytical inversion methods which require additional information on the NAP optical properties (e.g. absorption vs backscattering ratio). Empirical algorithms have been recently developed in order to overcome this limitation (Bélanger et al. 2006). Generally, current optical models usually regroup $a_{CDOM}(\lambda)$ and $a_{NAP}(\lambda)$ into a unique absorption coefficient referred to as $a_{dg}(\lambda)$ (for absorption of non-algal detritus + Gelbstoff) or $a_{CDM}(\lambda)$ (for absorption of Colored Detrital Material).

The absorption by phytoplankton ($a_{ph}(\lambda)$) and $a_{dg}(\lambda)$ has been recently archived for the European oceanic domain for the period 1998-2006 (SeaWiFS and MODIS data) using the multiband quasi-analytical algorithm developed by Lee et al. (2002). The latter has been subject to a recent validation exercise in the northern Adriatic waters (Mélin et al. 2007).

The characterization of CDOM spatio-temporal variability represents a key element in the context of this study. Indeed, knowledge of CDOM distribution is critical for (i) estimating the distribution of the ultraviolet and visible radiation spectrum at the ocean surface and interior, (ii) mapping the depth of its penetration, and (iii) calculating the levels of exposure in the water column. Furthermore, the accurate description of CDOM absorption coefficient is essential since the dissolved material represents the source element for the various photochemical processes that we plan to model.

The Figure 1.1 illustrates the spatial distribution of $a_{dg}(443)$ obtained from SeaWiFS observation in the Mediterranean Sea and Subarctic Atlantic region (SARC region, Longhurst 1995). Classical coastal to offshore decreasing gradients are observed in both basins. In the Mediterranean Sea, $a_{dg}(443)$ ranges from $< 0.01\ m^{-1}$ in the clear waters of the Levantine basin to $\approx 0.3\ m^{-1}$ in the more turbid coastal ecosystems. Similarly, in the SARC province high $a_{dg}(443)$ are located in the Baltic Sea while the lowest values are found in the Atlantic offshore waters.

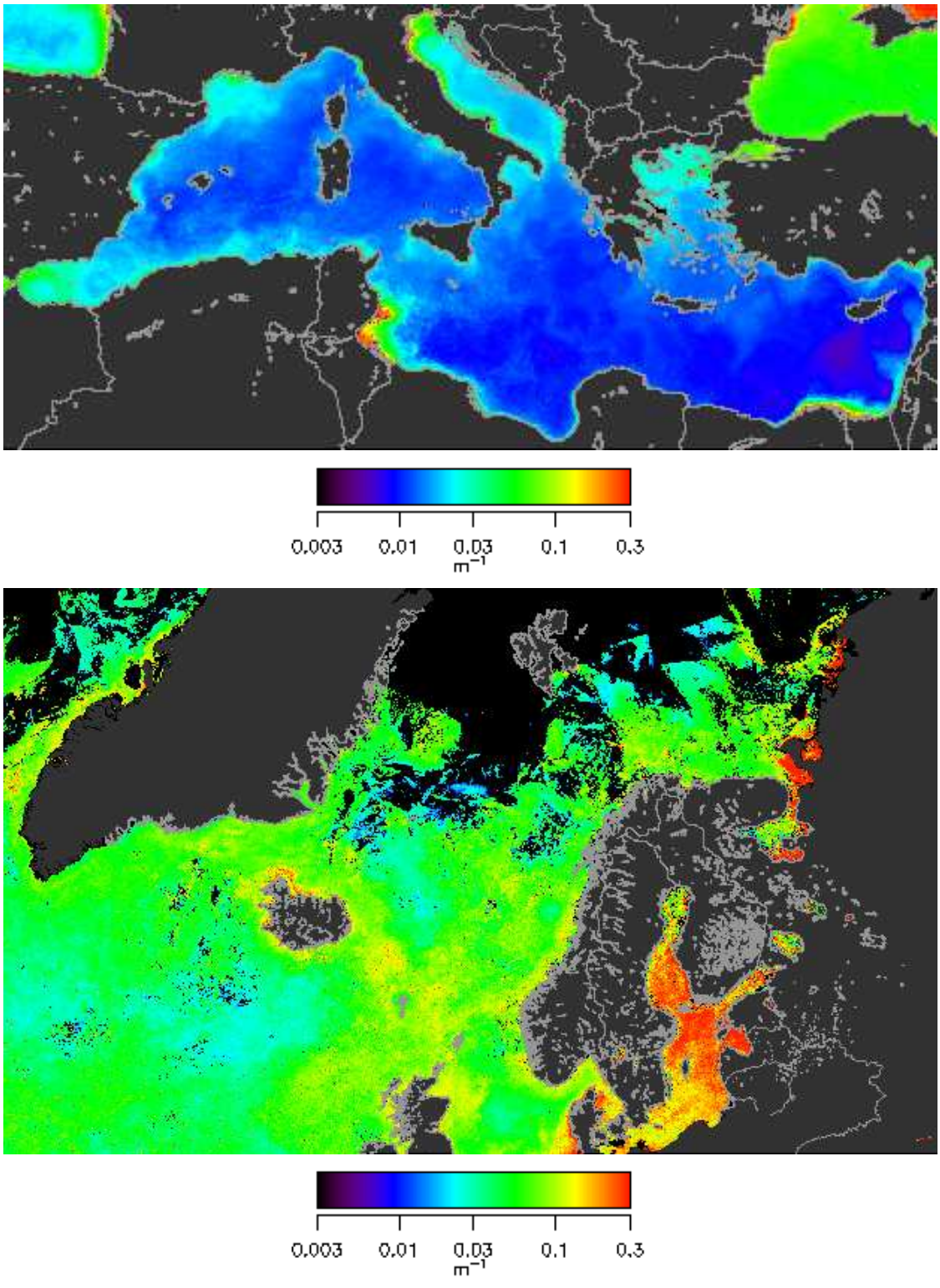

Figure 1.1: Field of colored detrital material absorption coefficient at 443 nm ($a_{dg}(443)$) in September 2003 in the Mediterranean Sea and subarctic Atlantic region given by Lee et al. (2002) inversion algorithm applied to SeaWiFS data.

On the temporal scale, monthly time series of SeaWiFS products including the concentration of chlorophyll a (chl$a$), $a_{dg}(443)$ and $a_{ph}(443)$ averages for each basin clearly emphasize the presence of a seasonal cycle for all parameters (Figures 1.2 and 1.3). The Mediterranean Sea is characterized by winter maxima and summer minima while $a_{dg}(443)$ in the Norwegian Sea globally exhibits an opposite trend. Note that these patterns are submitted to a low interannual variability.

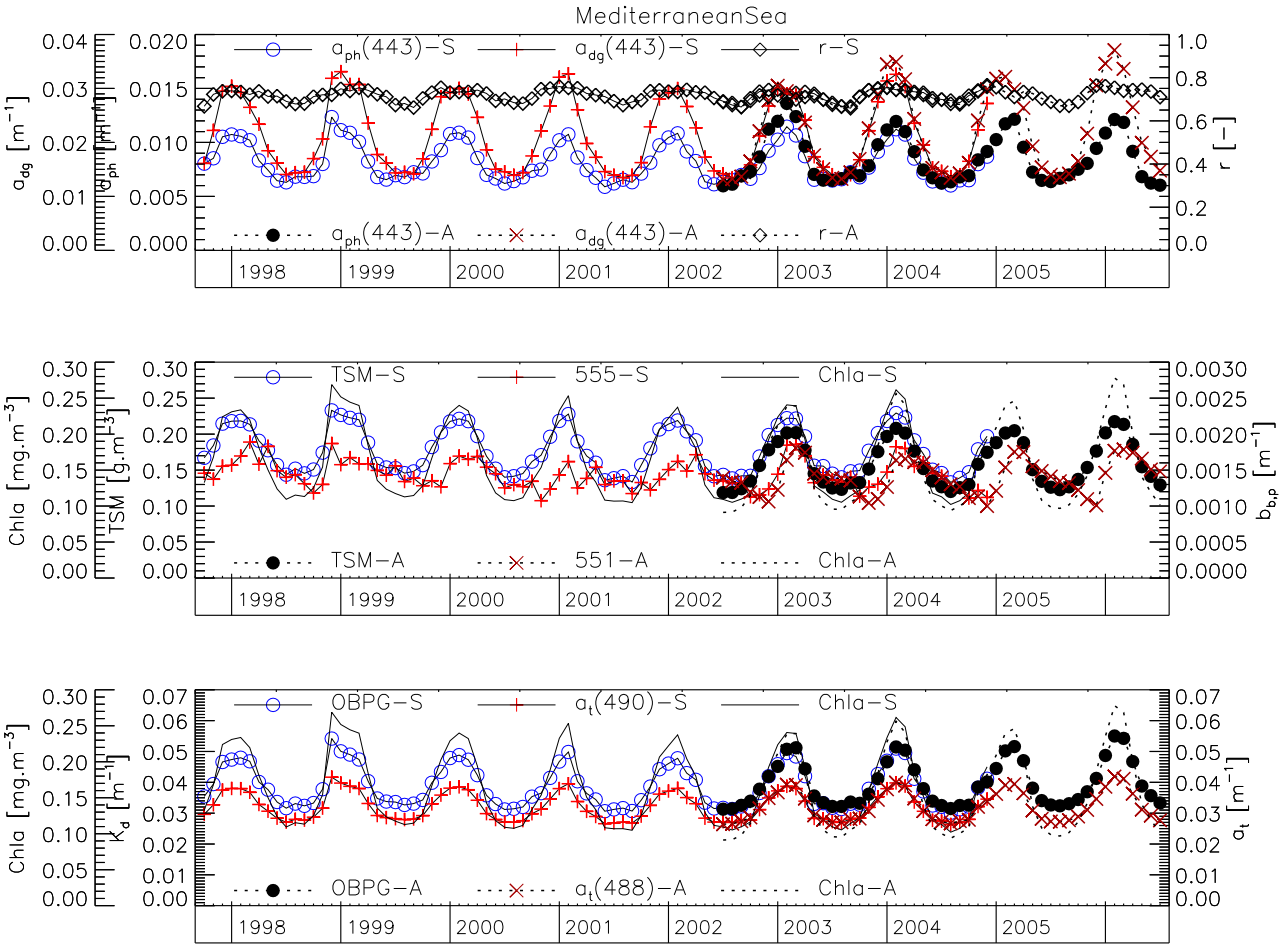

Figure 1.2: Monthly average time series of various SeaWiFS and MODIS products . The r-ratio represents : $a_{dg}(443)/(\ a_{ph}(443)+\ a_{dg}(443))$. The S and A extensions refer to SeaWiFS and MODIS respectively. a_t is total absorption and b_{bp} is particulate backscattering.

The comparison between $a_{dg}(443)$ and phytoplankton biomass and/ or absorption coefficient dynamics can provide relevant information on the origin of CDOM in open ocean which still remains poorly known. Indeed, some authors currently consider that CDOM in marine waters is predominantly of terrestrial origin while others argue that marine CDOM is mainly a by-product of *in situ* phytoplankton cells lysis, zooplankton grazing or bacterial activity. In the Mediterranean and Norwegian Seas, the apparent coupling existing between $a_{dg}(443)$ and $a_{ph}(443)$ (or chl$a$) monthly climatology (Figures 1.2 and 1.3) might confirm the relevant influence of the autochthonous biological activity for CDOM dynamics. However, more detailed analyses should be performed to derive relevant conclusions on the relationships existing between phytoplankton and CDOM evolution. In particularly, it would be necessary to identify more precisely the presence or the absence of a relationship at a lower spatial scale (regional) and further, in the case of the presence of a significant

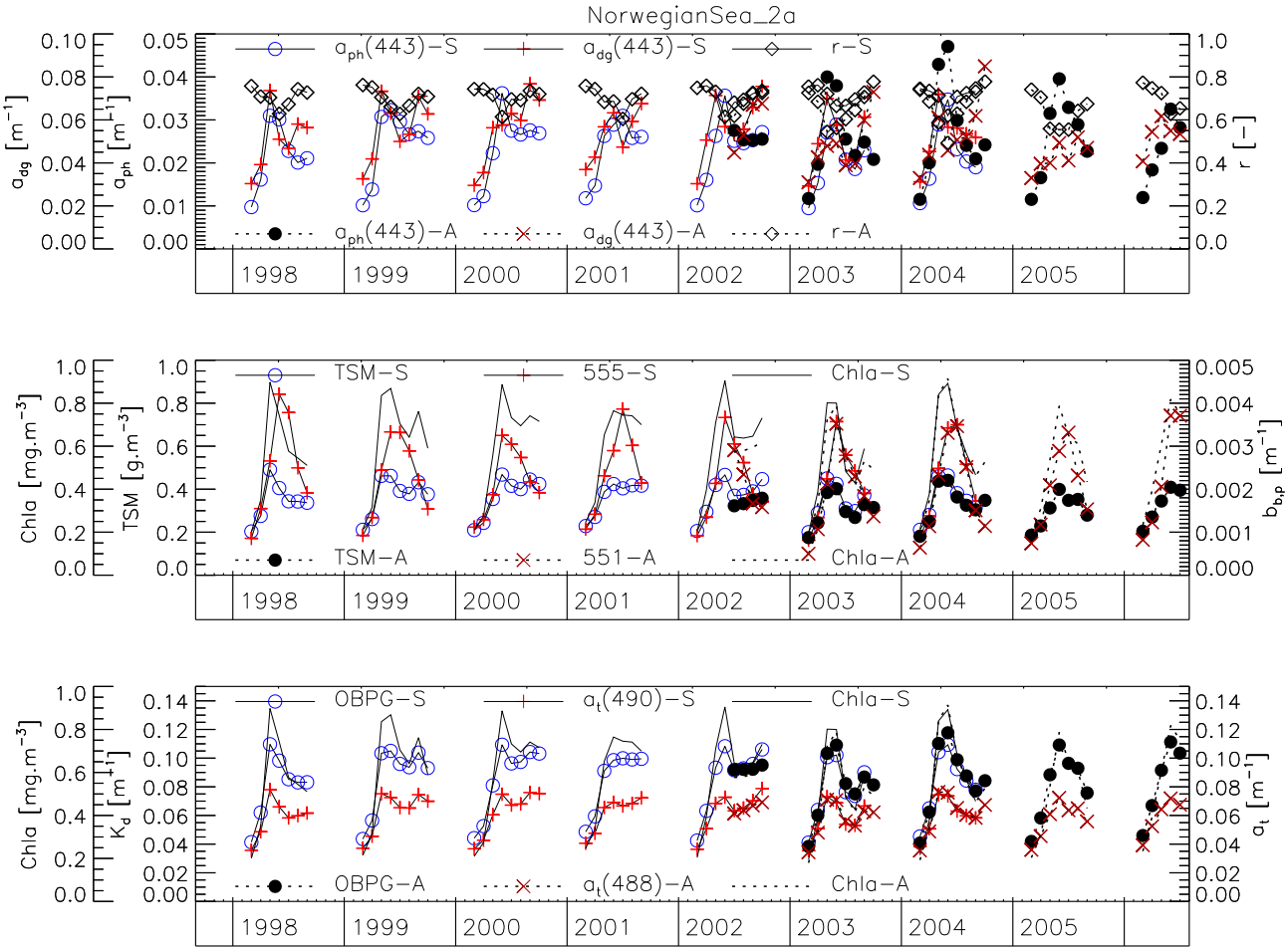

Figure 1.3: Monthly average time series of various SeaWiFS products in the subarctic Atlantic region. The r-ratio represents : $a_{dg}(443)/(\ a_{ph}(443)+\ a_{dg}(443))$. The S and A extensions refer to SeaWiFS and MODIS respectively. a_t is total absorption and b_{bp} is particulate backscattering.

covariation between $a_{ph}(443)$ and $a_{dg}(443)$ time series, to determine the eventual phase shift existing between these seasonal cycles considering a higher temporal resolution (e.g. weekly time series).

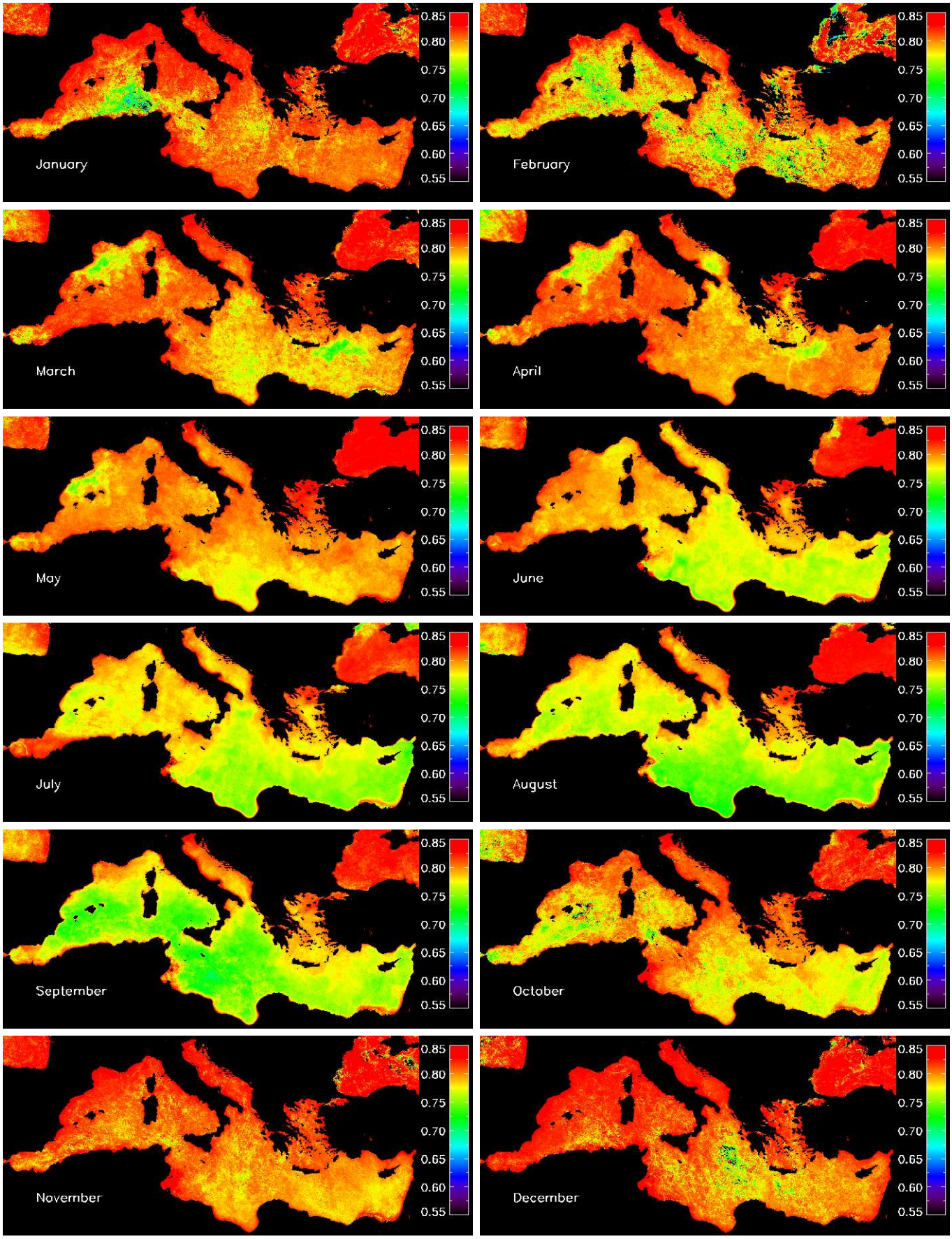

Figure 1.4: Monthly mean fields of the $a_{dg}(443)/(\ a_{ph}(443)+\ a_{dg}(443))$ ratio in 2003 in the Mediterranean Sea.

The contribution of the absorption of the colored detrital material with respect to total absorption of the seawater (expect pure water) at 443 nm ($a_{dg}(443)/(\ a_{ph}(443)+\ a_{dg}(443))$) varies spatially and temporally. At the basin scale, the $a_{dg}(443)/(\ a_{ph}(443)+\ a_{dg}(443))$ ratio ranges from ≈ 0.55 to 0.85 in the Mediterranean Sea and SARC region (Figures 1.5 and 1.4). Similar ranges of variation are observed on the temporal scale, with basin average for the $a_{dg}(443)/(\ a_{ph}(443)+\ a_{dg}(443))$ ratio oscillating between 0.65 and 0.8 for the Mediterranean and between 0.55 and 0.8 in the Norwegian Sea. Interestingly, the seasonal cycle of the $a_{dg}(443)/(\ a_{ph}(443)+\ a_{dg}(443))$ ratio in the Mediterranean Sea closely follows that of chl$a$, $a_{ph}(443)$, $a_{dg}(443)$ while in the Norwegian Sea high $a_{dg}(443)/(\ a_{ph}(443)+\ a_{dg}(443))$ values are found in late winter-early spring period when $a_{ph}(443)$ and $a_{dg}(443)$ minima are observed. This feature might indicate regional variations in the parameters controlling CDOM sink (photobleaching, bacterial activity) or source (terrestrial inputs, biologically mediated production) terms. The decrease observed in the $a_{dg}(443)/(\ a_{ph}(443)+\ a_{dg}(443))$ values from May to September in the Mediterranean Sea seems to start earlier in the eastern part than in the western part of the basin (Figure 1.4). This feature might be related to spatial differences in terms of water clarity and therefore in the magnitude of summer photobleaching processes between these two areas. Moreover, the relatively low $a_{dg}(443)/(\ a_{ph}(443)+\ a_{dg}(443))$ values (< 0.6) found in the Gulf of Lion from March to May, with respect to the overall Mediterranean Sea figure (Figure 1.4), might be related to the peculiar hydro-biological characteristics of this part of the Mediterranean Sea (upwelling zone and intense spring bloom event). Note that this feature is also clearly visible on the associated $a_{dg}(443)/(\ a_{ph}(443)+\ a_{dg}(443))$ monthly time series with the presence of a short spring minimum (Figure 1.6) coinciding with the regional chl$a$ maximum. The potential influence of spring bloom events is also illustrated by the similar situations found in April in the southern Adriatic as well as in the western part of the North Levantine basin.

Although there are significant spatio-temporal variations, the relative part of CDOM absorption in the overall absorption budget is much greater than previously thought, having relevant implications for optical modelling. Indeed, CDOM absorption is classically expressed in bio-optical models by its relative contribution to the total absorption coefficient of seawater, assuming that CDOM variation is related to that of particulate material and therefore to phytoplankton dynamics. More precisely, in the absence of any reliable alternative the ratio $a_{CDOM}(440)/(a_{CDOM}(440)/ + a_w(440) + a_p(440))$ has been often assumed constant and equal to 0.2 (Prieur and Sathyendranath 1981; Morel 1991). Hence, our results seems to confirm the slight underestimation made by this general assumption as already documented by various authors (e.g. Siegel et al. 2002; Siegel et al. 2005; Hu et al. 2006).

1.2 Relative contribution of NAP absorption to $a_{dg}(\lambda)$ estimated from satellite remote sensing

In the context of studies applied to the quantification of UV photochemical effects, it is useful to estimate the relative part of a_{dg} which can be effectively attributed to CDOM only and therefore to correct a_{dg} for the absorption of NAP. For this purpose, we estimated the relative proportion represented by NAP in the $a_{dg}(443)$ coefficient by calculating $a_{NAP}(443)$ from chl$a$ concentrations using an empirical parameterization from Bricaud et al. (1998):

$$a_{NAP} = 0.0124.chla^{0.724}.e^{-S_{NAP}(\lambda-440)} \tag{1.1}$$

with $S_{NAP} = 0.011\ nm^{-1}$.

NAP can account for $\approx$ 5 to 25% of the absorption of the colored detrital material at 443 nm

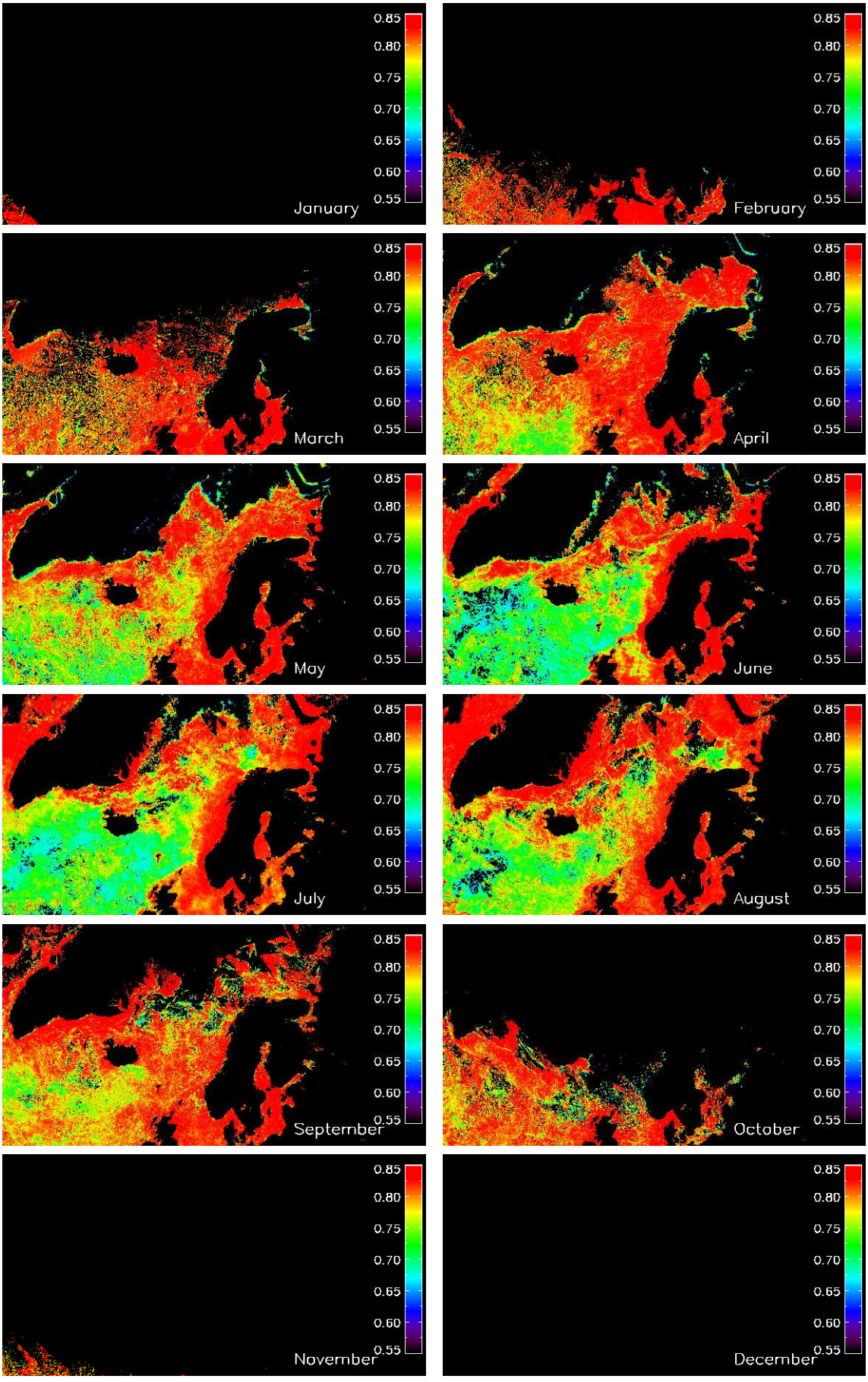

Figure 1.5: Monthly mean fields of the $a_{dg}(443)/(\ a_{ph}(443)+\ a_{dg}(443))$ ratio in 2003 in the Atlantic subarctic province.

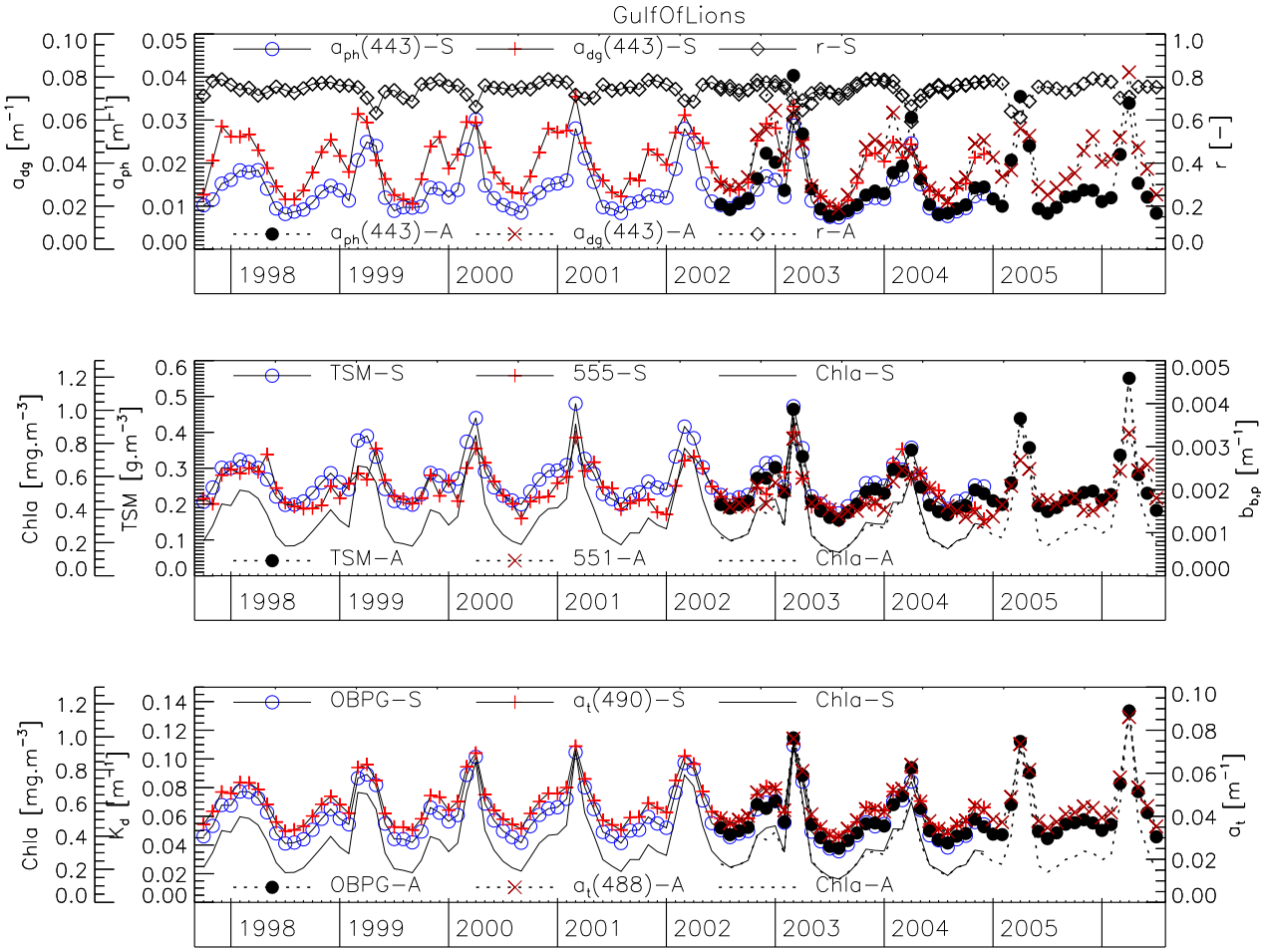

Figure 1.6: Monthly average time series of various SeaWiFS products in the Gulf of Lions. The r-ratio represents : $a_{dg}(443)/(\ a_{ph}(443)+\ a_{dg}(443))$. The S and A extensions refer to SeaWiFS and MODIS respectively. a_t is total absorption and b_{bp} is particulate backscattering.

with an average of 15 % (SD = 2.7%) and 16 % (SD = 7.8%) in the Mediterranean Sea and SARC region respectively (Figures 1.7, 1.8). These values obviously represent rough estimates since this estimation of $a_{NAP}(443)$ depends on the algorithm used to derived chl$a$ concentrations as well as on the choice of the NAP spectral slope. Moreover, these calculations do not explicitly take into account the presence of inorganic material including mineral particles from terrestrial inputs, and therefore certainly underestimate the relative influence of NAP in the coastal waters. However, these results are in agreement with the global estimations by Siegel et al. (2002; 2005) who reported an average a_{CDOM} contribution for a_{dg} of $\approx 81.7 \pm 13.7$ % at 440 nm from field measurements.

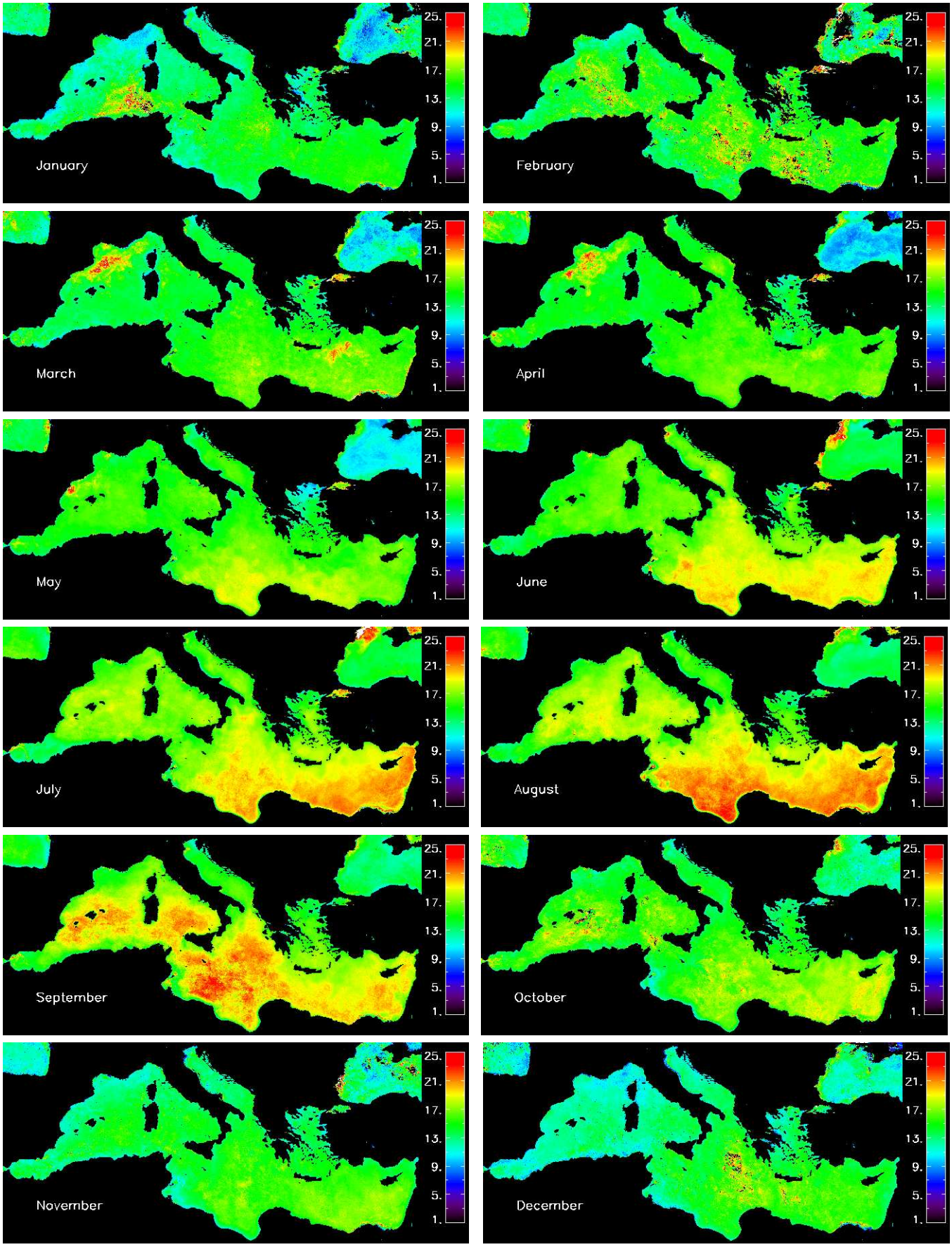

Figure 1.7: Monthly mean fields of the relative importance of NAP in the colored material absorption coefficient at 443 nm in 2003 in the Mediterranean Sea.

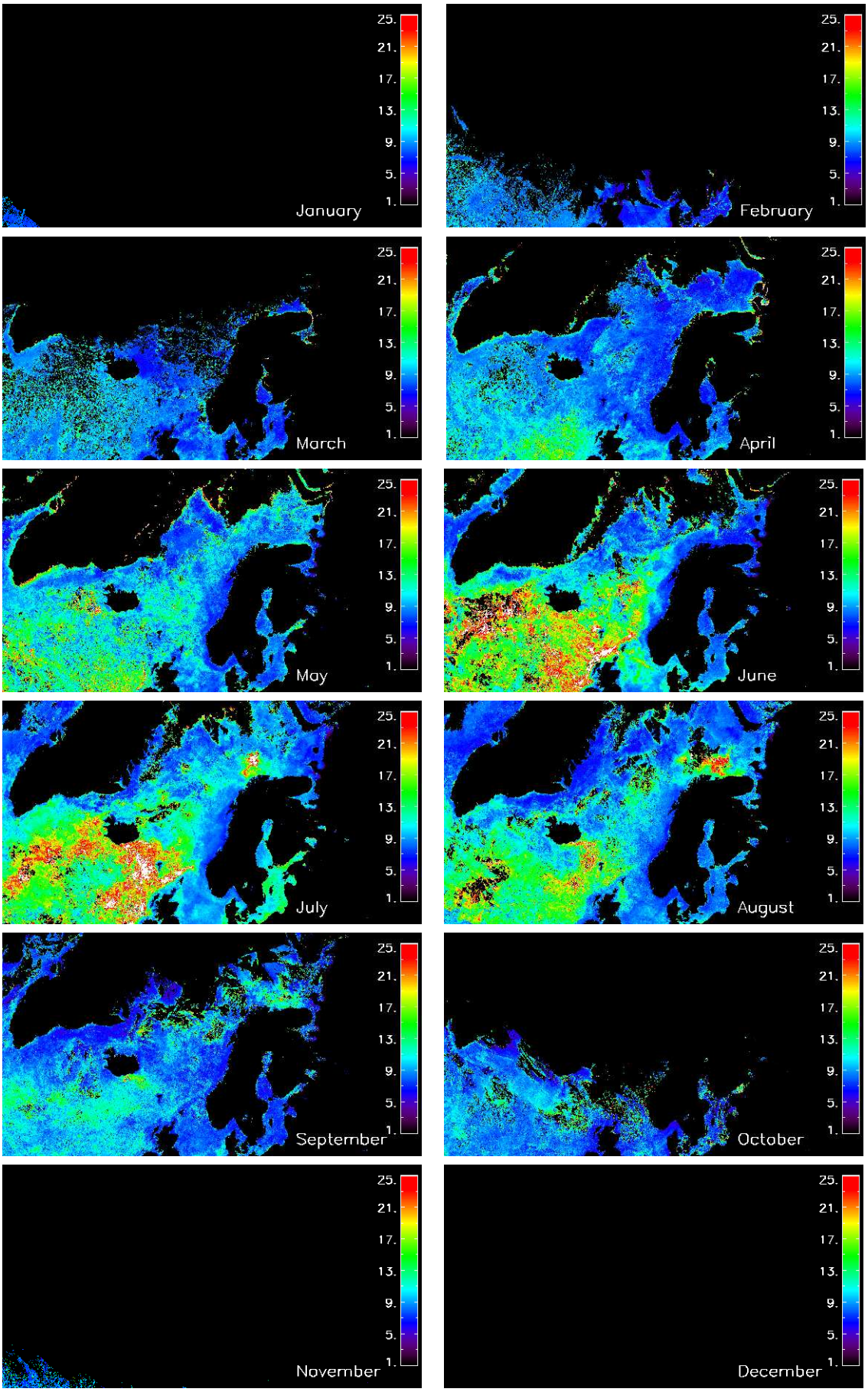

Figure 1.8: Monthly mean fields of the relative importance of NAP in the colored material absorption coefficient at 443 nm in 2003 in the SARC region.

Chapter 2

UV photochemical and photobiological effects: models description

2.1 CDOM Photobleaching

"Photobleaching" reactions refer to the process by which CDOM chromophores are altered due to their exposition to sunlight and especially to UV radiations. This alteration results in a decrease in the absorption (and flurorescence) coefficient also associated with changes in CDOM absorption spectra shape (Vodacek et al. 1997; Del Vecchio and Blough 2002; Twardowski and Donaghay 2002). CDOM photobleaching, which represents the "visible" manifestation of UVR degradation of CDOM, has been recently examined through numerous laboratory and field studies (Vodacek et al. 1997 ; Nelson et al. 1998; Whitehead et al. 2000; Vähätalo et al. 2000; Osburn et al. 2001; Del Vecchio and Blough 2002; Vähätalo et al. 2002; Goldstone et al. 2004; Vähätalo and Wetzel 2004). This process has been shown to represent the primary sink of CDOM in natural waters being responsible for an important part of the spatio-temporal dynamics of this optically active component of seawater (Nelson et al. 1998; Siegel et al. 2002; Del Vecchio and Blough 2004 ; Siegel et al. 2005; Hu et al. 2006). Moreover, the loss of CDOM absorption might lead to significant changes in the transparency of the surface waters for UVR and visible radiations (Morris and Hargreaves 1997; Vodacek et al. 1997; Nelson et al. 1998; Siegel et al. 2002) and therefore have significant ecological consequences (Zepp et al. 1998) by modifiying the level of exposure of marine compounds and organisms to UVR and therefore the extent of UVR damage and/or photo-repair processes.

The magnitude of photobleaching rates is expected to vary widely at the spatial and seasonal scale (Siegel et al. 2002) according to various parameters such as the water optical characteristics, the stratification of the water column, the seasonal changes in sunlight exposure, the origin and chemical composition of CDOM (e.g. Twardowski and Donaghay 2002).

As a matter of fact, the photobleaching rates and/or photobleaching half-life (time necessary to induce a reduction of 50 % of the CDOM absorption coefficient) currently reported in the literature for various aquatic ecosystems present large variations (Table 2.1).

Recently, several parametrisations have been proposed to characterize the kinetics of UVR photobleaching process:

1. **Osburn et al. (2001)**

   Osburn et al. (2001) have proposed a spectral weighting function for CDOM photobleaching in temperate lakes. The computation of CDOM photobleaching rates considers the solar energy absorbed by CDOM during a defined period (E_a in $J.m^{-2}$):

Reference	λ	Area	$t_{1/2}$	Rate
Twardowski and Donaghay (2002)	412 nm	WA USA	28 d	0.9145 d^{-1} RF
				0.0248 d^{-1} SF
Vodacek et al. (1997)	350 nm	Delaware Bay Mid-Atlantic	23.4 d	0.624 d^{-1} RF
				0.0072 d^{-1} SF
Whitehead et al. (2000)	280 nm	Saint-Laurent estuary	36.4 d	
	450 nm		13.5 d	
Nelson et al. (1998)	*N.D.*	Sargasso sea	90 d	0.011 d^{-1}
Boss et al. (2001)	*N.D.*	Mid-atlantic bight	$\approx$ 1 month	
Vähätalo et al. (2002)	280 nm	Lakes	120-455 d	

Table 2.1: Examples of CDOM photobleaching rates and photobleaching half-life currently published in the literature. Twardowski and Donaghay (2002) identified two fractions of CDOM showing differences in their sensitivity to photobleaching processes: RF: rapid fraction, SF: slow fraction.

$$E_a(\lambda) = E_d(\lambda).a_{CDOM}(\lambda)_{avg}.0.0177 \tag{2.1}$$

where $E_d(\lambda)$ is the spectrum of incident energy (Jm^{-2}), $a_{CDOM}(\lambda)_{avg}$ is the geometric mean of the initial and final (after UV exposition) dissolved absorption coefficients and 0.0177 represents the optical pathlength of the quartz tube used in these experiments. The weighting function is described by:

$$W(\lambda) = W(300).e^{(-S_W.[\lambda-300])} \tag{2.2}$$

where $W(\lambda)$ is the weight (in $m.J^{-1}$) at λ, $W(300)$ is the weight at the reference wavelength (300 nm) and S_W the slope of the exponential function. Then the predicted photobleaching (PB_{pred} in m^{-1}) is obtained by multiplying the absorbed energy (E_a in $J.m^{-2}$) by the spectral weight which converts the absorbed energy in photobleaching at each wavelength between 280 and 500 nm:

$$PB_{pred}(\lambda) = W(\lambda).E_a(\lambda) \tag{2.3}$$

The integrated photobleaching effect is obtained by:

$$PB_{pred} = \sum_{280}^{500} PB_{pred}(\lambda)d\lambda \tag{2.4}$$

The mean S_W value given by Osburn et al. (2001) is 0.0103 ($\pm$ 0.006) while the mean $W(300)$ is equal to $4.34.10^{-6}$ $m.J^{-1}$ ($\pm$ $-1.79.10^{-6}$)

2. **Vähätalo and Wetzel (2004)**

The rate of photobleaching of CDOM at the depth z (ble_z, $m^{-1}m^{-3}d^{-1}$) is defined by:

$$ble_z = \int_{\lambda_{min}}^{\lambda_{max}} \phi_{ble,\lambda} Q_{S,\lambda,z} a_{CDOM,\lambda} d\lambda \tag{2.5}$$

where $\phi_{ble,\lambda}$ represents the spectrum of apparent quantum yield at wavelength λ ($m^{-1}E^{-1}$), $Q_{S,\lambda,z}$ is the scalar photon density at wavelength λ and depth z ($Em^{-1}d^{-1}$) and $a_{CDOM,\lambda}$ is the absorption spectrum of CDOM (m^{-1}). λ_{min} and λ_{max} are the limits of the wavelengths contributing to photochemical decomposition.

For a deep water column this photodecomposition rate (ble) becomes:

$$ble = \int_{\lambda_{min}}^{\lambda_{max}} \phi_{ble,\lambda} Q_{a,\lambda} a_{CDOM,\lambda} / a_{tot,\lambda} d\lambda \tag{2.6}$$

where $Q_{a,\lambda}$ is the photons absorbed to the water column at the wavelength λ ($Em^{-2}d^{-1}$) and the ratio $a_{CDOM,\lambda}/a_{tot,\lambda}$ is the contribution of CDOM to the total absorption.

The apparent quantum yield is spectrally dependent and described as:

$$\phi_{ble,\lambda} = c.e^{-d\lambda} \tag{2.7}$$

where c ($m^{-1}E^{-1}$) and d (nm^{-1}) are constants determined experimentally. The coefficient c range from 0.145 to 0.161 $m^{-1}E^{-1}$ ($\bar{c} = 0.1551\ m^{-1}E^{-1}$) and d ranged from 0.00813 to 0.01096 nm^{-1} ($\bar{d} = 0.009637\ nm^{-1}$).

3. **Del Vecchio and Blough (2002)**

Recent experimental studies have emphasized that the loss of CDOM absorption at a defined wavelength might be induced by the absorption of the energy of photons from multiple wavelengths (Whitehead et al. 2000 ; Osburn et al. 2001). The model developed by Del Vecchio and Blough (2002) differs from the two previous models since it considers explicitly these indirect photobleaching processes through the definition of a cross-section matrix (Table 2.2, Figure 2.1).

(10^{-20})	λ_{irr}	λ_{irr}	λ_{irr}	λ_{irr}	λ_{irr}	λ_{irr}	λ_{irr}	λ_{irr}	λ_{irr}	λ_{irr}	λ_{irr}
σ_P	300	310	320	330	340	350	360	370	380	390	400
λ_{obs} 300	0.117	0.061	0.046	0.030	0.024	0.019	0.013	0.007	0.007	0.006	0.006
λ_{obs} 310	0.115	0.065	0.049	0.034	0.027	0.021	0.015	0.009	0.008	0.007	0.006
λ_{obs} 320	0.113	0.067	0.052	0.036	0.030	0.023	0.017	0.010	0.009	0.007	0.006
λ_{obs} 330	0.108	0.062	0.050	0.037	0.031	0.025	0.019	0.012	0.010	0.009	0.007
λ_{obs} 340	0.104	0.060	0.048	0.037	0.037	0.025	0.020	0.013	0.012	0.010	0.008
λ_{obs} 350	0.100	0.057	0.046	0.035	0.029	0.025	0.020	0.015	0.013	0.011	0.009
λ_{obs} 360	0.095	0.054	0.043	0.032	0.028	0.024	0.020	0.015	0.014	0.012	0.011
λ_{obs} 370	0.092	0.052	0.042	0.030	0.026	0.023	0.019	0.015	0.015	0.014	0.013
λ_{obs} 380	0.091	0.050	0.039	0.027	0.025	0.022	0.019	0.016	0.016	0.015	0.015
λ_{obs} 390	0.089	0.049	0.037	0.026	0.023	0.020	0.018	0.015	0.016	0.016	0.017
λ_{obs} 400	0.089	0.047	0.035	0.024	0.021	0.019	0.017	0.014	0.016	0.017	0.018

Table 2.2: CDOM photobleaching cross-section ($cm^{-2}s^{-1}$) from Del Vecchio and Blough (2002). λ_{irr} and λ_{obs} represent the irradiation and observation wavelengths respectively.

The depth and wavelength dependent photobleaching rate coefficients $F(\lambda, z)$ are obtained from:

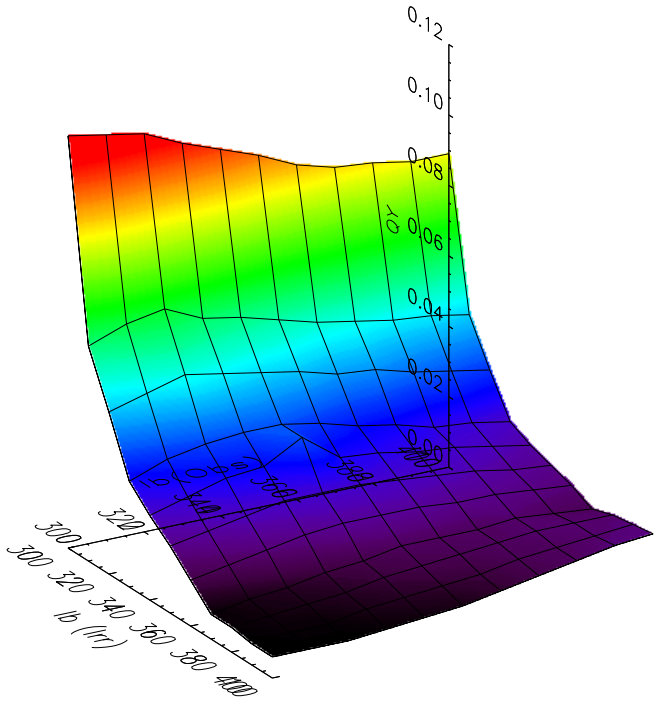

Figure 2.1: Photobleachimg cross section σ_P $(x10^{-20})$ matrix (Del Vecchio & Blough, 2002).

$$F(\lambda, z) = \sigma_P(\lambda).E_d(\lambda, z) \tag{2.8}$$

where $\sigma_P(\lambda)$ corresponds to the matrix of photobleaching cross-section ($cm^2.photon^{-1}$) reported in table 2.2 and $E_d(\lambda, z)$ is the solar irradiance at depth z ($photons.cm^{-2}.s^{-1}$). The absorption of CDOM obtained after an exposition to UV radiation for a short time interval (Δt) is obtained by:

$$a_{CDOM}(\lambda, z, \Delta t) = a_{CDOM}(\lambda, z).e^{-F(\lambda,z).(\Delta t)} \tag{2.9}$$

The average absorption of photobleached CDOM across the mixed layer is calculated as follows:

$$a_{CDOM}(\lambda) = \sum_n a_{CDOM_n}(\lambda, z)/(\#n) \tag{2.10}$$

where $\#n$ is the number of depth intervals. In this model, the new CDOM absorption obtained after a Δt interval was used to compute the new $K_d(\lambda, z)$.

2.2 CDOM photodegradation products

The quantification of the photochemical fluxes induced by the exposure of CDOM to solar irradiance needs knowledge on the efficiency of each absorbed photon to induce the photoproduction of a defined compound. The relationship between a defined photoproduct production rate and the spectral irradiance is represented by an "apparent quantum yield", usually noted $AQY(\lambda)$ or $\phi(\lambda)$.

The term "apparent" reflects the fact that the specific concentrations of CDOM chromophores in aquatic ecosytems are usually unknown and that therefore the quantum yields refer to the absorption of the entire CDOM. More precisely, the AQY represents the ratio between the number of molecules of photoproducts and the amount of photons effectively absorbed by the compound, from which the photoproduct is originating:

$$AQY(\lambda) = \frac{N_{photoproduct}}{N_{photons}(\lambda)} \tag{2.11}$$

where $AQY(\lambda)$ is the spectral quantum yield for a defined photoproduct (e.g. CO or DIC in mol(photoproduct). mol(photons)$^{-1}$), $N_{photoproduct}$ is the number of moles of photoproduct and $N_{photons}(\lambda)$ is the number of moles of photons absorbed by CDOM at the wavelength λ.

The photomineralisation rates are then derived by combining the AQY to the irradiance effectively absorbed by the reactive compound (e.g. CDOM). For a depth resolved model, the general formulation can be expressed as:

$$dP/dt(z) = \int_{\lambda_{min}}^{\lambda_{max}} \mathring{E}(\lambda, z).a_{CDOM}(\lambda, z).\phi(\lambda)d\lambda \tag{2.12}$$

where $dP/dt(z)$ is the photomineralisation rate at a defined depth (z) integrated through the spectral range [λ_{min},λ_{max}] which might vary according to the model considered. $\mathring{E}(\lambda, z)$ represents the scalar irradiance , $a_{CDOM}(\lambda, z)$ the absorption coefficient of CDOM at the wavelength λ and depth z, and $\phi(\lambda)$ the AQY specific to the photoproduct considered.

2.2.1 CO photoproduction

The photoproduction of carbon monoxide (CO) is the second largest identified product of CDOM photolysis after carbon dioxide (Miller and Zepp 1995; Mopper and Kieber 2000; Stubbins et al. 2006). CO fluxes have been used as a key tracer used to test models of photochemistry, bio-optics, mixing, air-sea exchanges (see Stubbins et al. 2006 and references therein). Recently, several quantum yields and CO photoproduction models have been documented in the literature. These quantum yields are usually described by an exponential or double exponential functions (see Figure 2.2):

1. **Ziolkowski (2000)**:

$$\phi_{CO}(\lambda) = e^{-[9.1341+0.0425(\lambda-290)]} + e^{-[11.3155+0.01425(\lambda-290)]} \tag{2.13}$$

2. **Zafiriou et al. (2003)**:

   - $\lambda \in$ [290-360]

$$\phi_{CO}(\lambda) = 5.78.10^{-6}e^{-0.05(\lambda-360)} - 6.99.10^{-7} \tag{2.14}$$

   - $\lambda \in$ [360-490]

$$\phi_{CO}(\lambda) = 5.24.10^{-6}e^{-0.0229(\lambda-360)} \tag{2.15}$$

   - Broadband formulation

$$\phi_{CO}(\lambda) = 9.18.10^{-6}e^{-0.0353(\lambda-360)} \tag{2.16}$$

The spectral CO production rates estimated from the models of Ziolkowski (2000) and Zafiriou et al. (2003) are integrated through the [280-490nm] domain following the equation 2.12.

3. **Miller et al. (2002)**:

   - Sapelo Islan (Georgia):
   $$\phi_{CO}(\lambda) = e^{-(8.001+0.037(\lambda-290))} \tag{2.17}$$
   - Altamaha River:
   $$\phi_{CO}(\lambda) = e^{-(8.004+0.059(\lambda-290))} \tag{2.18}$$

   The rate of CO photoproduction is integrated over the [280-450nm] spectral domain (equation 2.12).

   Further, Miller et al. (2002) also defined the photoproduct flux which corresponds to the integrated cross product of the net downwelling irradiance just under the surface ($\vec{E}_0(\lambda)$), considered equal to the downwelling irradiance according to Kirk (1994):

$$Flux = \int \vec{E}_0(\lambda).\phi_{CO}(\lambda)d\lambda \tag{2.19}$$

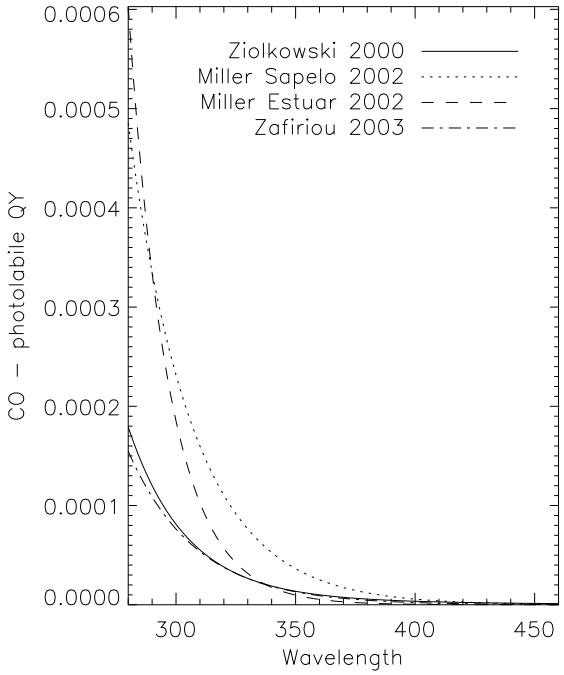

Figure 2.2: AQY for CO photoproduction currently reported in the literature.

2.2.2 DIC photoproduction and labile photoproducts

The photochemical oxidation of CDOM results in the formation of dissolved inorganic carbon (DIC) participating significantly to the global marine carbon cycle (Miller and Zepp 1995). The direct photoproduction of DIC (measured as the sum of CO_2, HCO_3^- and CO_3^{2-}) from CDOM exposure

to solar radiations represents a mineralization pathway independent from the microbial oxidation. Further, CDOM photo-oxidation can lead to the formation of biologically labile photoproducts (BLP) which include a variety of compounds such as ammonium and amino acids and low molecular weight organic compounds (Kieber et al. 1990; Moran and Zepp 1997; Miller et al. 2002).

The quantum yields for the formation of DIC and/or labile photoproducts are currently less characterized than for the CO photoproduction, in particularly for the marine ecosystems (see Figure 2.2):

1. **Vähätalo et al. (2000)**, cf section 2.1 for the whole model description:

$$\phi(\lambda) = 7.52.10^{-0.0122.\lambda} \tag{2.20}$$

2. **Johannessen and Miller (2001)**

   The quantum yield of DIC production (measured as the sum of CO_2, HCO_3^- and CO_3^{-2}) given by Johannessen and Miller (2001) is expressed as:

$$\phi(\lambda) = e^{-(m1+m2.(\lambda-290))} \tag{2.21}$$

   The production rate dP/dt (moles DIC produced $m^{-3}s^{-1}$) in an optical thin solution is then computed as followed:

$$dP/dt = \int_{280}^{480} (E_0(\lambda).a_{CDOM}(\lambda).\phi(\lambda)d\lambda) \tag{2.22}$$

   where $E_0(\lambda)$ is the scalar irradiance (moles photons $m^{-2}s^{-1}nm^{-1}$, $a_{CDOM}(\lambda)$ is the absorption coefficient of CDOM.

   These latter authors proposed parametrisations of the DIC quantum yield for three distinct water mass types distinguished from salinity criteria (Inshore waters: S <31 psu, Coastal waters 31 < S <35 psu, Offshore waters: S > 35 psu):

   - Inshore waters

$$\phi(\lambda) = e^{-(6.66+0.0285.(\lambda-290))} \tag{2.23}$$

   - Coastal waters

$$\phi(\lambda) = e^{-(6.36+0.014.(\lambda-290))} \tag{2.24}$$

   - Open Ocean waters

$$\phi(\lambda) = e^{-(5.53+0.00914.(\lambda-290))} \tag{2.25}$$

3. **Miller et al. (2002)**

   Similarly, Miller et al. (2002) proposed quantum yields for the formation of biologically labile products from CDOM photodegradation in the SE US estuarine waters.

   - Sapelo marsh

$$\phi(\lambda) = e^{-(5.633+0.0298.(\lambda-290)} \tag{2.26}$$

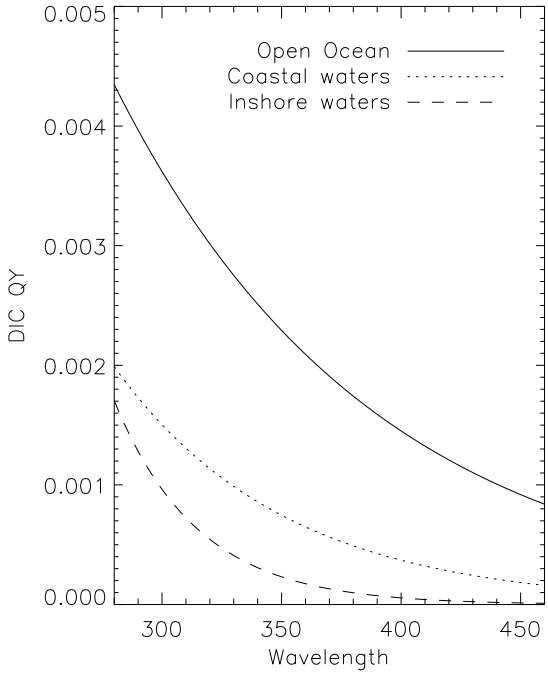

Figure 2.3: AQY for DIC photoproduction according to Johannessen & Miller (2001).

- Estuarine waters

$$\phi(\lambda) = e^{-(5.486+0.0273.(\lambda-290)} \tag{2.27}$$

2.2.3 Illustration of other selected AQYs

In addition to CO and DIC photoproduction, UVR have been shown to have a significant influence on the sulfured molecules such as Dimethyl sulfide (DMS) and carbonyl sulfide (COS) (Zepp and Andreae 1994; Weiss et al. 1995, Toole et al. 2003; Bouillon and Miller 2004). COS is an important gas for stratospheric processes and the oceans are considered as a sizable portion of the source term through photolysis of DOM by UVR. The DMS cycle has received particular attention since the description of potential climate feedbacks (Charlson et al. 1987) and is closely related to photobiological and photochemical processes for both production and removal. Since the quantification of the photolysis of DMS and/or photoproduction of COS rates are not considered in the context of this project, we briefly presented the parametrisations describing these processes in order to illustrate the similarities existing in the shape of these AQYs when compared to those for DIC and/or CO photoproduction (Figure 2.5).

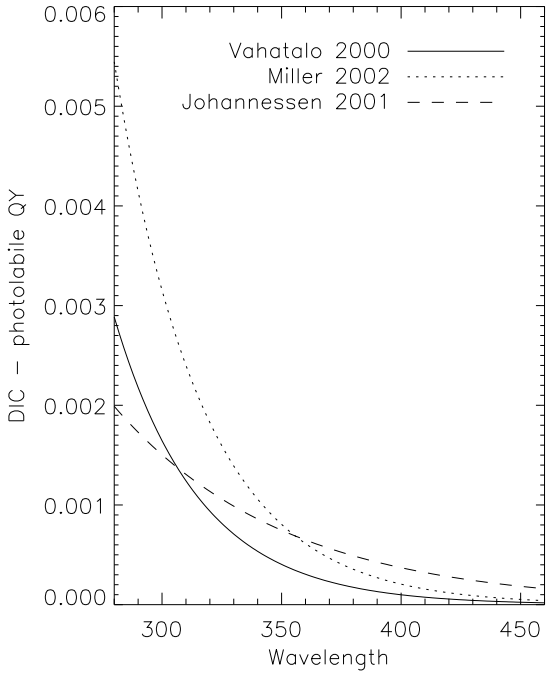

Figure 2.4: AQY for DIC and photolabile products.

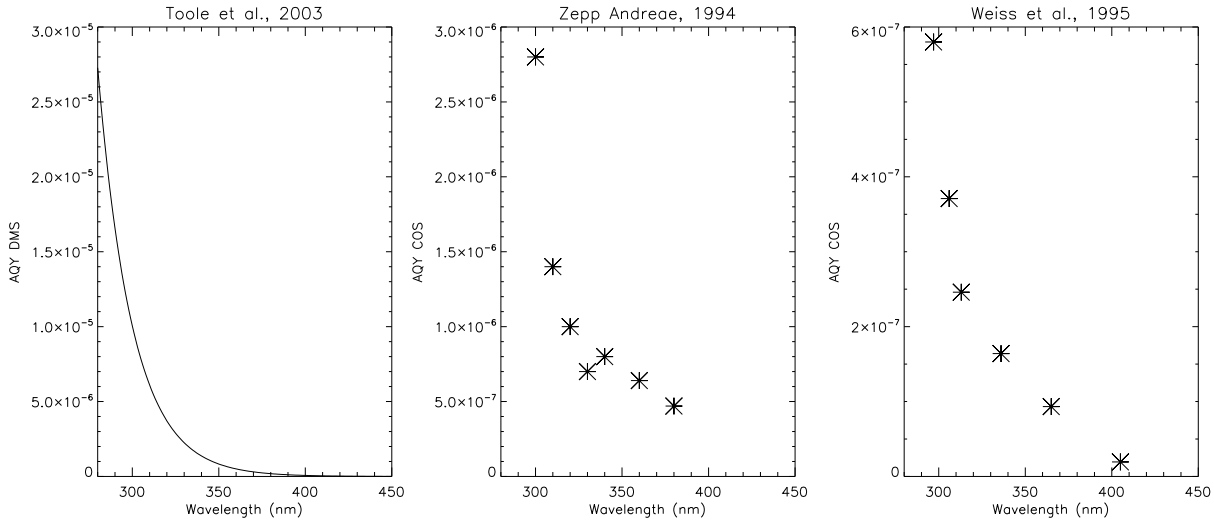

Figure 2.5: AQY for COS photoproduction and DMS photolysis.

Summary

The various AQYs illustrated previously present a strong spectral dependence, with the highest values observed in the UVB region. Conversely, the radiations at the highest wavelength in the near visible region do not have a sufficient energy to induce CDOM photodegradation processes and therefore the AQYs are falling to zero. However, the AQYs reported for a defined photoproduct also exhibit a strong inter-site variability as illustrated, for example, by the parameterizations reported by Johannessen and Miller (2001) for DIC photoproduction. According to these authors, CDOM in the open ocean water is more photosensitive to UV radiations for DIC production than the coastal and inland waters. This result is *a priori* surprising as one might expect that the highly colored terrestrial CDOM in estuarine and coastal waters is less degraded and therefore more sensitive to UVR. However, Johannessen and Miller (2001) attributed the higher efficiency in open waters to the structure of aromatic compounds forming CDOM molecules and more precisely to spatial variations in the proportions of DIC-producing and non-DIC producing chromophores. Indeed, they assumed that the terrestrially derived CDOM contains a high proportion of non-DIC producing chromophores contributing to a great part of CDOM absorbance. From the estuarine and coastal waters to the oceanic systems, the ratio between DIC producing and non-DIC producing chromophores increases due to the loss of aromatic non-DIC producing chromophores by fading and/or in reason of the domination of marine-derived CDOM. However, opposite results have been recently reported by White et al. (2006) and Bélanger et al. (2006) who obtained decreasing rates of DIC photoproduction from estuarine to oceanic ecosystems. Similarly, Zhang et al. (2006) recently documented that terrestrial CDOM is more efficient for photochemically producing CO than marine algae-derived CDOM. This apparent discrepancy between the recent studies underlines the current need of additional parameterizations in order to elucidate the high heterogeneity in the CDOM photolability according to variations in its origin and/or light history. The latter parameter in particular, which implicitly includes the influence of the vertical mixing on CDOM photolability, seems to be crucial for an accurate estimation of the spatio-temporal UV photochemical effects variability (Bélanger et al. 2006; Stubbins et al. 2006; Zhang et al. 2006). In addition, environmental conditions, which might vary spatially and seasonally for a defined site, have also been shown to have a significant influence on the efficiency of UVR for the production of DIC and/or CO. In particularly, a recent study from Zhang et al. (2006) demonstrates that the AQYs for CO production in the St Lawrence estuarine system are strongly affected, in addition to CDOM origin and light history, by the seasonal changes in the water temperature.

Ideally, an accurate modelling of DIC and/or CO photoproduction should take into account all these peculiarities by restraining the application of the AQY to the conditions (temperature, exposure dose) in which it has been determined in the laboratory. However, in practice, this approach is almost not feasible due to the complexity of an accurate determination of CDOM light history in natural environments where numerous timescales have to be considered. It is interesting to note that the global variability in CO AQYs is lower than that documented for the DIC photoproduction rates. Additionally, the fact that CO concentrations and production rates are relatively easy to measure explains that CO photoproduction has been proposed to be used as a proxy for the production of the other compounds resulting from the photodegradation of CDOM such as DIC and/or biologically labile photoproducts (see Stubbins et al. 2006 and references therein).

2.3 Primary production inhibition

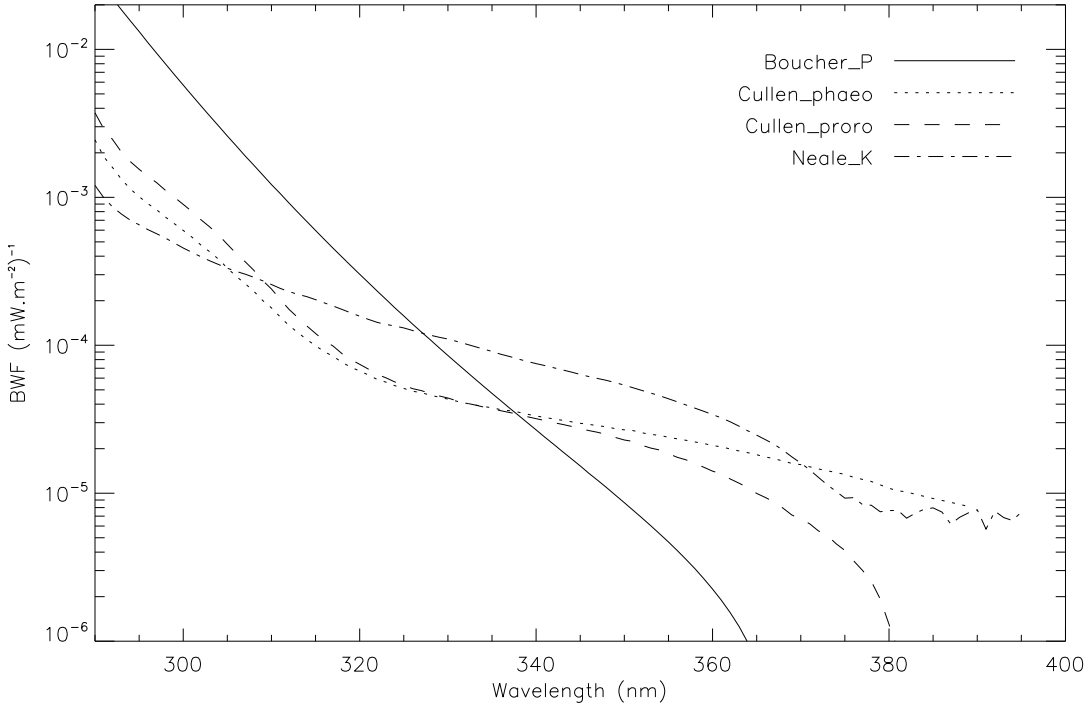

Figure 2.6: Selected Biological Weighting Functions (BWF) for UV inhibition of phytoplankton primary production. These BWFs are for weighted irradiance (E model,$(mW.m^{-2})^{-1}$) estimated for average daily irradiance on a coastal Antarctic assemblage (Boucher and Prezelin, 1996), the UV effect on a diatom (*Phaeodactylum* sp., Cullen et al., 1992) and a dinoflagellate (*Prorocentrum micans*, Cullen et al., 1992) and phytoplankton assemblage from the southern ocean for 1 h of exposure (Neale and Kieber, 2000).

The optimal rate of primary production, i.e. without inhibition processes ($P^B_{opt}(z)$ in $mgC.m^{-3}.h^{-1}$), is classically determined from Production-Irradiance (P-I) curves describing the kinetics of photosynthesis according to light changes. These P-I curves have been parametrised using various formulations:

- Smith (1936):

$$P^B_{opt}(z) = \frac{\Pi(z)}{\sqrt{1+(\Pi(z)/P^B_m)^2}} \tag{2.28}$$

$$\Pi(z) = \int_{400}^{700} \alpha^B(z,\lambda).\mathring{E}(z,\lambda).d\lambda \tag{2.29}$$

$$\alpha^B(z,\lambda) = \alpha^B.a_{ph}(z,\lambda).\int_{400}^{700} d\lambda / \int_{400}^{700} a_{ph}(z,\lambda)d\lambda \tag{2.30}$$

- Jassby and Platt (1976) :

$$P^B_{opt}(z) = P^B_m.tanh(\alpha^B.E(z)/P^B_m) \tag{2.31}$$

- Exponential (Webb et al. 1974 ; Platt et al. 1980):

$$P^B_{opt}(z) = P^B_m.(1 - e^{(-\alpha^B.E(z)/P^B_m)}) \tag{2.32}$$

where, E(z) can correspond to PAR(z) or PUR(z), α^B is the initial slope of the production-irradiance curve and P^B_m the saturation rate of photosynthesis, both normalised by the biomass.

Numerous works on various aquatic systems have shown that the environmental UVR, independently of changes in ozone phenomena, represents an important ecological stress for the organisms populating the surface layer of the oceanic and freshwater ecosystems. This high influence of UVR on marine photosynthesis has recently induced the development of diverse parameterizations describing the dependence of these inhibition phenomena on the UV exposure rate. The relationships, called Biological Weighting Functions (BWF), have been determined experimentally for various phytoplankton species and environmental conditions (Behrenfeld et al. 1993, Cullen et al. 1992; Boucher and Prézelin 1996 ; Neale et al. 1998a; Neale and Kieber 2000; Neale 2000; Banaszak and Neale 2001). In spite of the large variations reported for the weighting functions according to phytoplankton species, region, water mass characteristics or season, BWFs present a conservative shape, with biological weighting decreasing from the UVB to the UVA and visible spectral domain (Figure 2.6). Boucher and Prézelin (1996) reported negative BWFs for irradiance at wavelengths greater than ± 380 nm emphasizing that UVR radiations are not necessarily detrimental for primary production (Williamson et al. 2001; Mengelt and Prézelin 2005) and illustrating the great complexity of the related physiological processes.

In addition to the BWF, the quantitative estimation of the UVR impact on phytoplankton primary production requires the definition of an Exposure-Response Curve (ERC) describing the variation of the UV effect on phytoplankton with exposure (Cullen and Neale 1997a; (Cullen and Neale 1997b). The ERC definition implicitly depends on the balance between damage and repair processes and therefore on the time scale considered. More precisely, to determine the ERC adapted for a defined model, one must define if the measured damage on photosynthesis is function of cumulative exposure of phytoplankton to UVR or whether it is function of instantaneous exposure rate.

Two distinct model formulations can be therefore distinguished:

- $BWF_E P - I$ model

  If repair is active and if the objective is to estimate the steady-state response of photosynthesis during UVR and visible exposure, the adapted approach is to calculate the inhibitory irradiance $E^*_{inh}(z)$ for a depth z corresponding to the sum over a series of narrow wavelength bands ($\Delta\lambda$) of the product between spectral irradiance ($E(\lambda, z)$, in $mWm^{-2}nm^{-1}$) and the BWF($\in (\lambda)$, in $(mWm^{-2})^{-1}$):

$$E^*_{inh}(z) = \sum_{\lambda_{min}}^{\lambda_{max}} \in (\lambda).E(\lambda, z).\Delta(\lambda) \tag{2.33}$$

  The response at a defined depth z is then obtained using an hyperbolic function of this weighted irradiance allowing to correct the optimal rate of photosynthesis ($P^B_{opt}(z)$) for UV inhibition:

$$P^B(z) = P^B_{opt}(z).\left(\frac{1}{1 + E^*_{inh}(z)}\right) \tag{2.34}$$

where P^B_{opt}(z) is the maximum potential rate of photosynthesis in the absence of photoinhibition.

Theoritically, the weighted irradiance for inhibition E^*_{inh} can be determined for UV and PAR radiations since visible radiations can also have an inhibitory effect on primary production (Neale 2000). In practice, the damaging effect of PAR is poorly known and this parameter is represented by a single average weighting coefficient for the whole PAR ($\in (PAR)$), or is not considered.

- BWF_HP-I model

  The previous BWF-PI model is modified if it is assumed that repair processes are not active and if the objective is to estimate the average photosynthetic rate over a period of exposure (Neale et al., 1998b). In this case, the approach is to compute the weight radiant exposure ($H(\lambda)$, $J.m^{-2}nm^{-1}$) used to determine the weighted exposure (H^*_{inh}) for inhibition:

$$H^*_{inh}(z) = \sum_{\lambda_{max}}^{\lambda_{min}} \in_H (\lambda).H(\lambda, z).\Delta(\lambda) \tag{2.35}$$

  where $H(\lambda, z) = \int E0(\lambda, z, t).dt$. Then the average production over the period of cumulative exposure is obtained by:

$$P^B_{avg}(z) = P^B_{opt}(z).\frac{(1 - e^{H^*_{inh}(z)})}{H^*_{inh}} \tag{2.36}$$

  This model is called the $BWF_H - PI$ model because it depends on the parameter H while the previous model is denoted $BWF_E - PI$ model.

The BWF_EP-I and BWF_HP-I models are both useful for the description of inhibition processes occurring in phytoplankton assemblages. However, the development of these models and their application have resulted in the definition of two classes of BWFs which are not directly comparable (Neale et al. 2001). Moreover, the choice of the ERC (Exposure Response Curve) depends on the kinetic of damage-repair processes (Cullen et al. 1992; Neale et al., 1998a; Neale et al., 1998b; Neale 2001). If repair is active and the exposure time is sufficiently long to attain a steady state response of photosynthesis during UV exposure, e.g. as it has been observed in cultures of temperate phytoplankton (Lesser et al. 1994), the appropriated approach is to use the weighted irradiance and describe the response using an hyperbolic function of this irradiance (Eq. 2.3). If the objective is to predict the average inhibited photosynthetic rate over a certain exposure period, the radiant exposure should be used to compute $H^*_{inh}(z)$. The temporal scale considered is therefore critical to justify the use of a H or E model. A model applied to well-mixed waters should consider a model based on the duration of the exposure, since phytoplankton response is function of its cumulative exposure to UVR along its vertical movements and repair rates are considered to be slow. Conversely, a steady state model should be used when recovery rates are rapid and when inhibition is function of irradiance level (reciprocity principle fails).

Chapter 3

UV effects: General characteristics

The following computations performed to quantify the selected UVR photochemical and photobiological effects are based on a synthetic dataset covering various water types (N=42) obtained by combining each of 6 chl$a$ concentrations (0.03, 0.1, 0.3, 1, 3, 10 $mg.m^{-3}$) to each of 7 CDOM concentrations (with CDOM absorption coefficient used as a proxy for CDOM concentration) representative of the average ranges of variation observed on natural marine ecosystems. The bio-optical model is detailed in Vantrepotte and Mélin (2006). Briefly, CDOM absorption is expressed through the relative proportion of the absportion at 440 nm of dissolved material with respect to the absorption of particulate matter ($a_{CDOM}(440)$ /$a_p(440) = \%CDOM$ = 0., 0.15, 0.30, 0.45, 0.60, 0.75, 0.9, see the detailed method in Vantrepotte and Mélin 2006). In a first approximation, vertical profiles of chl$a$ and related dissolved and particulate matter absorptions have been considered to be homogeneous throughout the water column. We considered fixed P-I curve parameters corresponding to those classically reported for the Mediterranean Sea (P_m^B = 4 $mgC\ (mgchla)^{-1}\ h^{-1}$, α^B = 0.099 $mgC\ (mgchla)^{-1}\ h^{-1}(W\ m^{-2})^{-1}$).

The atmosphere characteristics considered for these computations were globally representative of an average European atmosphere under clear sky conditions. Reference calculations were performed with an ozone of 325 DU. Finally, for the sun geometry we considered a latitude of 45^oN and summer soltice conditions (Julian day : 180).

3.1 CDOM photobleaching

We simulated the decrease of CDOM absorption due to photobleaching processes considering the models defined by Osburn et al. (2001) and Del Vecchio and Blough (2002) for a 1 day exposure. In practice, the CDOM absorption coefficient obtained at the time t has been used as an input to the spectral irradiance propagation model at the time t+1.

Figures 3.1, 3.2, 3.3 and 3.4 illustrate the variations of CDOM photobleaching along the spectral and water column vertical dimensions estimated using the two models considered. The estimations provided by these two different models are globally in good agreement especially for surface values. After 1 day of exposure CDOM absorption can be reduced by up to 6% at the surface of the water body. Then, the influence of photobleaching rapidly decreases within the first meters of the water column becoming negligible below $\approx$ 5 to 20 m depth according to the water transparency.

In all cases (Figures 3.3 and 3.4), the relative loss of CDOM absorption is greater at longer wavelengths, despite the lower efficiency of these photons for inducing photobleaching. According to Del Vecchio and Blough (2002) this feature can be related to two factors: (i) the greater amount of longer-wavelength photon penetrating in the water column (ii) the higher rates of indirect absorption loss produced at longer wavelengths by the influence of short wavelength photons absorbed by the

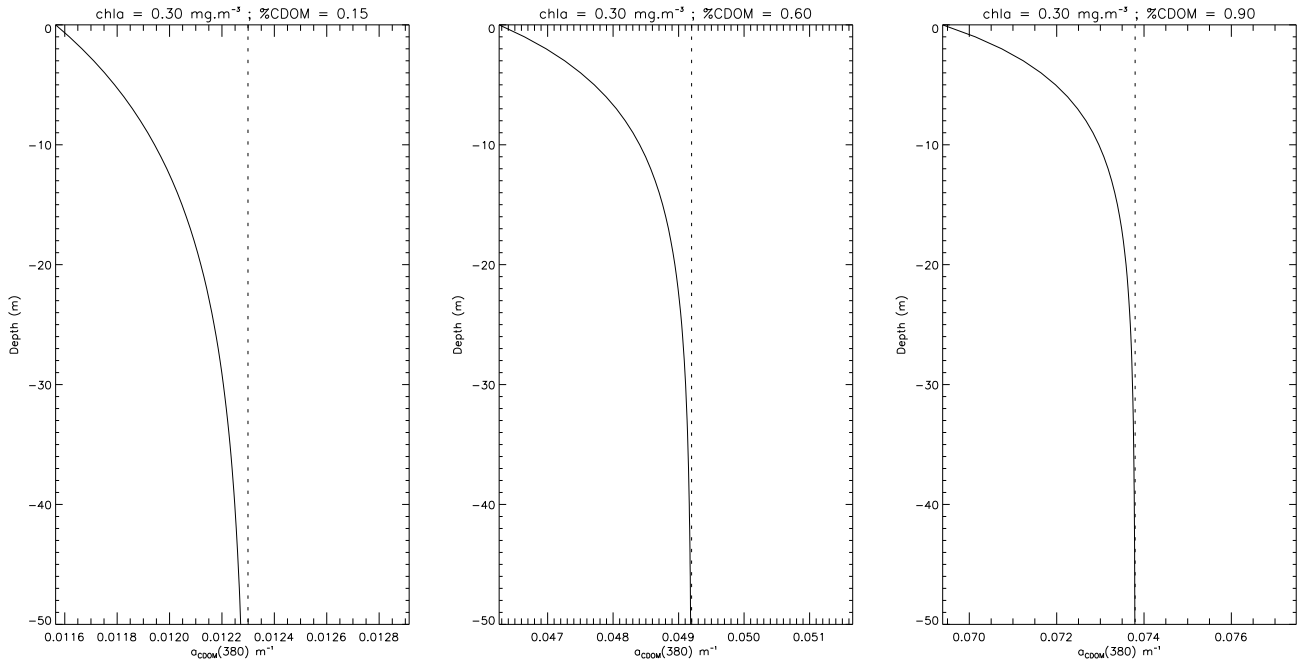

Figure 3.1: Influence of photobleaching on the CDOM absorption vertical profile at 380 nm after 1 day of exposure according to the model by DelVecchio and Blough 2002.

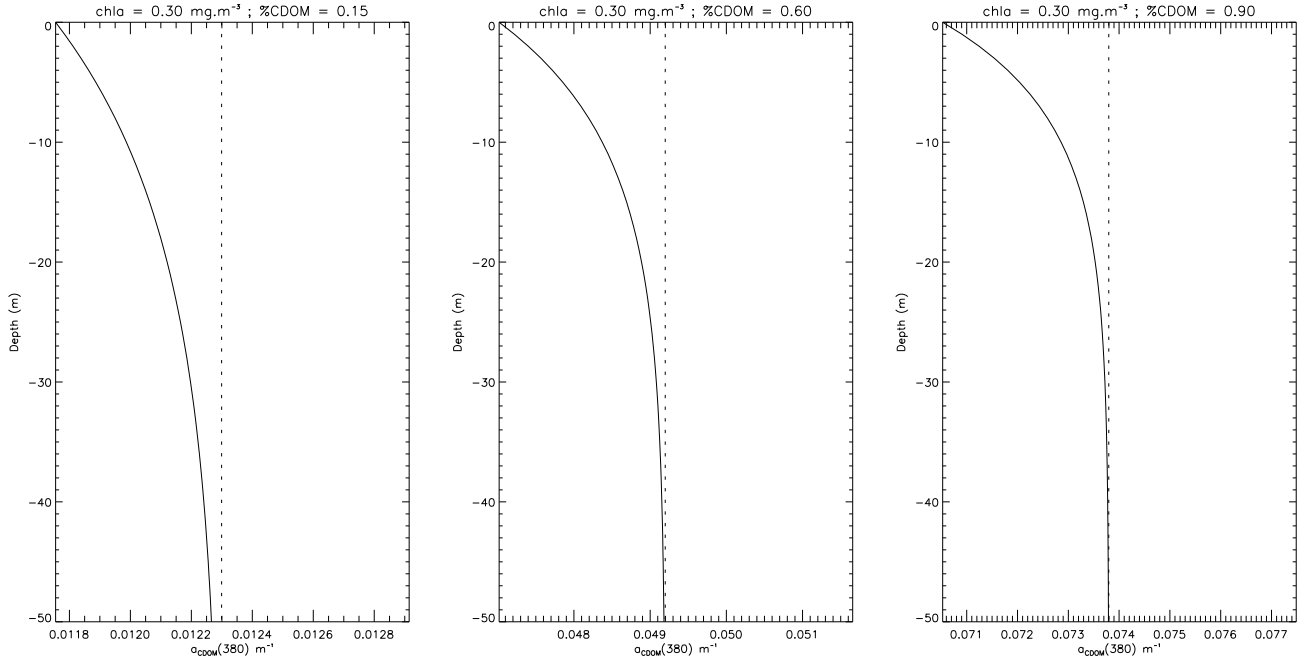

Figure 3.2: Influence of photobleaching on the CDOM absorption vertical profile at 380 nm after 1 day of exposure according to the model by Osburn et al., 2001.

CDOM molecules. Thus, this preferential loss of absorption would lead to an increase in the CDOM spectral slope in agreement with field observations (e.g. Vodacek et al. 1997; Twardowski and Donaghay 2002).

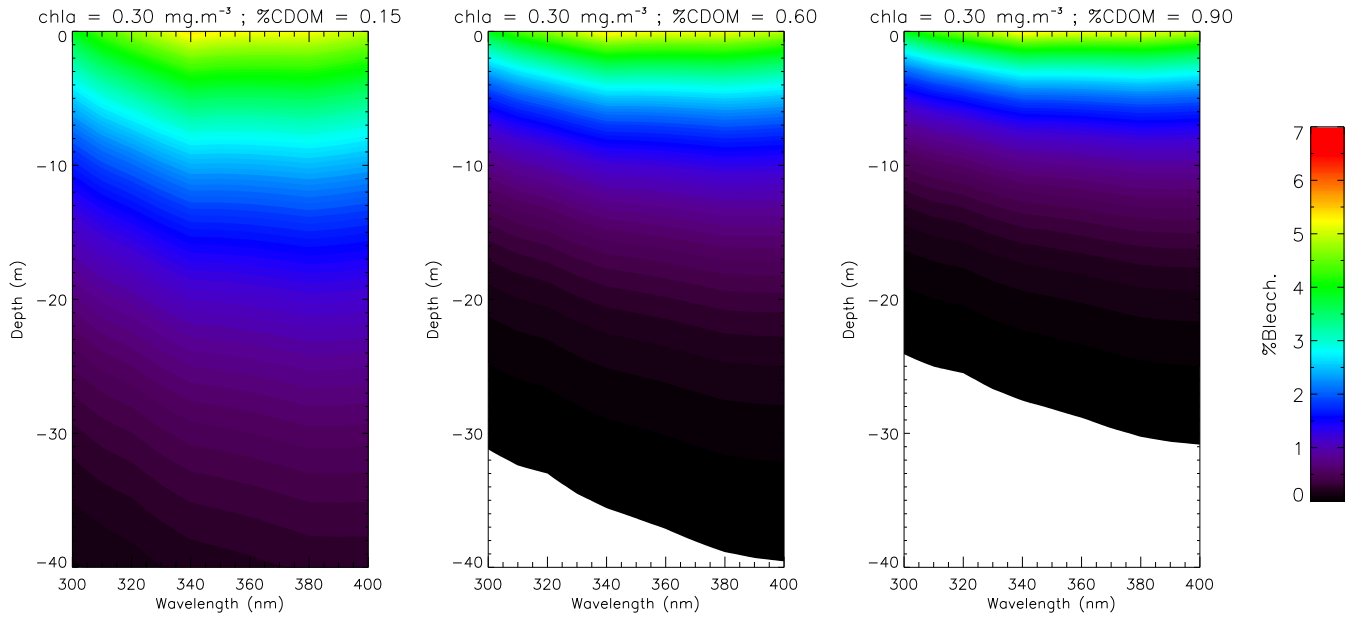

Figure 3.3: Spectral and vertical dependence of the relative rates of CDOM photobleaching after 1 day of exposure according to the model by DelVecchio and Blough 2002.

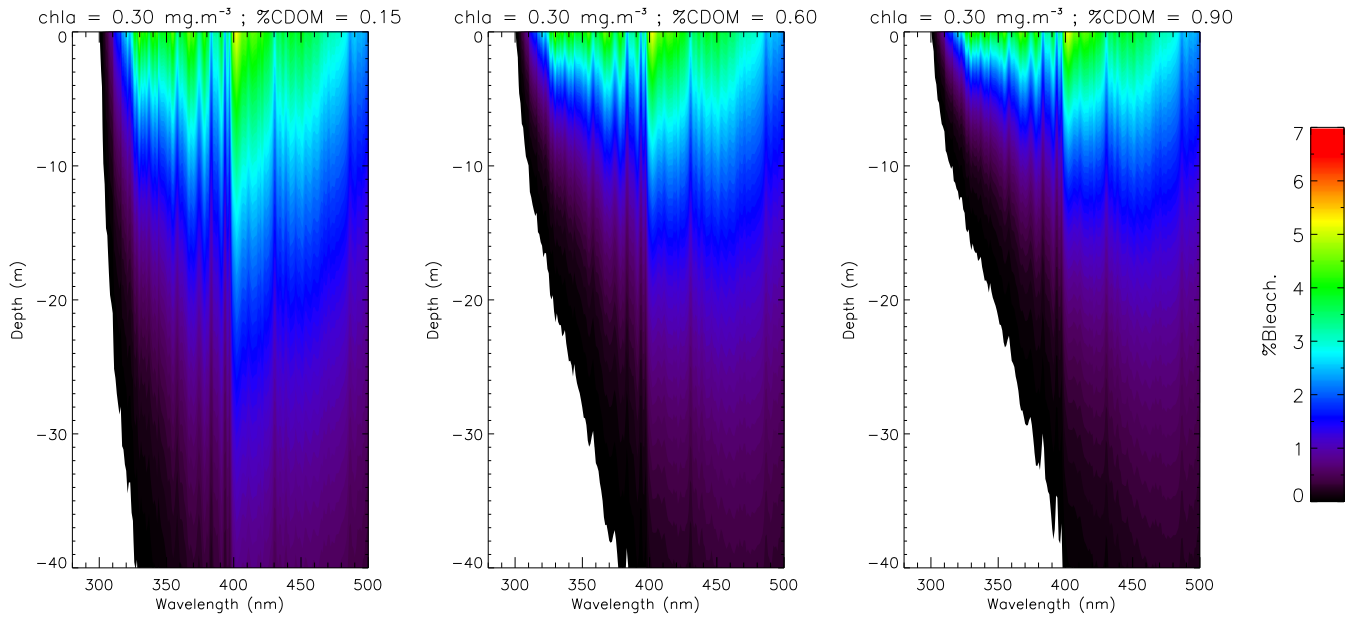

Figure 3.4: Spectral and vertical dependence of the relative rates of CDOM photobleaching after 1 day of exposure according to the model by Osburn et al., 2001.

3.2 DIC-CO photoproduction

Reference	Area	Product	Rate
Granéli et al. (1996)	Swedish Lakes	DIC	50-171 $mgC\,m^{-2}\,d^{-1}$
Johannessen and Miller (2001)	Gulf Stream	DIC	Order of $x.10^{-3}$ $mol\,DIC\,m^{-3}$
White et al. (2006)	NW Atl., Delaware estu.	DIC (CO_2)	Riverine: $\approx 1.4\ \mu mol\,l^{-1}\,h^{-1}$
			Coastal: $\approx$ 0.18-0.75 $\mu mol\,l^{-1}\,h^{-1}$
			Oceanic: $\leq 0.1\ \mu mol\,l^{-1}\,h^{-1}$
Bertilsson and Tranvik (2000)	Swedish Lakes	DIC	0.5-158 $\mu C\,l^{-1}\,h^{-1}$
Miller and Moran (1997)	Sapelo Island	DIC	$0.3 - 2.3 \mu mol\,C\,h^{-1}(vol\ N.D.)$
		CO	$40 - 147 nmol\,C\,h^{-1}(vol\ N.D.)$
Bélanger et al. (2006)	Arctic coast.	DIC	2-3.6 $mgC\,m^{-2}\,d^{-1}$
Miller et al. (2002)	SW US shelf	CO	Surface (graphic) 3.10^{-7} $mol\,l^{-1}\,d^{-1}$
		Labile Photop.	Surface (graphic) 4.10^{-6} $mol\,l^{-1}\,d^{-1}$
Fichot (2004)	Surface (graphic)	CO	Oligo: $0.05.10^{-4}\,mol\,CO\,m^{-3}\,d^{-1}$
			Estuarine : $1.10^{-4} mol\,CO\,m^{-3}\,d^{-1}$
			1-6 $10^{-5} mol\,CO\,m^{-2}\,d^{-1}$

Table 3.1: Examples of some referenced CO and DIC production rates for various sites and aquatic ecosystems.

After several decades of research into CO (and/or DIC) production in various aquatic ecosystems (Table 3.1), it is now widely recognized that CDOM photomineralisation processes play an important role for the global marine carbon cycle. However, the actual amount of carbon actually represented by the total photochemical sources of CO and DIC at the global ocean scale is still poorly constrained and remains an open field of study. Indeed, estimates of global oceanic CO photoproduction vary between 30 and 820 $TgCO - C.yr^{-1}$ (see the review by Stubbins et al. 2006). The most recent estimates suggest however that the earlier work may have largely overestimated the actual oceanic CO photoproduction which should rather fall into the narrow range of 30-50 $TgCO - C.yr^{-1}$ (Zafiriou et al. 2003; Fichot 2004; Stubbins et al. 2006). Similarly, estimates for the global oceanic flux of photoproduced DIC range from 2.7 $PgC.yr^{-1}$ (Mopper and Kieber 2000) to $\approx$ 12 $PgC.yr^{-1}$ (Kudela 2000).

Note that these quantifications are usually based on spatial extrapolations considering the product of local estimations of the water column photoproduction rates by the surface of the whole ocean. To date only few studies are related to the quantification of DIC and/or CO annual photoproduction at global or basin scales using satellite remote sensing techniques (Fichot 2004; Bélanger et al. 2006).

The relative importance of UVB, UVA and PAR domain for the photodegradation of CDOM reflects the combination between photon effectiveness and the amount of photons penetrating within the water column. As a matter of fact, the DIC photoproduction rate seems to be negligible below 300 nm, even in the clearest water bodies (Figure 3.5) in spite of the high efficiency of the shortest radiations for inducing a photodegradation of CDOM.

Photodegradation processes can be mainly attributed to photons in the UVA domain (Figures 3.6 and 3.7, Table 3.2). Note that the strong contribution of UVA radiations is slightly sensitive to changes in the dissolved and particulate material loads as underlined by the relatively low variations around average values in Table 3.2. The relative proportion of the DIC and CO photoproduction which can be attributed to UVB and PAR radiations presents large variations according to the AQYs definition, reflecting the diversity existing in AQYs shape and spectral ranges of application. The relative importance of UVB radiations remains relatively low and varies between 3-32 % according to the different AQYs models reflecting the high attenuation of UVB radiations both within the atmosphere and through the water column.

	UVB	UVA	PAR
Johannessen Ocean	4.80 (0.69)	56.64 (3.19)	38.56 (3.73)
Johannessen Coastal	2.97 (0.48)	46.76 (3.54)	50.27 (3.93)
Johannessen Inshore	7.05 (0.88)	67.40 (2.31)	25.55 (2.99)
Miller labile	14.57 (1.29)	75.38 (0.91)	10.05 (1.49)
Miller labile river	13.24 (1.24)	74.92 (1.03)	11.84 (1.71)
Vähätalo	13.65 (1.26)	75.10 (0.99)	11.25 (1.64)
Ziokolowski CO	15.40 (1.44)	69.12 (1.38)	15.48 (2.22)
Zafiriou CO	17.50 (1.40)	74.88 (0.89)	7.62 (1.17)
Miller CO	18.61 (1.43)	75.28 (0.90)	6.11 (0.96)
Miller CO river	31.70 (1.63)	67.18 (1.48)	1.12 (0.20)

Table 3.2: Means and standard deviations of the relative contribution (in %) of UVB, UVA and PAR domain to the daily DIC production.

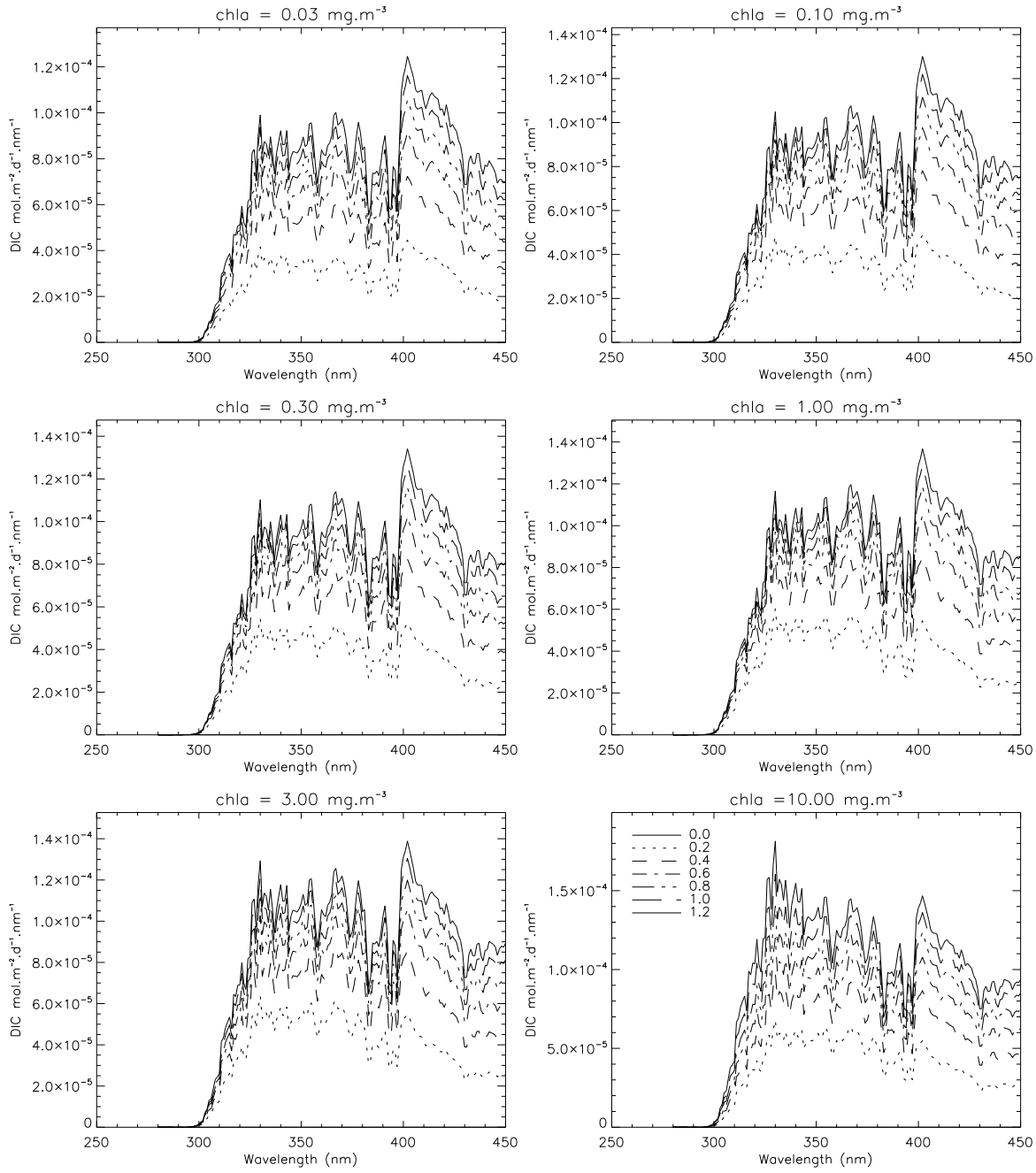

Figure 3.5: Spectral dependence of daily DIC production for different loads of phytoplankton biomass and CDOM proportions.

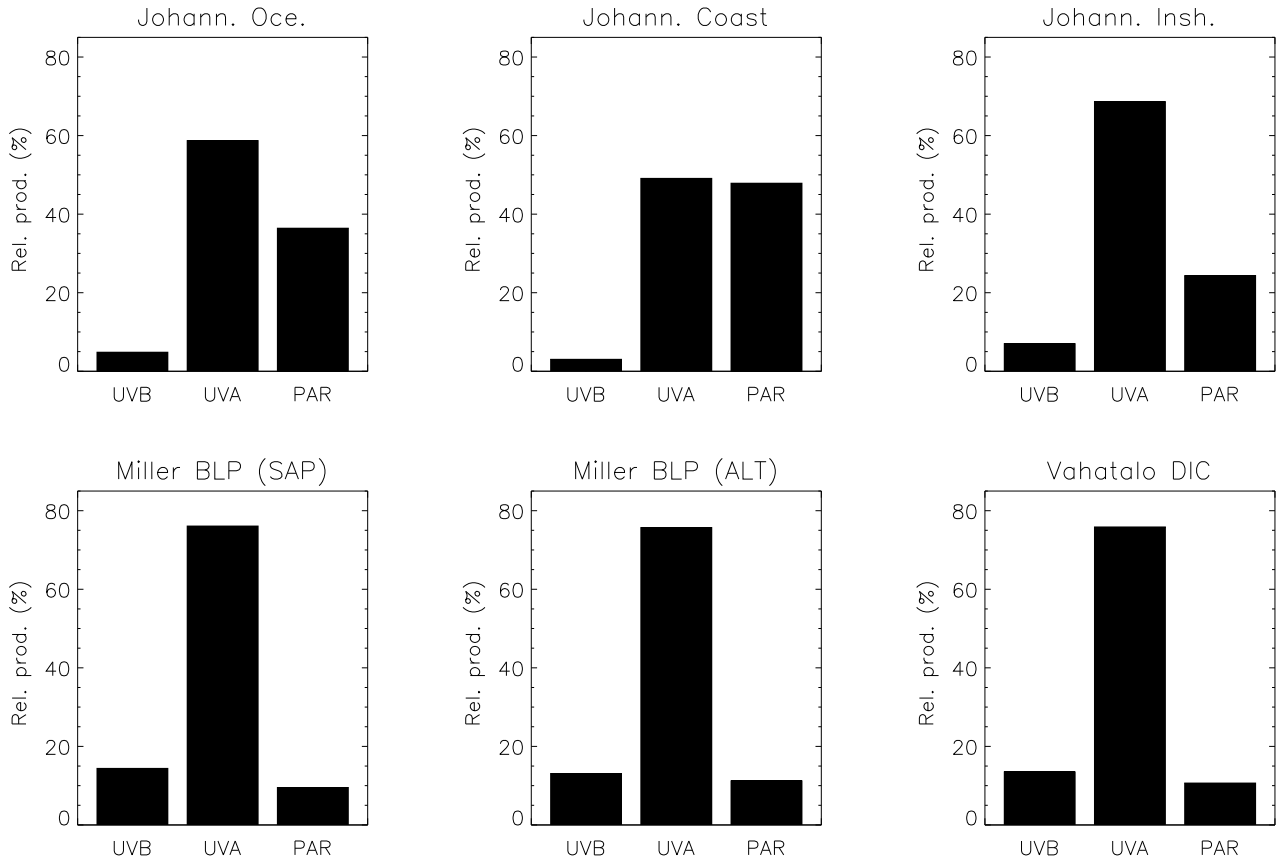

Figure 3.6: Relative contribution of UVB, UVA and PAR domains to the DIC photoproduction (average values on the 42 water types of the synthetic dataset).

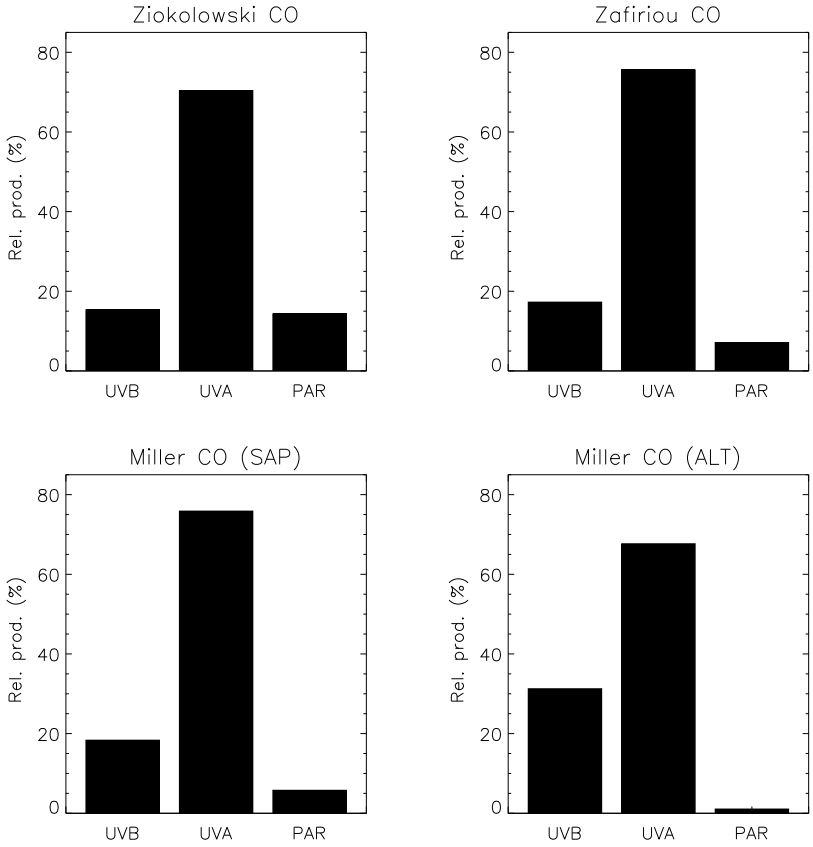

Figure 3.7: Relative contribution of UVB, UVA and PAR domains to the CO photoproduction (average values on the 42 water types of the synthetic dataset).

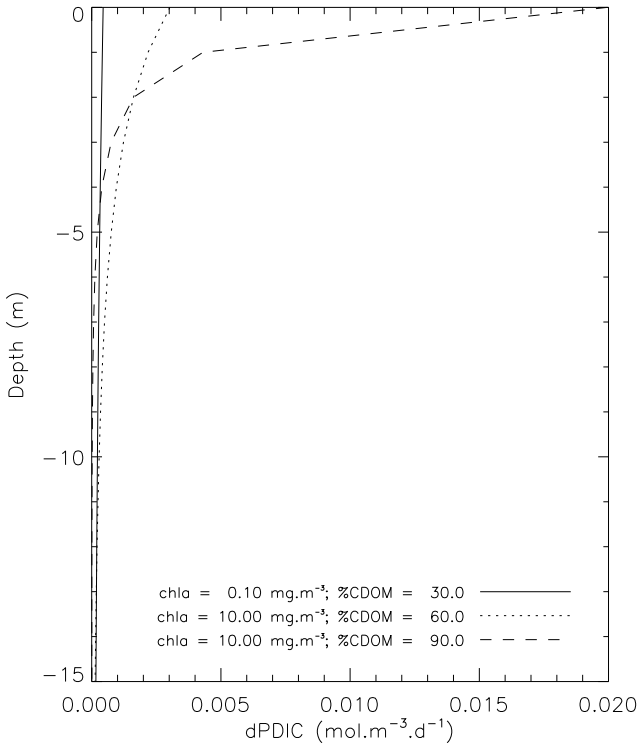

Figure 3.8: Example of daily DIC profiles for different water types obtained from Johannessen and Miller (2001) Open-ocean AQY model.

DIC production rates rapidly decrease from the surface to the deep waters (Figure 3.8) following a quasi exponential shape. In the context of a depth-resolved modelling of UV photochemical effects, it is interesting to evaluate the layer of the water column in which the major part of the DIC production is performed. For this purpose, the $Z(90\%)DIC$ depth, representing the depth range in which 90 % of the total depth-integrated DIC photoproduction occurs, is defined by (Fichot, 2004):

$$\int_0^{Z(90\%)DIC} PDIC(z)dz = 0.90PDIC_t \tag{3.1}$$

The Figure 3.9 represents the variations of the $Z(90\%)DIC$ depth according to changes in chl$a$ and CDOM loads. $Z(90\%)DIC$ values can range from several tens (up to 80 m) for the clearest (oligotrophic) waters to few meters only (< 5 m) for the more turbid ones.

This feature reflects obviously changes in the water transparency as described by the significant relationships found between $Z(90\%)DIC$ and UVA, UVB or PAR 1% penetration depths (Figure 3.10, Table 3.3).

Furthermore, changes in the underwater light field quality with depth (Vantrepotte and Mélin 2006) induce vertical variations in the relative importance of each spectral domain to the total DIC production throughout the water column. As a matter of fact, the relative contribution of UVB radiations to the DIC production quickly decays in the first meters of the water column due to the very low penetration of the short wavelength radiations in the water body. Conversely, the PAR contribution increases from the surface to the deep waters (Figure 3.11) as UVA contribution decreases even though this spectral domain remains the main contributor for the photodegradation of

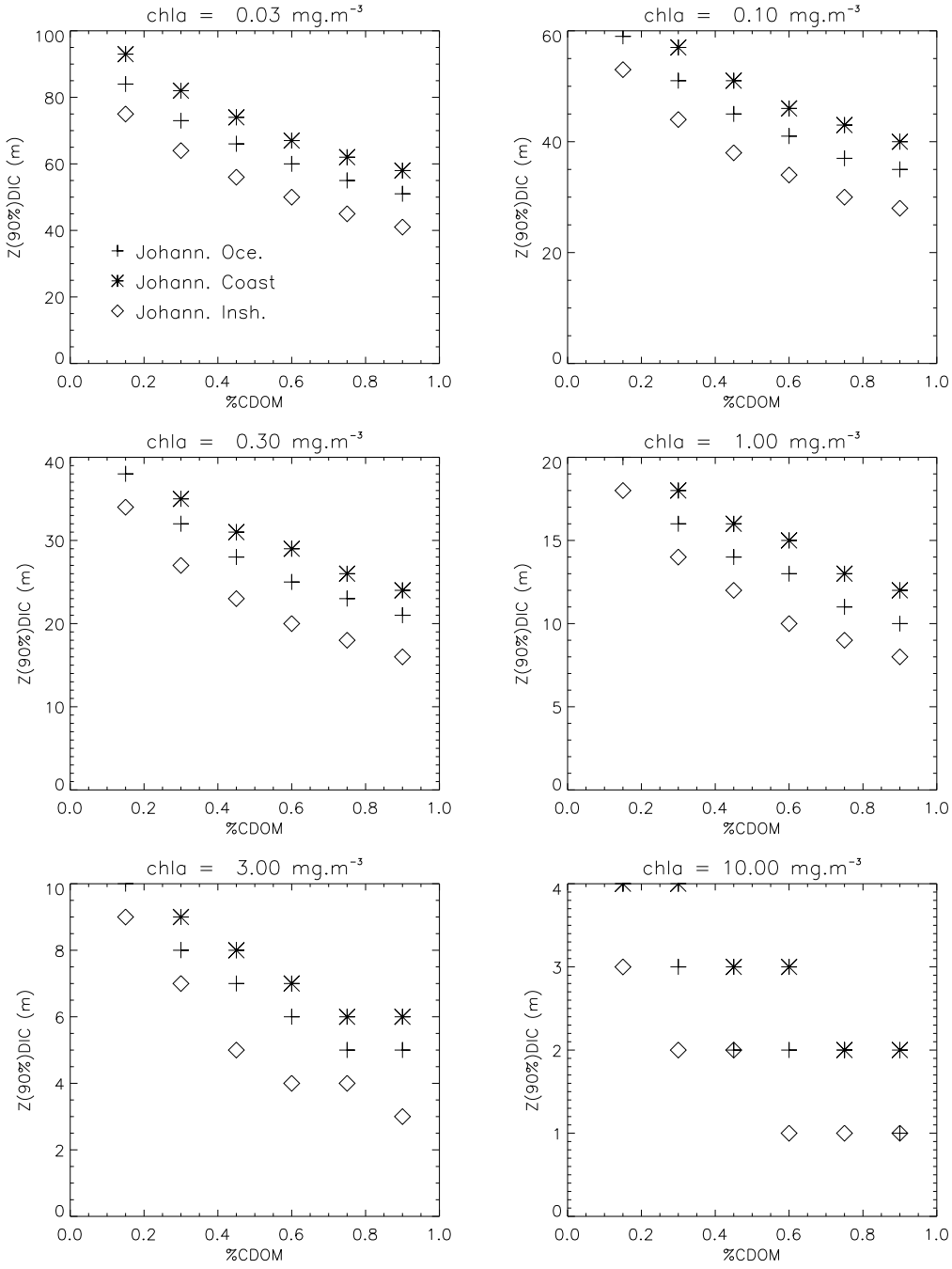

Figure 3.9: $Z(90\%)DIC$ depth which corresponds to the depth at which the vertically integrated DIC production is equal to 90% of the water column integrated value.

CDOM within the surface productive layer, independently of the water mass characteristics (Figure 3.11).

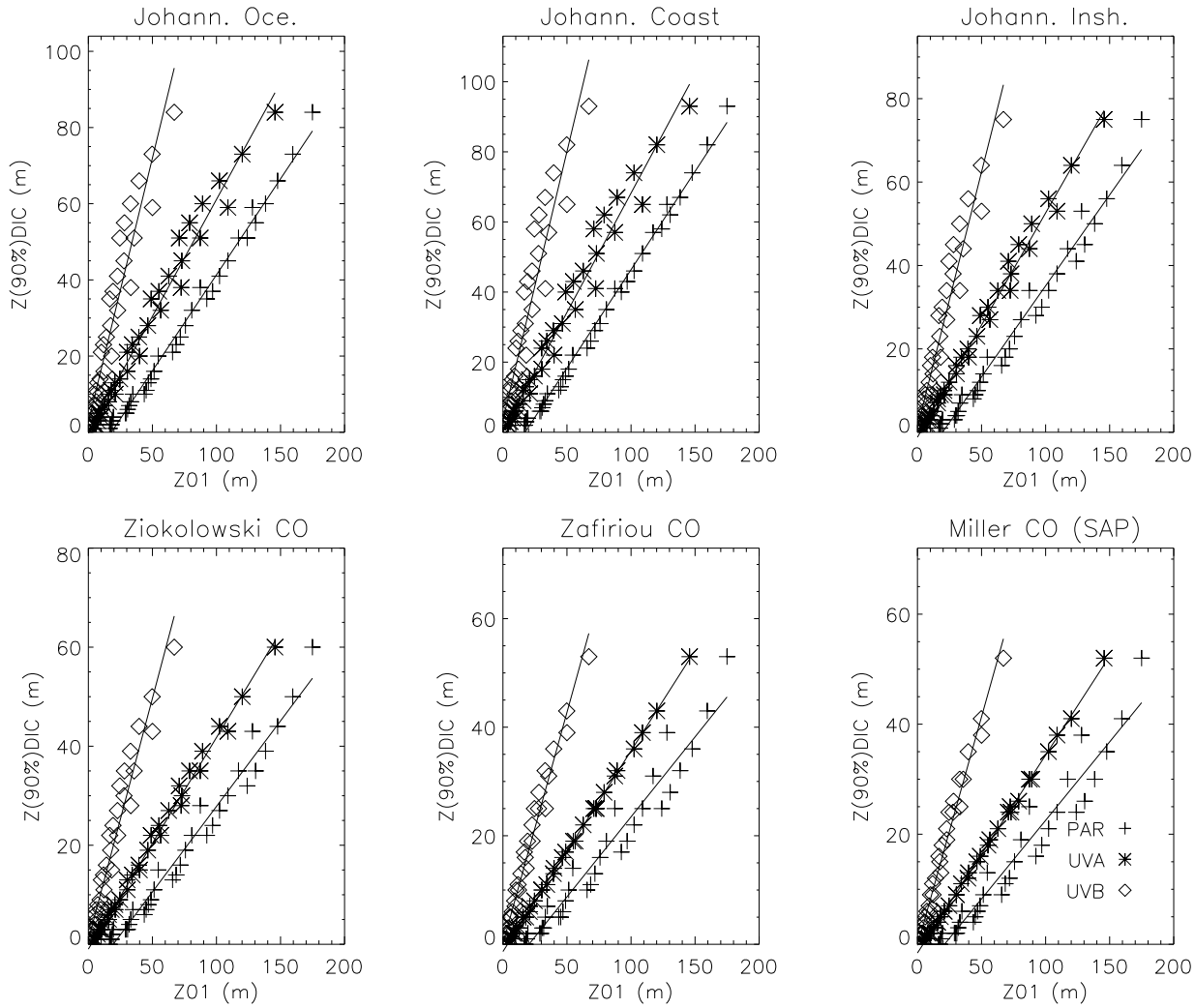

Figure 3.10: Relationships between the 90% depth for DIC production and UVB, UVA and PAR penetration. The equation corresponding to the linear regression illustrated by the solid lines are reported in the Table 3.3.

	UVB			UVA			PAR		
	A	B	R^2	A	B	R^2	A	B	R^2
Johannessen Ocean	2.66	1.39	0.96	-0.26	0.61	0.99	-9.05	0.50	1.00
Johannessen Coastal	3.51	1.53	0.96	0.20	0.68	0.99	-9.70	0.56	1.00
Johannessen Inshore	1.19	1.22	0.97	-1.20	0.54	1.00	-8.53	0.44	0.99
Ziokolowski CO	0.89	0.98	0.98	-0.97	0.43	1.00	-6.71	0.35	0.99
Zafiriou CO	0.13	0.85	0.99	-1.33	0.37	1.00	-5.99	0.29	0.98
Miller CO	-0.19	0.83	0.99	-1.58	0.36	1.00	-6.03	0.29	0.97

Table 3.3: Linear regression parameters for the relationships between $Z(90\%)DIC$ and the 1 % UVB, UVA and PAR penetration depths: $Z(90\%)DIC$ = A +B. Z10(UVB, UVA, PAR), (N=42).

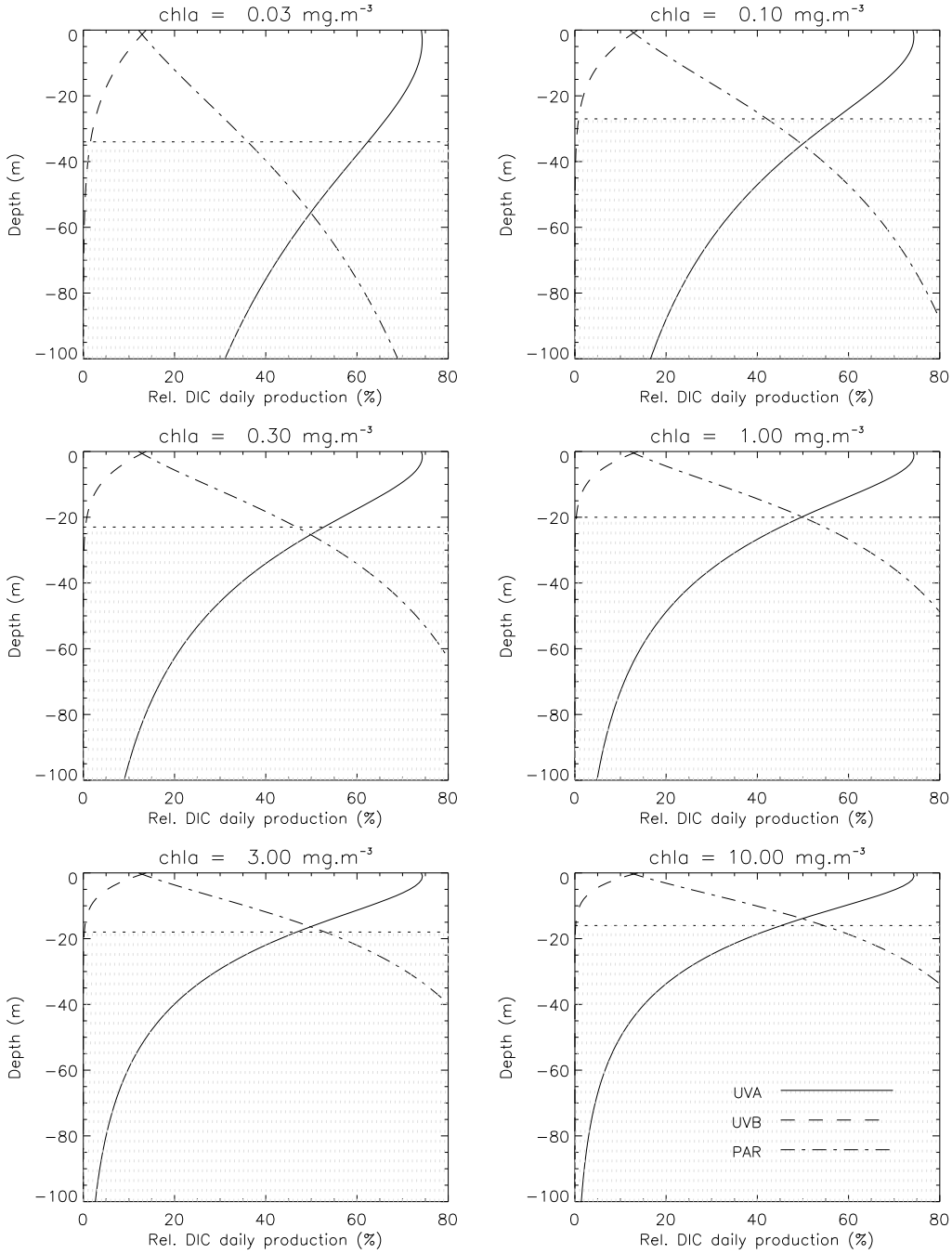

Figure 3.11: Vertical profiles of the relative contribution of UVB, UVA and PAR radiations to the total DIC production. The shaded area correspond to the area where the verticaly integrated production is < to 90 % of the total production of the water column.

3.3 UV inhibition of primary production

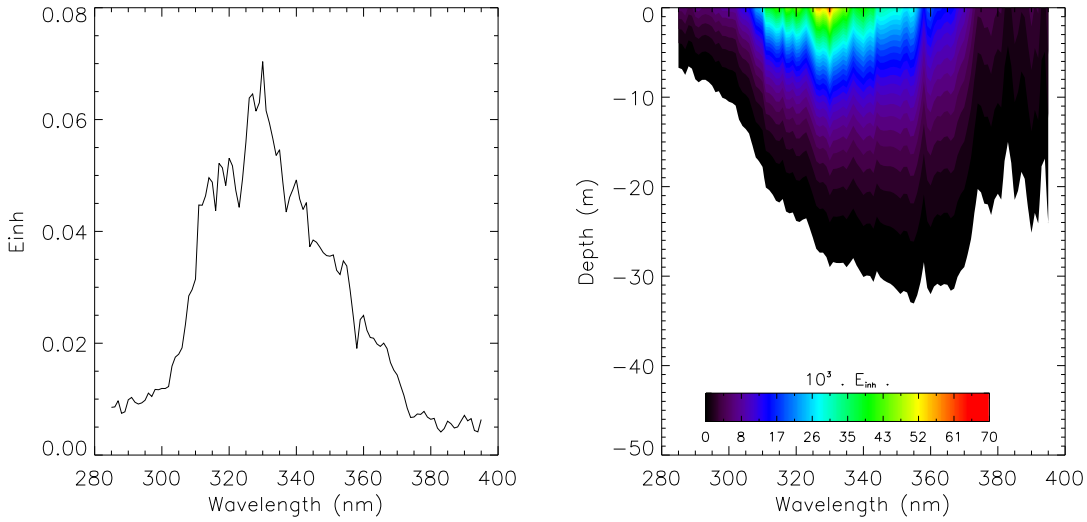

Figure 3.12: Example of E_{inh} spectrum in surface (left side) and along the water column (right side)

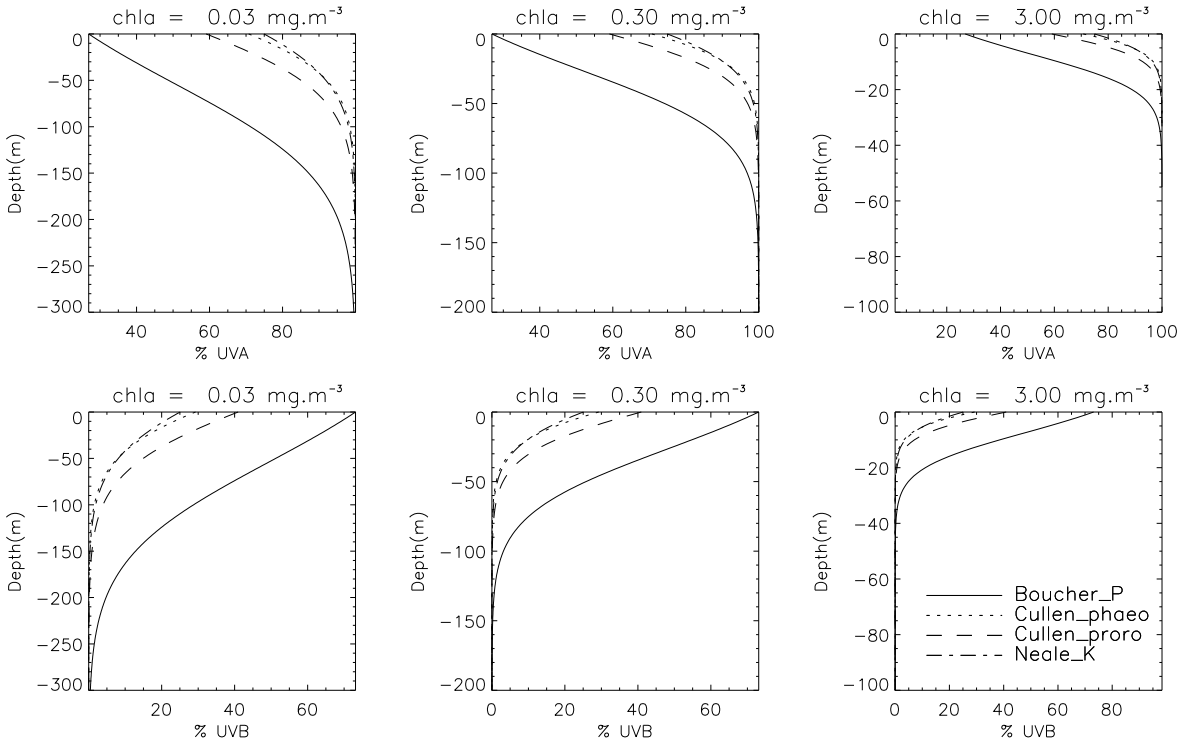

Figure 3.13: Vertical distribution of the relative contribution of UVB and UVA radiations to the E_{inh} inhibition parameter of primary production for the several BWFs models at noon.

The Figure 3.12 presents an example of the spectral distribution of the weighted irradiance E_{inh} illustrating the combined effect of the irradiance spectral quality at a defined depth and biological weightings (see section 2.3). In this example, the most inhibiting effects in surface are related to

the UV radiations located around 330 nm while the values of E_{inh} are negligible for the shortest wavelengths in the UVB as well as in the near visible region. However, this pattern varies along the vertical scale. Indeed, there is a small shift of the most efficient radiations from the wavelengths around 330 nm to those around 360 nm from the surface to the bottom of the water column respectively (Figure 3.12). The same pattern is clearly illustrated by Figure 3.13 with a net increase of the relative contribution of UVA for E_{inh} (and a reciprocal decrease of UVB impact) with depth. This spectral dependence of UV inhibiting effects varies according to the BWFs definition as illustrated by the greater weight given to UVA radiations when considering the Boucher and Prézelin (1996)'s formulation.

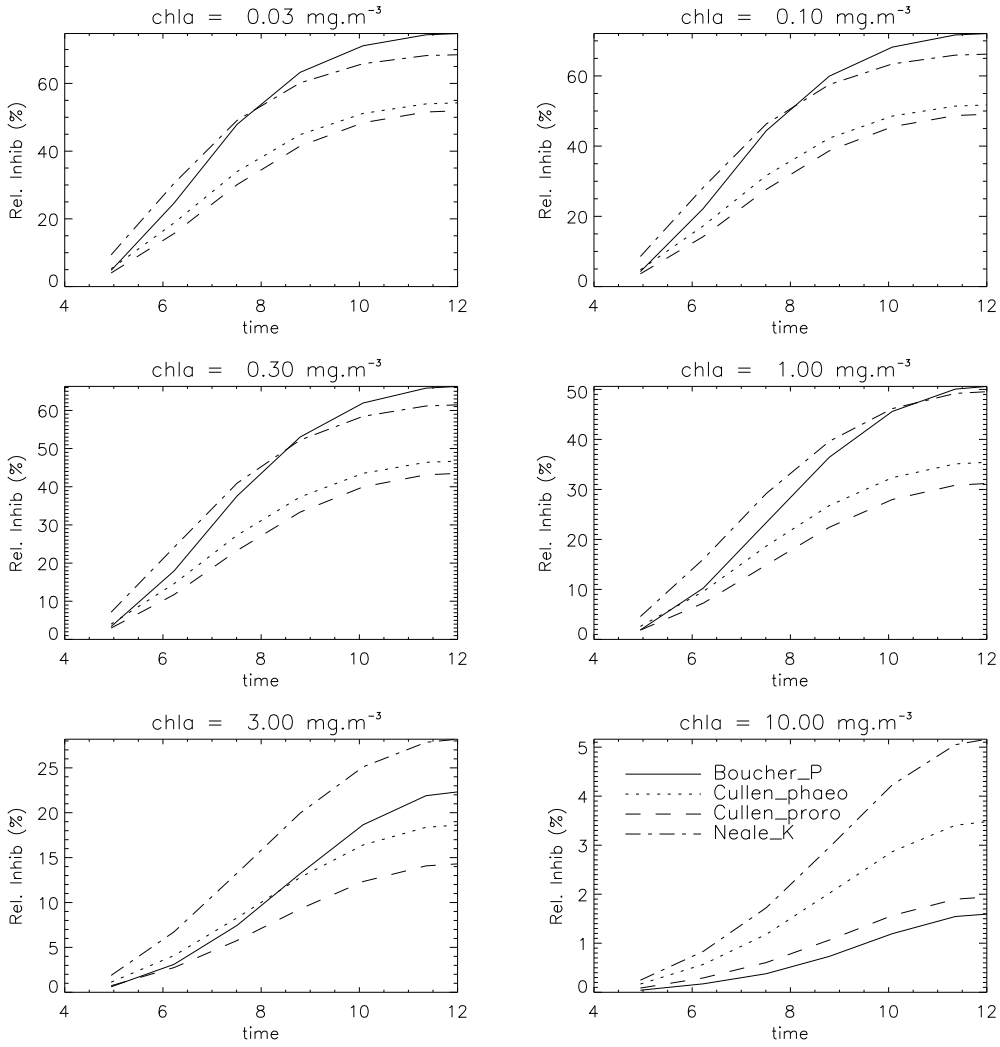

Figure 3.14: Time course of primary production inhibition at 5 m depth for different chl$a$ concentration and for the various BWFs.

Figure 3.14 presents some examples of the time course of UV inhibition of primary production during the day at 5m depth. In the clearest waters, the inhibition induced by the exposure of phytoplankton to UVR can lead to a decrease of up to 60 % of the initial primary production rates at noon. Conversely, the exposure of phytoplankton to UVR in the more turbid waters has a more restricted impact on the photosynthetic process since the relative inhibition rates of primary production account for less than 10 % at noon.

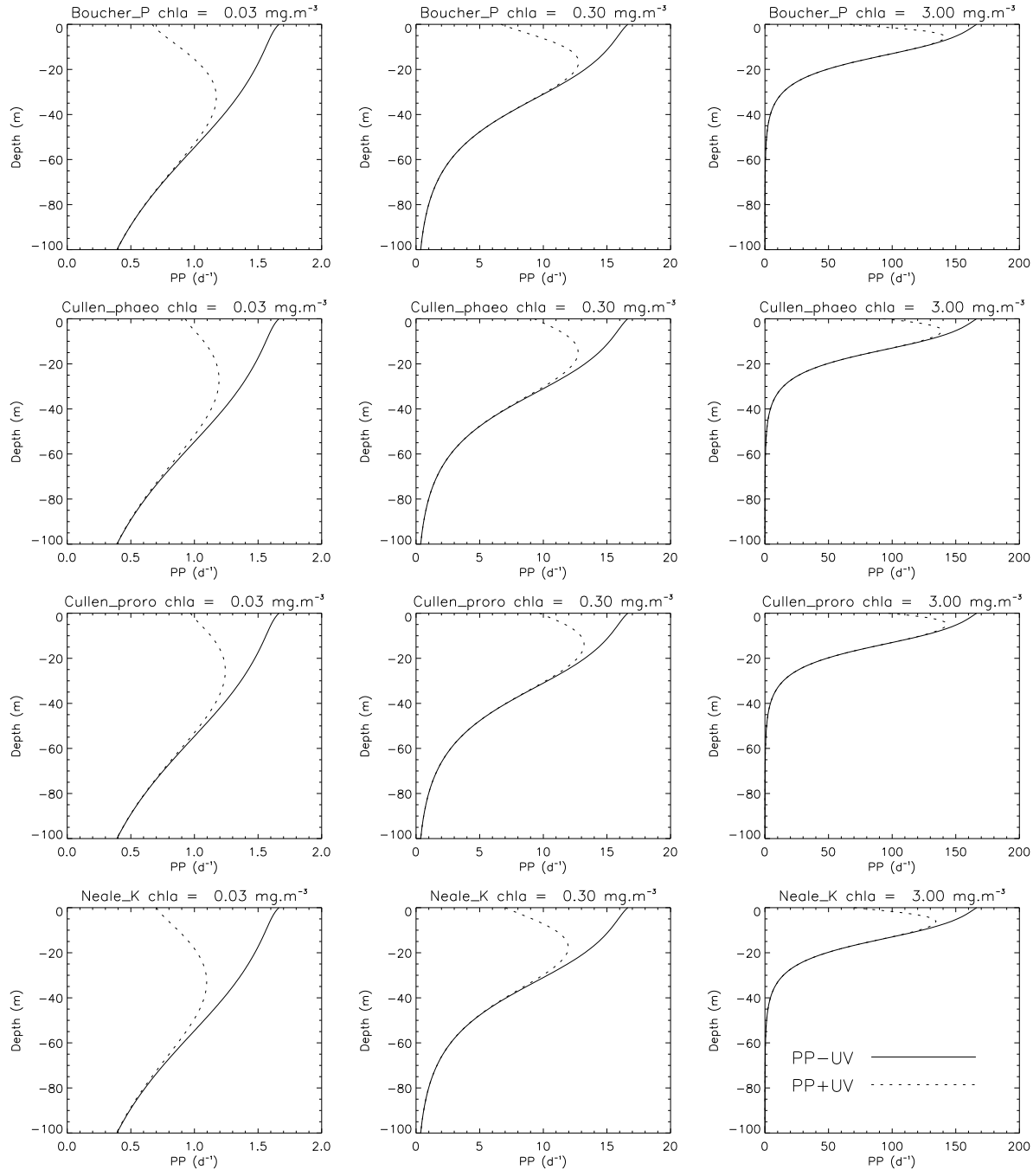

Figure 3.15: Daily primary production vertical profiles with and without UV inhibition for various chl*a* levels and BWFs (%CDOM =45).

On the daily scale, the phytoplankton exposure to UVR can induce a decrease in the uninhibited production (PP-UV) by $\approx 5\%$ to 30 % from the more turbid to the clearest ecosystems (Figure 3.17). Similar relative inhibition rates are usually reported in the literature from *in situ* laboratory and/or modelling studies (Furgal and Smith 1997; Neale et al. 1998a; Neale et al. 1998b; Neale et al. 2001). These results provide the evidence of the importance of the integration of an UV-dependent inhibition term for the study of marine global carbon cycling.

UV inhibition processes obviously modify the shape of the vertical profiles of primary production.

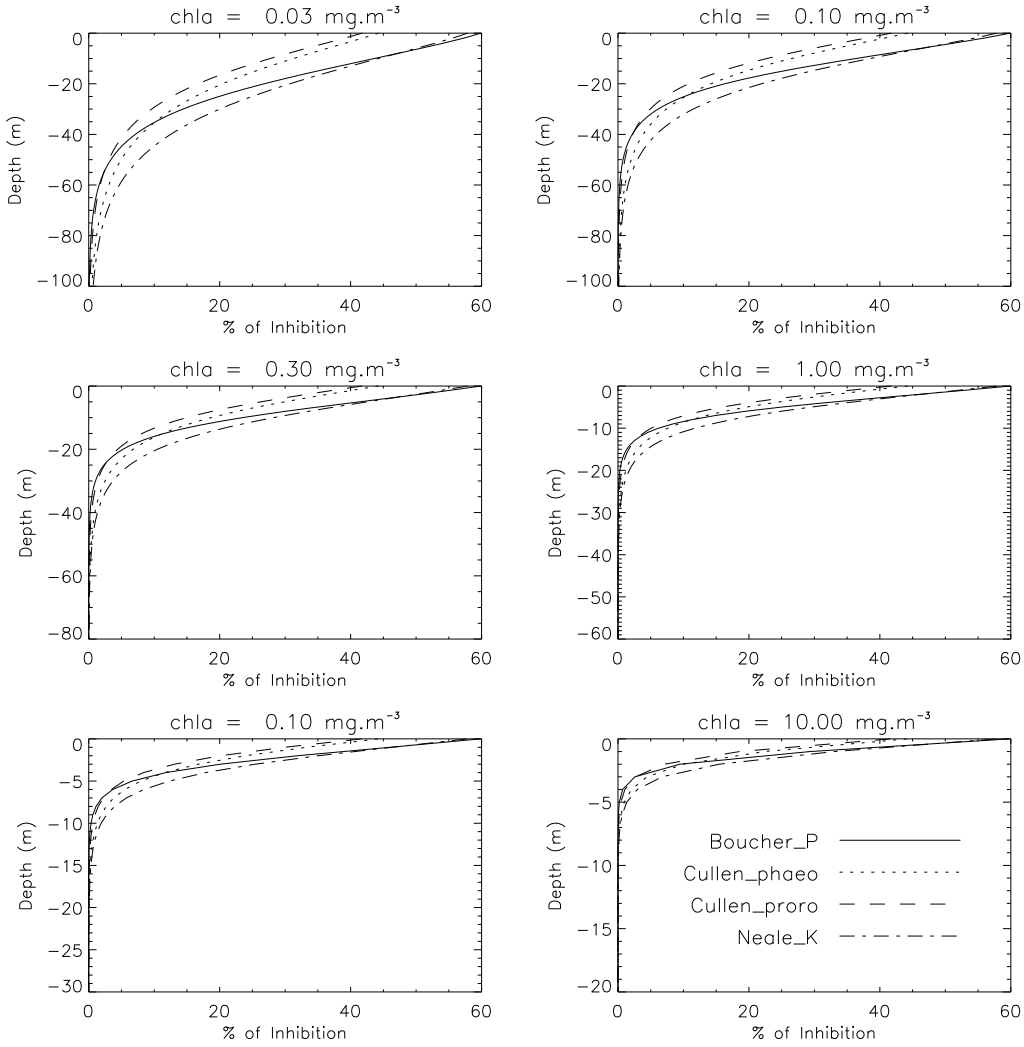

Figure 3.16: Daily profile of UV inhibition of primary production (%) (%CDOM =45).

Indeed, the consideration of the influence of the exposure of phytoplankton to UVR leads to a sharp decrease of the water column production level in the first meters of the water column (Figure 3.15). At the surface of the water column, UV inhibition can for instance induce a decrease of up to 60 % of the optimal carbon fixation rates. Then, the relative inhibition rate of primary production (PP+UV-PP-UV)/PP-UV.100) decreases exponentially with depth (Figure 3.16).

The vertical extent of UV primary production inhibition processes can be characterised by the definition of the ZPP50% depth corresponding to the depth at which the primary production is reduced to half of its uninhibited value. Variations in the ZPP50% are related to the water transparency for UVR with values ranging from up to 15 m to less than 2 m (Figure 3.18). In the more turbid water bodies, the ZPP50% depth is not reached since the penetration of UVR is not sufficient enough to induce a large inhibition of phytoplankton primary production.

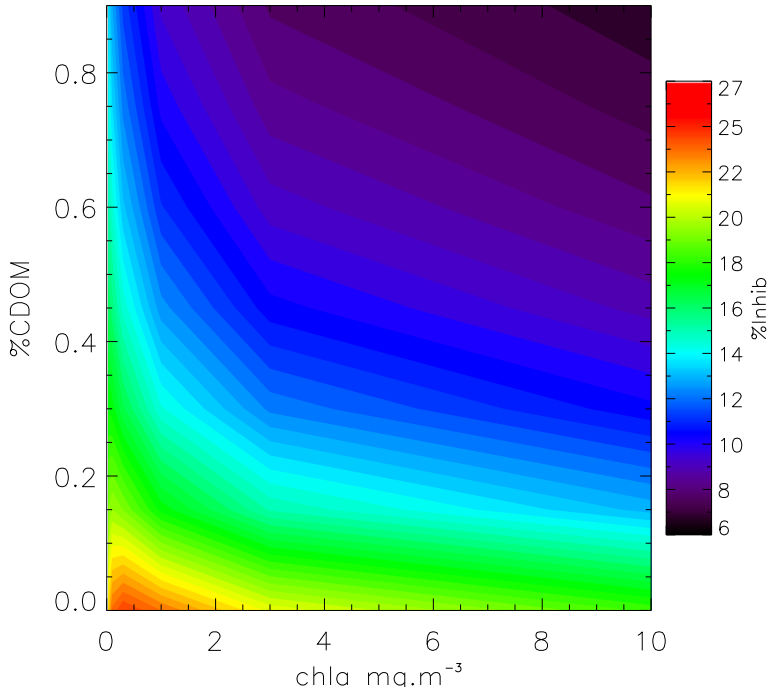

Figure 3.17: Daily water column inhibition variations according variations in chl*a* and CDOM loads.

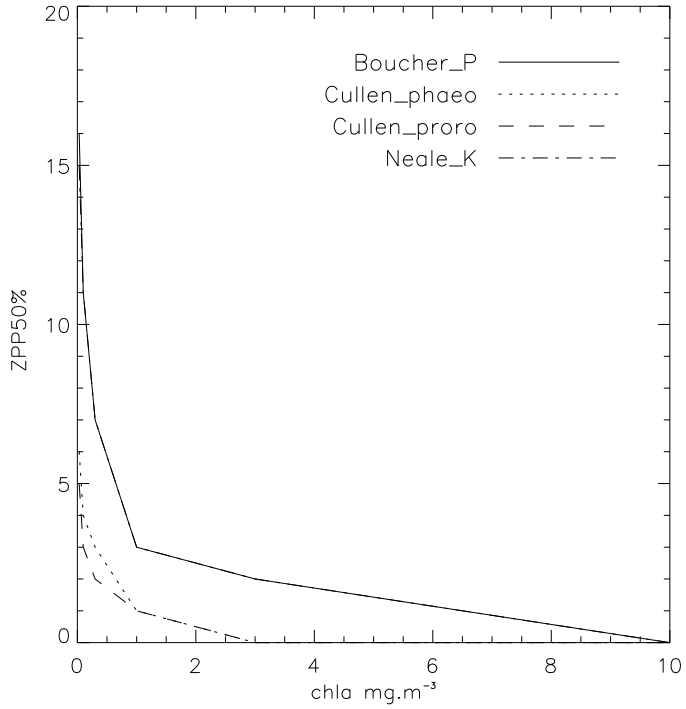

Figure 3.18: Depth corresponding to a level of UVR inhibition of primary production of 50% at noon (%CDOM =45).

Chapter 4

Sensitivity analyses

4.1 Influence of the AQY definition on UV DIC and CO photoproduction rates

The impact of the AQYs definition on DIC and CO daily and vertically integrated photoproduction rates has been quantified by considering the various AQYs formulations reported in the section 2.2.

- DIC photoproduction rates

Col./Row	Johan. Ocean	Johan. Coastal	Johan. Inshore	Vähätalo	BLP (SAP)	BLP (ALT)
Johan. Ocean	1	0.61	0.26	0.12	0.18	0.25
Johan. Coastal	1.64	1	0.43	0.20	0.30	0.40
Johan. Inshore	3.79	2.31	1	0.47	0.69	0.93
Vähätalo	8.16	4.98	2.15	1	1.48	2.00
BLP (SAP)	5.52	3.37	1.45	0.68	1	1.35
BLP (ALT)	4.08	2.49	1.08	0.50	0.74	1

Table 4.1: DIC production mean ratios. Biological Labile Photoproduct production (BLP) has been added for comparison. Note that the BLP vs DIC photoproduction rates is usually assumed to be approximately equal to 1 (e.g., Stubbins et al., 2006).

The estimation of the water column DIC daily production (dPDIC, $molDIC.m^{-2}.d^{-1}$) varies widely according to the AQY definition (Figure 4.2). Discrepancies in dPDIC calculations are particularly marked between results obtained from AQYs defined for different aquatic bodies (from freshwaters to oceanic waters) but also between estimations derived from AQYs determined for a same water type. For example, the mean ratio between DIC productions derived from Johannessen and Miller (2001) coastal and offshore AQYs reaches 1.64 while a ratio of 3.79 has been found between the offshore and inshore AQY formulations (Table 4.1, Figure 4.1). Moreover, a relatively high ratio of 2.15 was obtained between computations derived from the freshwater AQYs described by Johannessen and Miller (2001) and Vähätalo et al. (2000). This result reflects the high spatial heterogeneity of CDOM photolability for DIC production (see section 2.2) and emphasizes the current need to document AQY in order to understand its variations according to changes in environmental forcing. Therefore, it is clear that a peculiar attention should be paid on the choice of the AQY considered in the photochemical model

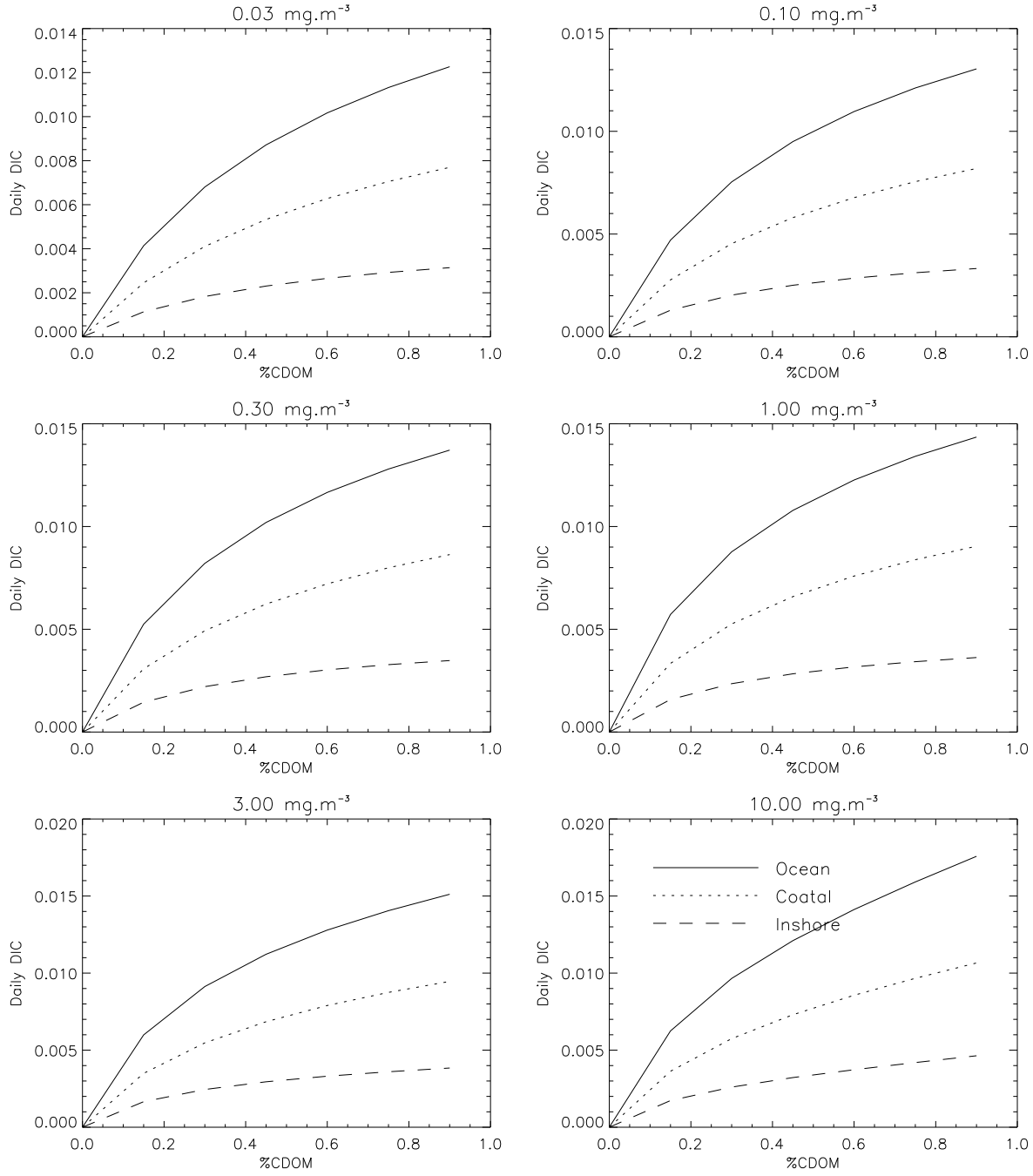

Figure 4.1: Comparison of the DIC daily production considering the AQYs (Apparent Quantum Yields) from Johannessen and Miller (2001).

which should ideally be adapted to the characteristics of CDOM (origin, light history...) in the area selected. However, the current lack of AQY documentation represents a strong limitation for achieving this goal. Nevertheless, it seems necessary, at least in a first approximation, to consider in a separated way the oceanic and coastal water masses (Traykovski et al. 2002).

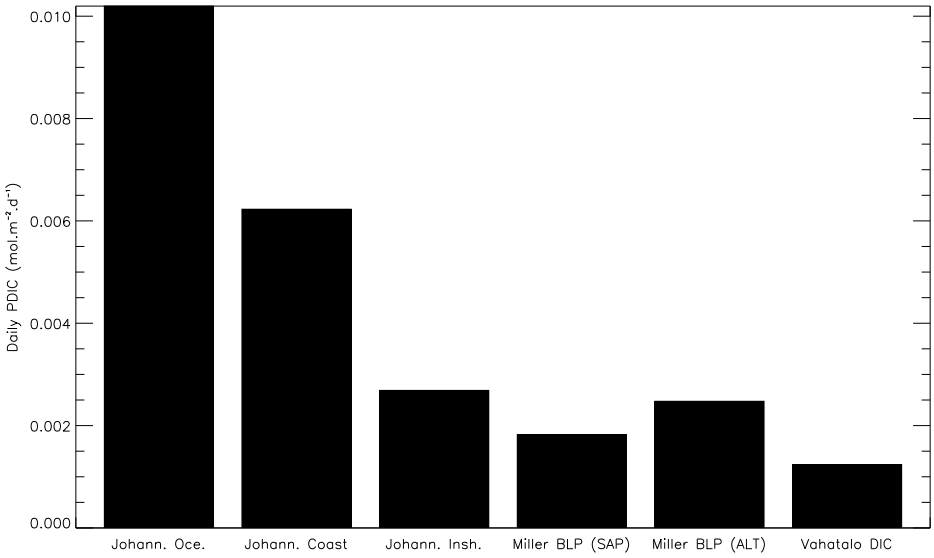

Figure 4.2: Comparison of DIC daily production according to the various existing parametrisations (chl$a$ = 0.3 $mg.m^{-3}$, %CDOM = 0.45).

- CO photoproduction rates

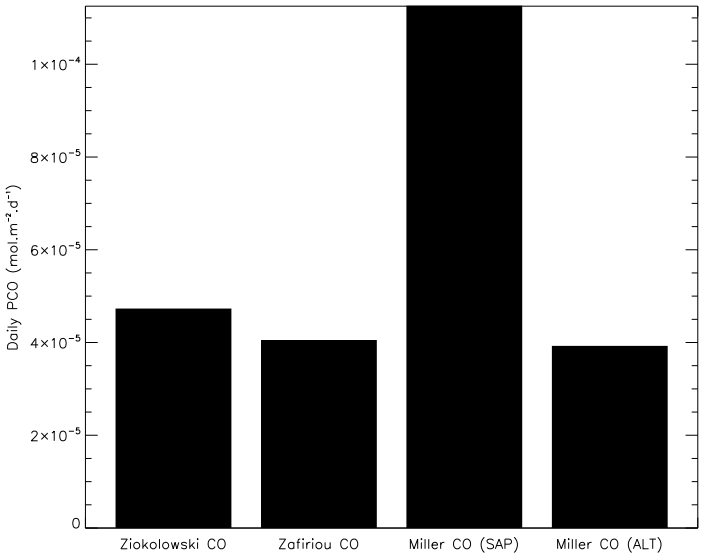

Figure 4.3: Comparison of CO daily production according to the various existing parametrisations (chl$a$ = 0.3 $mg.m^{-3}$, %CDOM = 0.45).

C/R	Zafiriou	Ziolkowski	Miller SAP	Miller ALT
Zafiriou	1	0.86	2.39	0.84
Ziolkowski	1.17	1	2.79	0.98
Miller SAP	0.42	0.36	1	0.35
Miller ALT	1.19	1.02	2.84	1

Table 4.2: CO daily photoproduction mean ratios.

The influence of the AQY definition has a lower impact for the estimation of the water column daily CO production (dPCO, $molDIC.m^{-2}.d^{-1}$) than for the computation of DIC production (Figure 4.3, Table 4.2). Indeed, if we except the AQY from Miller et al. (2002) in the Sapelo marsh which leads to at least twice greater CO production estimation when compared to the other models, a broad consistency exists in the dPCO estimations obtained from the different AQYs as illustrated by the ratios ≈ 1 in Table 4.2 (Fichot 2004, Stubbins et al. 2006).

4.2 Effect of the model definition on UV inhibition of primary production estimation

This section describes the results of the sensitivity analyses performed on the different steps of photobiological model used to compute the daily UV inhibited primary production rates.

- *P-I curves definition*

  The impact of the choice of the P-I curve description for the computation of the water column daily integrated primary production optimal rate (i.e., without inhibition) has been estimated using 3 formalisms described in the section 2.3: (i) the quadratic (eq. 2.30, "Quadra") (ii) the hyperbolic tangent (eq. 2.31, "Tan") and (iii) the exponential (eq. 2.32, "Exp") formulations.

  Figure 4.4 illustrates the primary production profiles obtained from these 3 formalisms. The relative differences the between the 3 P-I curves remain relatively low for the daily uninhibited ("PP-UV"), inhibited ("PP+UV") or the PP relative inhibition rate (Δ PP). Indeed, differences between the quadratic model and the other ones are lower than $\approx$ 5 % while the greatest discrepancies are observed between the hyperbolic tangent and the exponential formulation ($<$ 9.8% for the daily PP-UV, PP+UV or PP relative inhibition rate, Table 4.3). These results are in agreement with the values reported by Frenette et al. (1993) for uninhibited primary production estimations. Note that the extent of the differences between the P-I curve models varies only weakly with the water mass characteristics.

		Quadra. (eq. 2.30)	Tan.(eq. 2.31)	Exp. (eq. 2.32)
PP-UV	Quadra (eq. 2.30)	/	-4.36	4.94
	Tan. (eq. 2.31)	/	/	8.92
		Quadra. (eq. 2.30)	Tan. (eq. 2.31)	Exp. (eq. 2.32)
PP+UV	Quadra. (eq. 2.30)	/	-4.63	5.62
	Tan. (eq. 2.31)	/	/	9.80
		Quadr. (eq. 2.30)	Tan. (eq. 2.31)	Exp. (eq. 2.32)
Rel. Inhib. (%)	Quadra. (eq. 2.30)	/	2.13	-5.56
	Tan. (eq. 2.31)	/	/	-7.9

Table 4.3: Relative differences (%) between PI curve formalisms for the estimation of primary production without UV inhibition (PP), with PP inhibition (PPUV) and the relative amount of inhibition ((PP-UV)-(PP+UV))/(PP-UV).100 (with PUR considered in the calculations).

- *Biological Weighting Function (BWF) definition*

  The choice of the BWF parametrization can have a significant effect on the computation of PP+UV as illustrated in Figures 4.5 and 4.6. Variations in the estimation of PP UV inhibition rates from one BWF formulation to the others are particularly marked in the surface of the water column where the difference between maximum and minimum values relative to the overall average can reach up to 38 %. Conversely the variation in BWF has a weaker impact on water column integrated daily primary production since maximal relative differences range from 19 % for the clearest waters to less than 5 % in the more turbid ones. Similar effects of BWF variability on PP+UV have been reported by Neale (2001) in the Rhode river where variations in the phytoplankton sensitivity to UV can induce a variation of $\pm$ 8% in the estimation of primary production inhibition (4.4). The importance of the accurate definition of BWF

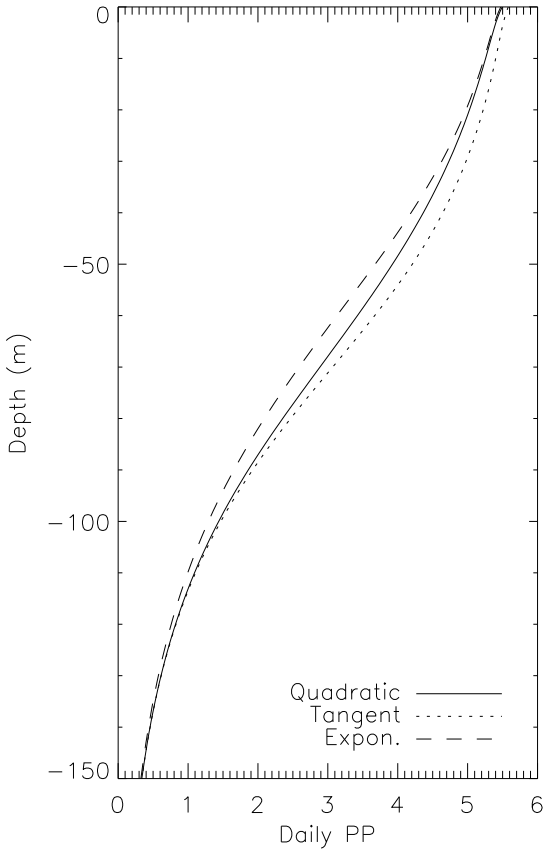

Figure 4.4: Comparison of the daily PP profile considering the various PI models.

is further underlined by Neale et al. (1998b) who reported that under some conditions the variability in the sensitivity of phytoplankton to UV radiation (i.e BWF) in the Weddel-Scotia confluence can induce variations in PP+UV by as much as ± 46 % depending on the BWF of the assemblage (more typically ± 25 %).

	Boucher P.	Cullen Ph.	Cullen Pr.	Neale K.
Boucher P.	/			
Cullen Ph.	2.93 [-3.44; 7.52]	/		
Cullen Pr.	7.74 [-0.72; 13.97]	5.00 [2.35; 6.96]	/	
Neale K.	12.38 [2.84; 19.38]	9.80 [5.51; 12.82]	5.07 [3.23; 6.29]	/

Table 4.4: Effect of the BWF on the estimation of the inhibited water column daily primary production. Results (average [minimum;maximum]) are quantified as the relative differences existing between the various estimations: $(PP + UV(Col_i) - PP + UV(Row_j))/PP + UV(Col_i).100$.

- *Exposure-Response-Curve definition*

  The comparison of the water column inhibition rates of primary production obtained with the BWF_E and BWF_H models shows that the choice of the Exposure-Response Curve (ERC), on the basis of two distinct concepts and assumptions (see section 2.3), can have a significant

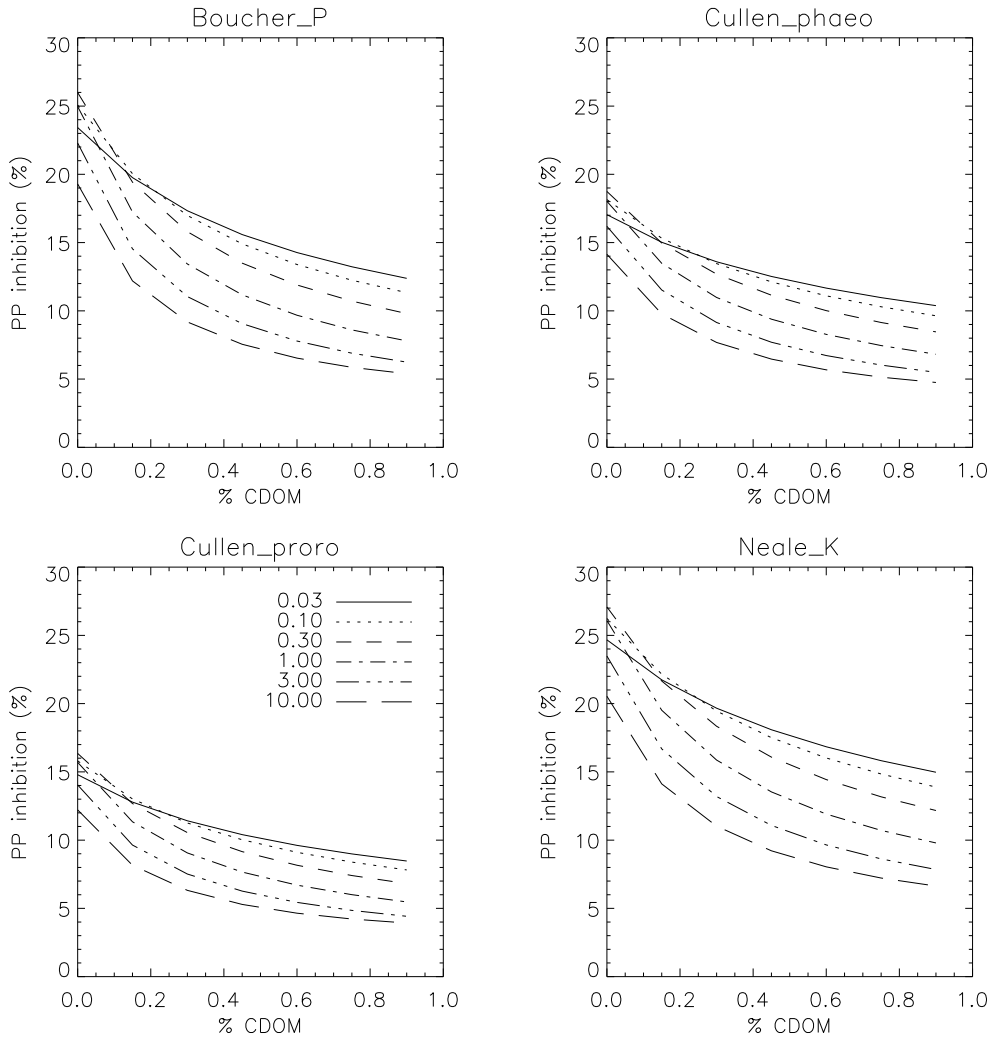

Figure 4.5: Daily water column inhibited primary production variations obtained according to the variations in Biological Weighting Functions (BWFs) definition.

influence on the estimation of the rate of primary production inhibition for a same exposure to UV radiations (Figure 4.7). Indeed, the BWF_H model tends to lower the PP+UV estimation of about 20% when compared to the BWF_E model. This result is in agreement with Neale (2001) who reported that the H_{inh} values has to be about 32 % higher than E_{inh} to result in the same relative inhibition of photosynthesis (i.e. $(1 - exp(-H_{inh}.1.32))/(H_{inh}.1.32) \approx 1/1 + E_{inh}$).

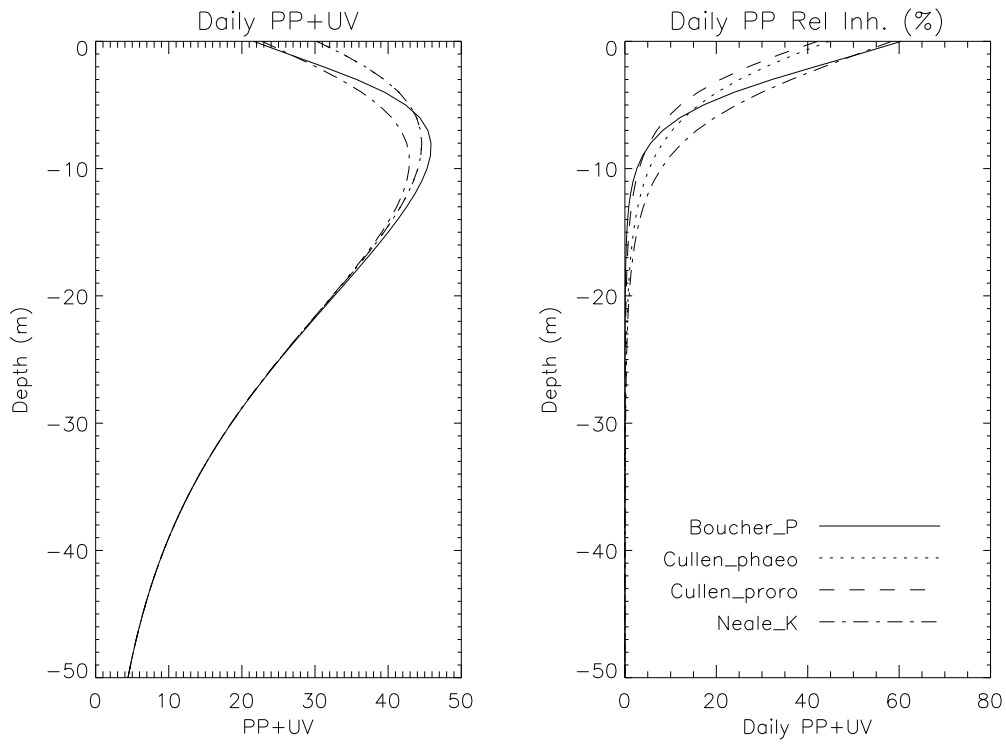

Figure 4.6: Variation in daily inhibited primary production profile (PP+UV) and relative UV inhibition rate according to the Biological Weighting Functions (BWFs) for different chl$a$ values.

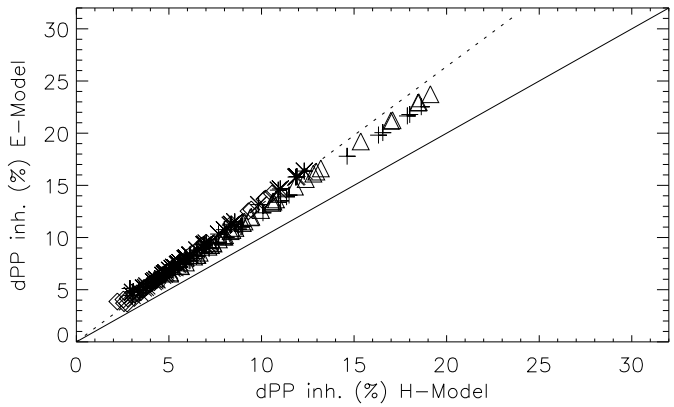

Figure 4.7: Influence of the ERC on primary production inhibition (mean differences $\approx 20\%$, $E/H \approx 1.32$ (cf Neale et al., 2001). The thin line represents the first bissectrice while the dashed line corresponds to the UV effect with a modified exposure: H_{inh} is multiplied by a scaling factor 1.32 which brings the two ERCs into a close agreement.

4.3 Effect of ozone concentration changes on UV DIC production and phytoplankton primary production inhibition

Several computations have been performed in order to appreciate the influence of changes in the amount of ozone in the atmosphere on the UVR photochemical and photobiological effects. For this purpose, series of simulations were undertaken considering variations in the total atmospheric ozone amount ranging from 125 to 575 DU by 25 DU increments. The "reference" calculation was performed by considering an ozone amount of 325 DU that is globally representative of an average European atmosphere.

Our results underline that changes in the atmospheric ozone concentrations have only a restricted effect on both UV DIC photoproduction and primary production inhibition (Figures 4.8, 4.9). Indeed, a decrease in ozone concentrations from 325 DU to 125 DU would induce an increase of the daily water column integrated DIC production and primary production inhibition of 4 % and 8 % respectively. Similarly, an increase in the ozone concentration from 325 DU to 575 DU limiting the amount of UV reaching the surface of the sea would induce a decrease of less than 3 and 5 % of DIC photoproduction and phytoplankton photosynthesis inhibition rates respectively.

This feature, already reported in several studies dedicated especially to UV photobiological effects (Neale et al. 1998a; Neale et al. 1998b, Neale 2000, Neale 2001), reflects the limited transparency of the water column to UVR and in particularly to UVB which are the more affected by changes in the atmospheric ozone amount (Vantrepotte and Mélin 2006). Moreover, this result might indicate that short term variations in the ozone amount might be obscured by concomitant changes in the other atmospheric conditions. In particularly, changes in cloud cover, which are expected to greatly modulate the amount of UVA radiations reaching the surface of the sea, might have a more relevant impact on these processes. Interestingly, the highest influence of ozone concentration changes on the relative rate of inhibition of primary production was not observed at the surface of the water column (Figure 4.10) illustrating that modification in the ozone concentration also influence the underwater light quality, however according to a nonlinear pattern.

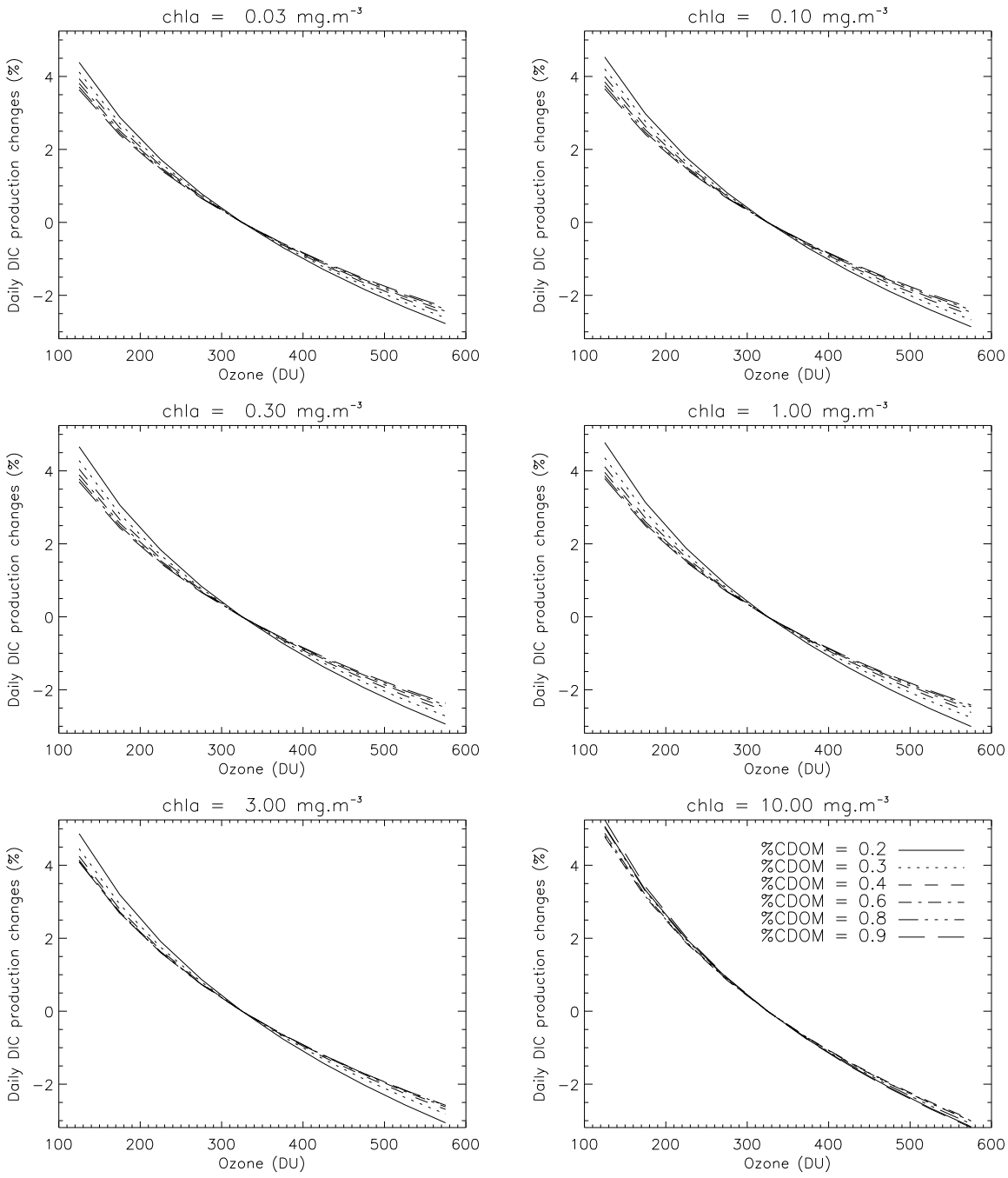

Figure 4.8: Influence of ozone concentration changes on the water column daily DIC photoproduction (325 DU taken for reference calculation).

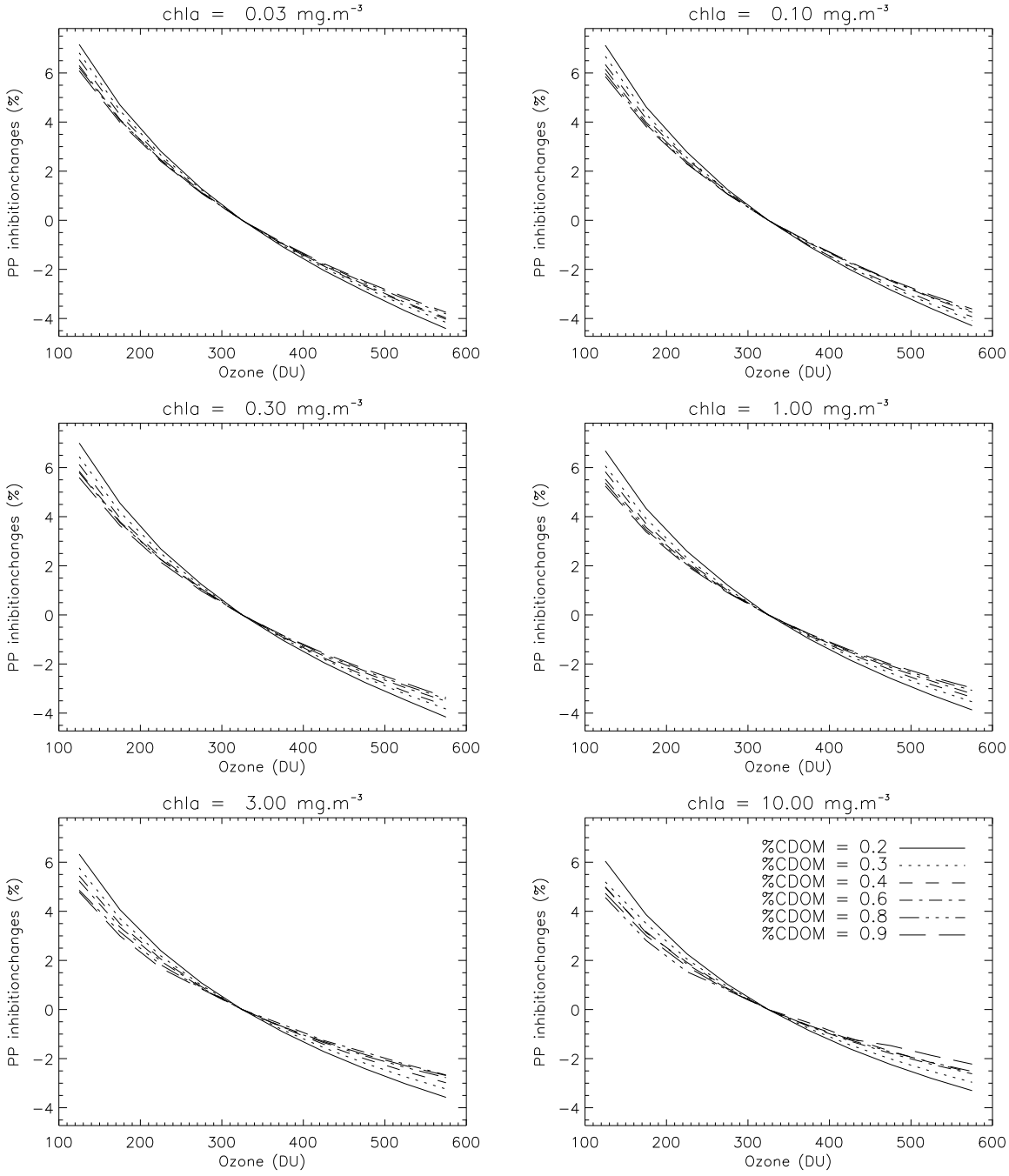

Figure 4.9: Influence of ozone concentration changes on the water column daily primary production inhibition (325 DU taken for reference calculation).

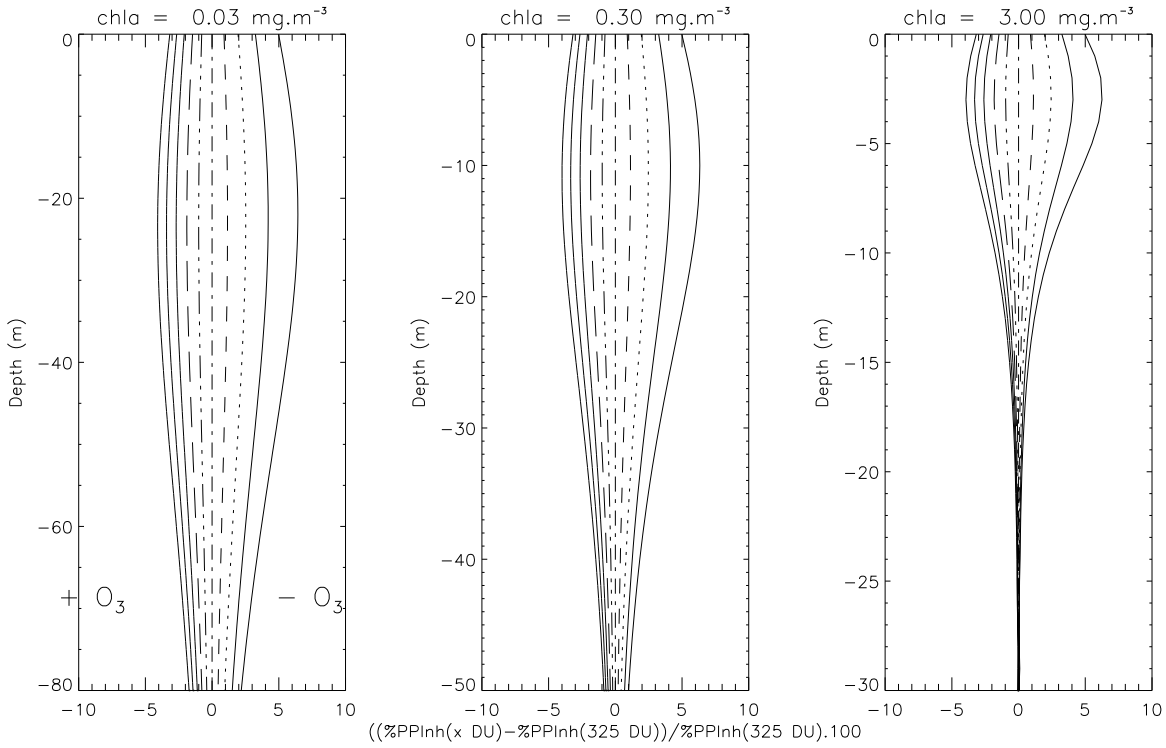

Figure 4.10: Influence of ozone concentration changes on the vertical profile of primary production inhibition (325 DU taken for the reference calculation).

4.4 Effect of water column vertical structure on UV DIC photoproduction and phytoplankton primary production inhibition

Several algorithms are currently available to derive chl$a$ concentrations and estimate IOPs at the surface of the ocean from satellite remote sensing data (e.g. Carder et al. 1999 ; Lee et al. 2002). However, in the context of photochemical and/or photobiological applications based on satellite information, the consideration of the sub-surface layer accessible from satellite measurements (i.e., Zeu/4.6) is not sufficient and a description of the vertical distribution of phytoplankton biomass (and/or of particulate matter and CDOM concentrations) is needed. Several models have been proposed to derive the marine vertical chl$a$ profile from the surface concentration. Morel and Berthon (1989) proposed an heuristic model for case 1 waters based on 4000 vertical chl$a$ profile measurements from fluorometric technique. This model allows the derivation of the chl$a$ vertical profile for diverse trophic regimes classified according to the surface layer chl$a$ concentration and characterized by specific parameterizations. Very recently, Uitz et al. (2006) have proposed similar parameterizations of the vertical profiles of chl$a$ considering different marine trophic states in case 1 (oceanic) waters from a dataset of 2419 profiles of HPLC pigment concentrations (with [chl$a$] ranging from 0.03 to 6 $mg.m^{-3}$). These revised parametrizations are in a broad agreement with the previous findings of Morel and Berthon (1989). Another approach developed by Longhurst (1995) considers that the global ocean can be partitioned in several provinces or biomes on the basis of diverse factors including the light climate, the physical circulation patterns, the inputs of macro- and micro-nutrients, the

distance to continental masses... . From the analysis of more than 21000 chl*a* profiles, each province has been characterized by a set of parameters allowing the derivation of the vertical structure of biomass from a general Gaussian-shape formulation (see Mélin and Hoepffner 2004).

Conversely, no equivalent general parameterization is currently available for the CDOM vertical structure due to the presence of numerous controlling factors such as the photobleaching process that modulates the CDOM absorption in the surface layer of the water column (Twardowski and Donaghay 2002; Oubelkheir et al. 2005). The amount of measurements of vertical profiles of CDOM is also much lower than for chl*a*. Therefore, in absence of reliable alternative, the actual modelling approaches used to compute CDOM vertical distribution are based on many assumptions. Globally, two major approaches can be distinguished:

- Homogeneous vertical profile of CDOM:

  A first approximation is to consider a homogeneous vertical profile of CDOM from the surface to the bottom of the water column. This approach has been used in recent studies on UVR penetration and biogeochemical effects (Vasilkov et al. 2002; Vasilkov et al. 2005).

- CDOM absorption profile inferred from chl*a* vertical distribution:

  Another classical approach is to relate the CDOM absorption to that of particulate matter absorption and therefore to derive the vertical CDOM distribution from the vertical structure of chl*a* concentration. This method considers that the CDOM in open-ocean originates from an autochthonous biological marine production. More precisely, $a_{CDOM}(440)$ estimation is based on a general bio-optical assumption (Prieur and Sathyendranath 1981, Morel 1991) which considers that (i) a covariation exist between ch*a* and CDOM concentration, (ii) the relative proportion of the absorption due to CDOM with respect to the sum of the absorption of other absorbing compounds at 440 nm is globally constant (previously fixed at 20 % of the sum of pure water and particulate matter absorption). However, several authors (Carder et al. 1989, Nelson et al. 1998, Siegel et al. 2002, 2005) have underlined the limits of this general assumption (see discussion in Vantrepotte and Mélin 2006). Focusing on the vertical scale, Oubelkheir et al. (2005) have reported an absence of direct covariation between CDOM absorption coefficient and the chl*a* concentration in the Mediterranean Sea due to the occurrence of surface photobleaching or bacterial activity. However, the current lack of similar *in situ* comparison does not allow general conclusions and an improved determination of CDOM vertical structure still remains a complex and open field of studies.

In this context of an application of the model to ocean color data, we performed several simulations in order to *estimate the relative importance of the description of both phytoplankton biomass and CDOM absorption vertical structure on the computation of UV photochemical and photobiological effects*. For this purpose, we compared the calculations of the daily DIC production and PP+UV rates obtained with uniform and stratified vertical profiles considering:

- the Gaussian formulation reported for the Atlantic subarctic (SARC) and Mediterranean sea (MED) provinces defined by Longhurst (1995).

- the trophic status from Uitz et al. (2006):

  chl*a* profiles have been derived from Uitz et al. (2006) formulation by defining 9 cases of study (Figure 4.12) corresponding to the different stratified water types ("trophic states") defined by

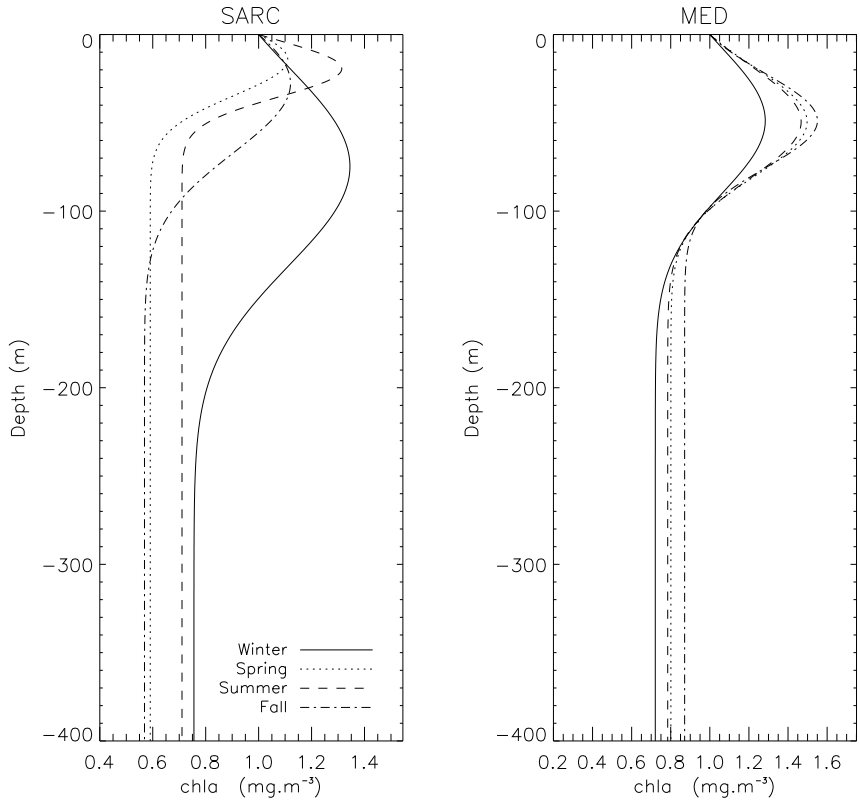

Figure 4.11: Vertical biomass profiles in the Mediterranean Sea (MED) and Atlantic Subarctic (SARC) areas according to Longhurst (1995) climatology (provided by the Biological Institute for Oceanography, Halifax), with [chla(z=0)] = 1 $mg.m^{-3}$.

		Mean($\|X\|$)	SD($\|X\|$)	Min	Max
MED	DIC	0.61	0.43	-1.98	-0.14
	PP	10.73	5.05	-20.01	-2.36
	PPUV	12.46	6.70	-25.02	-2.09
	%Inh	5.53	2.98	-4.39	12.19
SARC	DIC	0.42	0.27	-1.27	0.68
	PP	6.68	4.85	-16.34	22.16
	PPUV	6.79	4.88	-17.50	22.35
	%Inh	5.11	4.18	-18.43	8.60

Table 4.5: Influence of the vertical structure of biomass on PP, PP inhibition and PDIC estimation for the Mediterranean sea and SARC area ((P(Homog)-P(Stratif))/P(Homog) .100). Average ($\|X$), standard deviation (SD), minimum and maximum (Min and Max respectively) values have been calculated considering the various water types (N = 42) defined in the synthetic dataset (6 chl$a$ concentration and 7 CDOM proportions), DIC production rates have been calculated using the AQY by Johannessen and Miller (2001) for oceanic waters.

the latter authors ($[chla_{surf}]$ = 0.03, 0.06, 0.1, 0.16, 0.25, 0.35, 0.6, 1.5 and 3.0 $mg.m^{-3}$). Statistics on the differences observed between stratified and homogeneous simulations are reported in Table 4.6.

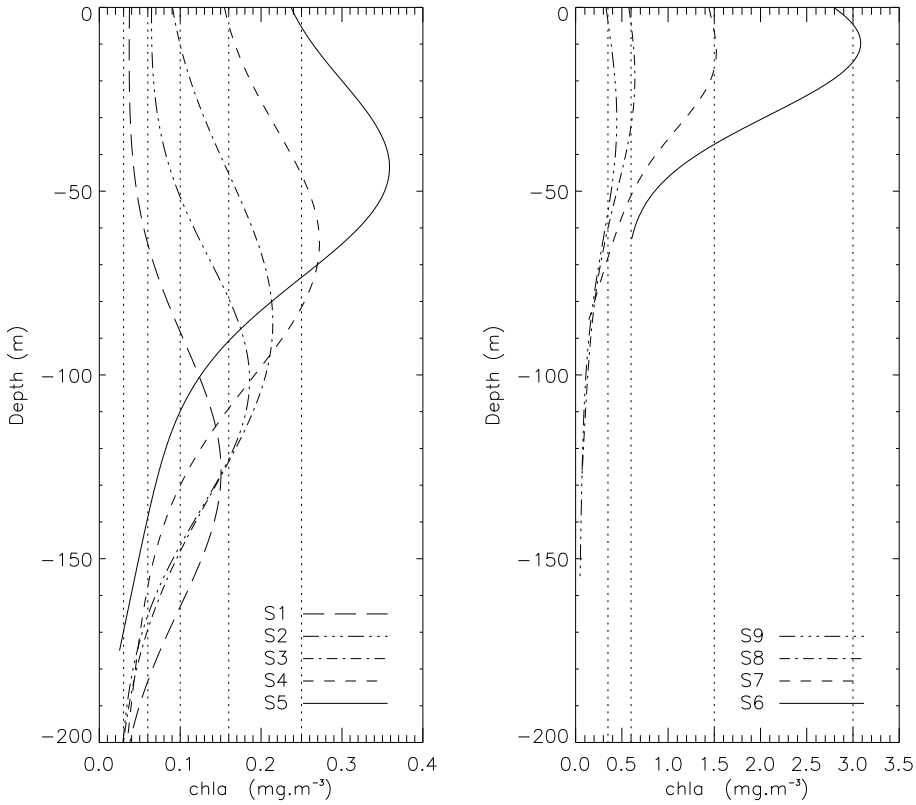

Figure 4.12: Vertical biomass profiles for the different trophic states defined by Uitz et al., 2006. The dotted lines represent the corresponding homogeneous profiles.

The approximation of a homogeneous vertical profile of chl*a* (and therefore CDOM) has only a restricted effect on the estimation of DIC photoproduction rates. Indeed, the relative differences in the DIC water column integrated daily production obtained from homogeneous and stratified simulations remain lower than 4 % considering both vertical profile models (Tables 4.5 and 4.6). This feature can be explained by the fact that the major part of the DIC production occurs in the first meters of the water column (see Figures 3.9 and 4.13). As a matter of fact, the shape of the vertical DIC production profiles seems to be mainly related to the vertical decrease of irradiance throughout the water column (Figure 4.13).

Conversely, the description of the water column vertical structure is more relevant for the estimation of primary production with and/or without UV inhibition (PP+UV and PP-UV respectively). Indeed, mean differences between water column daily primary production estimations computed with homogeneous and/or stratified vertical profiles can reach ≈ 90 % for PP-UV and ≈ 65 % for PP+UV (Table 4.6, Figure 4.14) in absolute values. The higher impact of the vertical structure description for the primary production than for the DIC photoproduction estimation can be explained by the difference existing in the thickness of the productive layer between these two photodependent processes (see sections 3.2, 3.3).

Moreover, the relative importance of the vertical structure description for the primary production modelling varies according to the water mass characteristics (Table 4.6, Figure 4.15). Indeed, differences between homogeneous and stratified simulations are relatively low for the high chl*a* concentrations, when the major part of the primary production is performed within the top layer of the water column. Conversely, the impact of the vertical structure is greater when the primary pro-

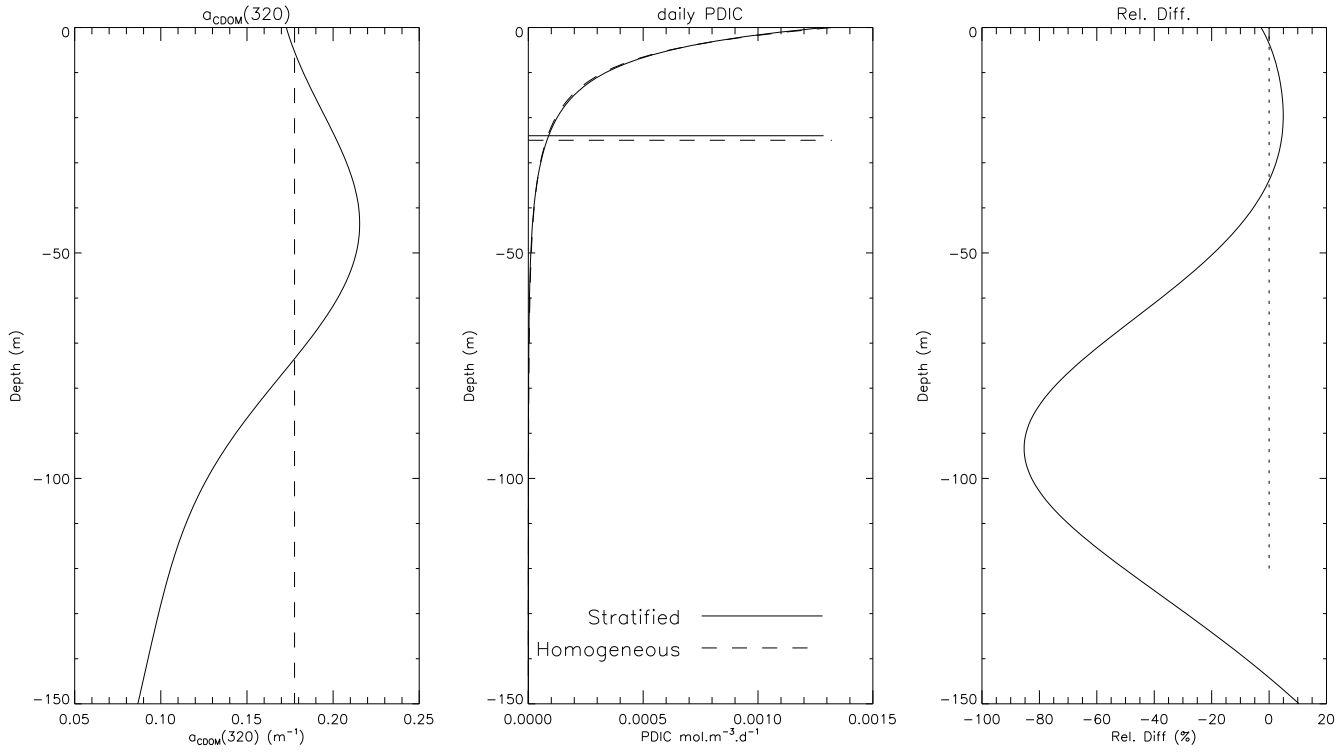

Figure 4.13: Example of the vertical distribution of the CDOM absorption coefficient at 320 nm, the daily profile of DIC photoproduction ($mol.m^{-3}.d^{-1}$ and the relative difference between homogeneous and stratified profiles with $[chla_{surf}] = 0.25\ mg.m^{-3}$ and %CDOM = 60. The horizontal lines represent the $Z(90\%)DIC$ depths for both homogeneous (solid line) and stratified (dashed line) distributions.

duction occurs within a deep layer. Further, the sign of these relative differences is also related to the trophic state. Indeed, the consideration of homogenous rather than stratified water columns can lead to a large underestimation of the water column daily primary production for the oligotrophic waters characterized by a deep mixed layer (e.g. from S1 to S6, Figure 4.15). On the opposite, in the more eutrophic waters, for which the chlorophyll maximum is located near the surface of the water column, the consideration of a homogeneous profile tends to overestimate the water integrated primary production (e.g. S7 to S9, Figure 4.15). Note that the same feature is observed for the SARC Gaussian profiles formulation in spring and/or summer when the chlorophyll maximum is located in the 20 first meters of the water column.

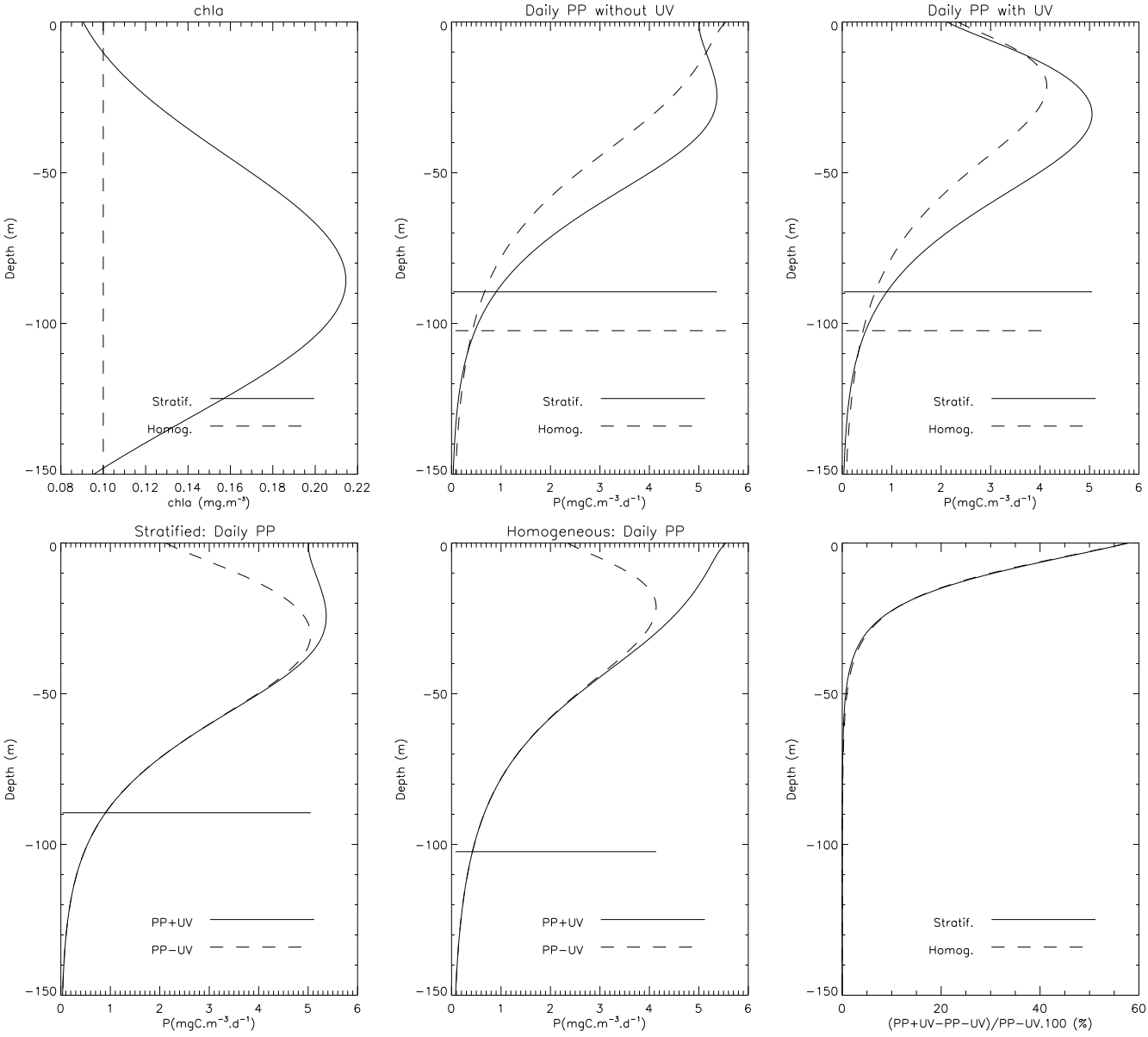

Figure 4.14: Example of the vertical distribution of chl*a*, primary production without UV effects (PP-UV), primary production with UV inhibition (PP+UV), (PP-UV) and (PP+UV) for homogeneous and stratified profiles and relative differences between (PP-UV) and (PP+UV) considering stratified and/or homogenous profiles. The horizontal lines represent the Z01(PAR) depth for both stratified and homogeneous profiles (S3, %CDOM = 60).

		S1	S2	S3	S4	S5	S6	S7	S8	S9	all
	$[chla_{surf}]$	0.03	0.06	0.1	0.16	0.25	0.35	0.6	1.5	3.0	/
DIC	Mean($\|X\|$)	2.09	1.23	0.67	0.66	0.48	0.48	0.11	0.03	0.13	0.65
	SD($\|X\|$)	0.92	0.64	0.44	0.34	0.19	0.10	0.05	0.03	0.07	0.73
	Min	-3.67	-2.34	-1.44	-1.26	-0.82	-0.65	-0.14	-0.03	-0.21	-3.67
	Max	-1.20	-0.64	-0.28	-0.35	-0.30	-0.38	-0.01	0.09	0.06	0.09
PP	Mean($\|X\|$)	87.53	50.85	31.76	21.13	11.76	5.70	2.95	5.48	3.34	24.50
	SD($\|X\|$)	15.69	6.72	3.03	0.69	1.94	2.52	2.29	1.88	1.19	27.70
	Min	-110.39	-59.77	-35.64	-21.88	-13.27	-8.22	0.54	3.37	2.18	-110.39
	Max	-67.53	-41.70	-27.50	-20.04	-8.02	-1.15	6.98	8.65	5.36	8.65
PP_{UV}	Mean($\|X\|$)	64.94	40.58	28.58	21.06	14.33	9.32	1.25	3.83	2.12	20.67
	SD($\|X\|$)	15.20	8.26	4.52	1.96	0.69	1.53	1.24	1.60	0.96	20.92
	Min	-89.66	-53.35	-35.21	-23.37	-14.98	-10.46	-1.14	2.17	1.24	-89.66
	Max	-47.62	-30.67	-22.88	-18.35	-12.98	-6.21	3.78	6.69	3.87	6.69
dPP (%)	Mean($\|X\|$)	27.13	21.62	19.01	12.63	8.84	5.33	1.33	2.57	1.03	11.06
	SD($\|X\|$)	3.54	2.06	3.22	2.97	3.48	2.86	1.12	1.15	1.00	9.46
	Min	-31.53	-23.82	-21.03	-14.65	-11.82	-8.46	-1.26	1.14	-0.12	-31.53
	Max	-21.72	-18.18	-12.26	-6.58	-2.20	0.83	3.40	4.25	2.63	4.25

Table 4.6: Influence of the vertical structure of biomass on PP, PP inhibition and PDIC estimation considering the various trophic states defined by Uitz et al. (2006) ((P(Homog)-P(Stratif))/P(Homog) .100).

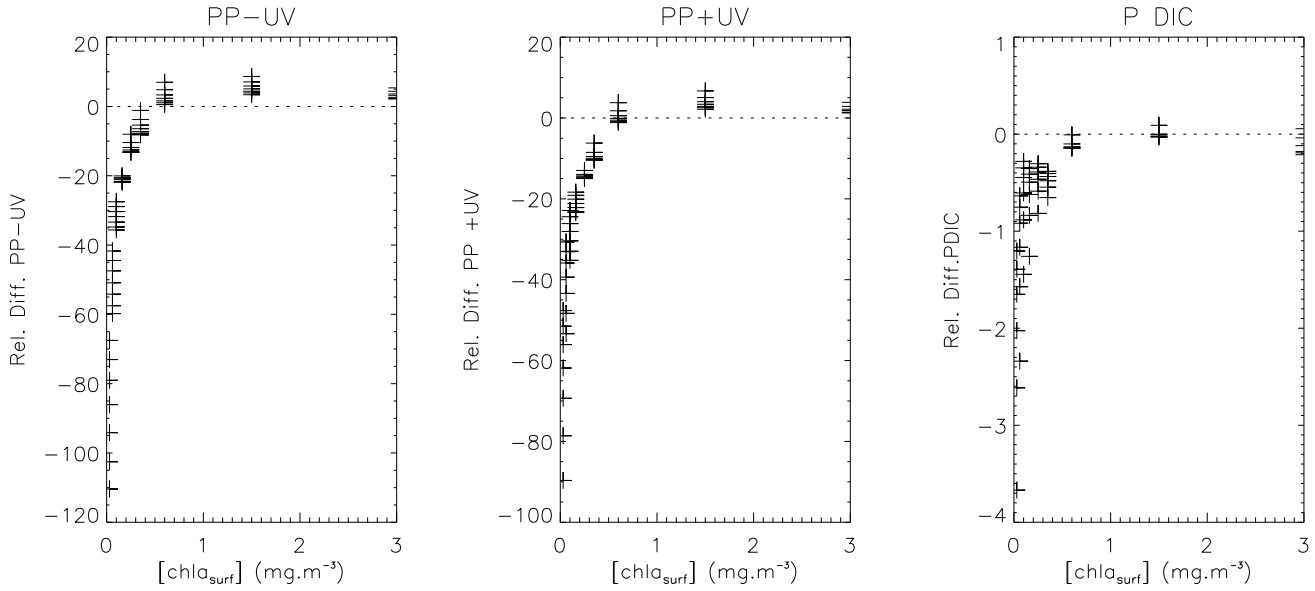

Figure 4.15: Relationship between $chla_{surf}$ concentration and the relative differences between homogenous and stratified vertical profiles description calculated for PP-UV, PP+UV and PDIC (Rel. Diff. = (Homogeneous-Stratified)/Homogeneous.100).

4.5 Effect of Mixing on UV DIC production and primary production inhibition

Mixing effects have been shown to be relevant for the description of UV photochemical and photobiological effects on aquatic ecosystems and they are recognized to represent a major complication in attempting to quantify them (Cullen and Lesser 1991; Neale et al. 1998b; Simó and Pedrós-Alió 1999; Neale 2001; Bélanger et al. 2006).

Phytoplankton cells are exposed to different irradiance intensities and spectral fields during their vertical motions. This feature induces that the exposure dose as well as the balance between damage and repair processes will be modulated by the mixing depth and vertical velocity (Belzile et al. 1998; Neale 2001). The importance of the vertical mixing events is further increased by the fact that phytoplankton blooms are often associated with a seasonal stratification of the water column which usually coincides with periods of high irradiance, including both PAR and UVR. The various experimental and modelling studies which have been conducted in the recent years in order to evaluate the effects of vertical mixing on phytoplankton photosynthetic response have emphasized the high complexity of this environmental forcing (Helbling et al. 1994; Neale et al. 1998b; Köhler et al. 2001; Barbieri et al. 2002; Hernandom and Ferreyra 2005). Indeed, works by Helbling et al. (1994), Prezelin et al. (1994) or Neale et al. (1998b) have demonstrated that the sign as well as the magnitude of the differences for primary production inhibition existing between static and vertically mixed situations can vary widely according to the position of the vertical stratification, the velocity of phytoplankton vertical movements and the water column optical quality (i.e. the thickness of the photic layer).

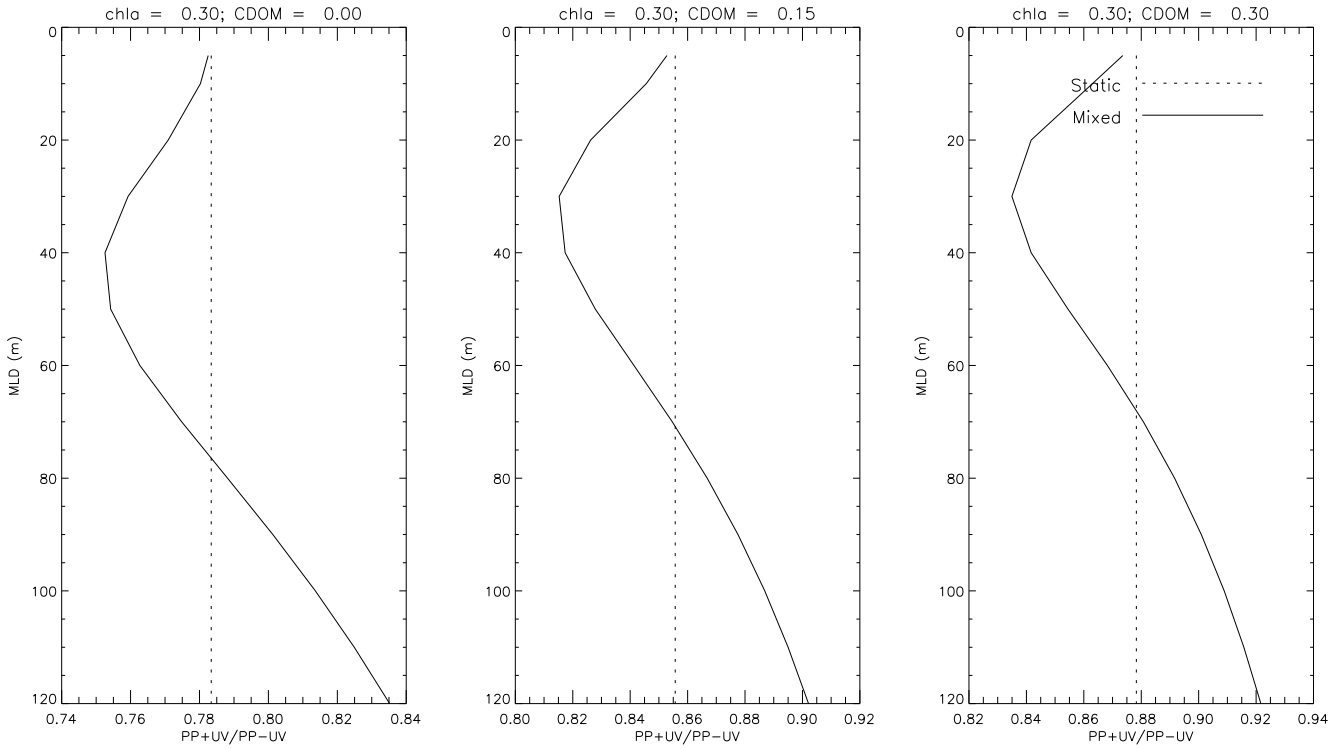

Figure 4.16: Dependence of the relative water column daily inhibition rates (PP+UV/PP-UV) on changes in the MLD, the dotted line represents the results obtained for static conditions.

In particular, Neale et al. (1998b), using a cumulative exposure model (H-model) allowing to consider the phytoplankton cells light history, have reported variations in PP+UV rates ranging from -43.8 to 30.9 % due to the action of vertical mixing. Further, they demonstrated that mixing within the photic zone has a global negative effect on PP+UV since it brings less inhibited cells to the surface of the water column, increasing therefore the overall phytoplankton community inhibition (Figure 4.16). Further, in the same time inhibited cells are transported to the lower photic zone where light-limited rates are low with respect to static conditions.

Conversely, deep mixing condition is assumed to have a net positive effect on the daily PP+UV levels since (i) it lessens the overall rate of photoinhibition (Figure 4.16) and (ii) it transports deep phytoplankton, unproductive during static conditions, to the surface productive layer.

However, these general patterns might be significantly modulated since the impact of vertical mixing on a defined biological response is related to the time scale considered and therefore to the specific kinetic of the photodependent process (e.g. phytoplankton balance between damage and repair processes). Indeed, if the time scale for a photodependent process (e.g. UV inhibition of primary production) is short when compared to that for the vertical mixing, phytoplankton will exhibit a vertical gradient of this photodependent response (Lewis et al. 1984). On the contrary, if the biological response occurs on a time scale longer than that for vertical mixing, the gradient of the photodependent response is not observed.

From a modelling point of view, diverse approaches are possible in order to simulate the water column vertical mixing:

- Single-multiple layer model

  A first approximation is to average, across the mixed layer (ML), the irradiance and/or the concentration of the compound concerned by a defined photodependent effect. This idealized approach can be applied by considering the ML as a whole or be more detailed by considering different layers within the ML in order to take into account the decrease of mixing magnitude with depth. Such single and/or multilayer models have been applied by several authors in order to examine the effects of mixing on CDOM photobleaching (Del Vecchio and Blough 2002, single layer with average of bleached a_{CDOM}), phytoplankton UV photoprotection process (Morrison and Nelson 2004, single and multilayer, irradiance averaged) or UV inhibition of photosynthesis (Neale et al. 1998b using "effective phytoplankton biomass" averages).

- Lagrangian mixing model

  A more detailed approach is to simulate vertical mixing by using a Lagrangian mixing model reproducing the vertical trajectory of individual marine organisms or compounds and therefore the temporal variation in their exposure to various levels of irradiance (e.g. Neale et al. 1998b for UV effects on photosynthesis, Farmer and McNeil 1999; Han et al. 2000; Oliver et al. 2003 for phytoplankton photo-adaptation to changes in visible radiations).

The effects of mixing on CDOM photomineralization processes are currently poorly known. We simulated mixing conditions by setting the exposure at all depths in the ML equal to the mean irradiance within this layer (from 0 m to the MLD) at each time step of the daily calculation. In the deep layer, from the MLD to the bottom of the water column (max 400 m), the irradiance vertical decrease was classically described by an exponential function (Figure 4.17). Thus, using this approach we assume that irradiance exposure in a completely mixed layer is not dependent on depth and that the total exposure should be equivalent for both mixed and homogeneous conditions. For this simple case study, the vertical distribution of chl$a$ related CDOM is assumed to be homogeneous along the water column while three MLD have been considered: 10 m, 50 m and 100 m. The results of the

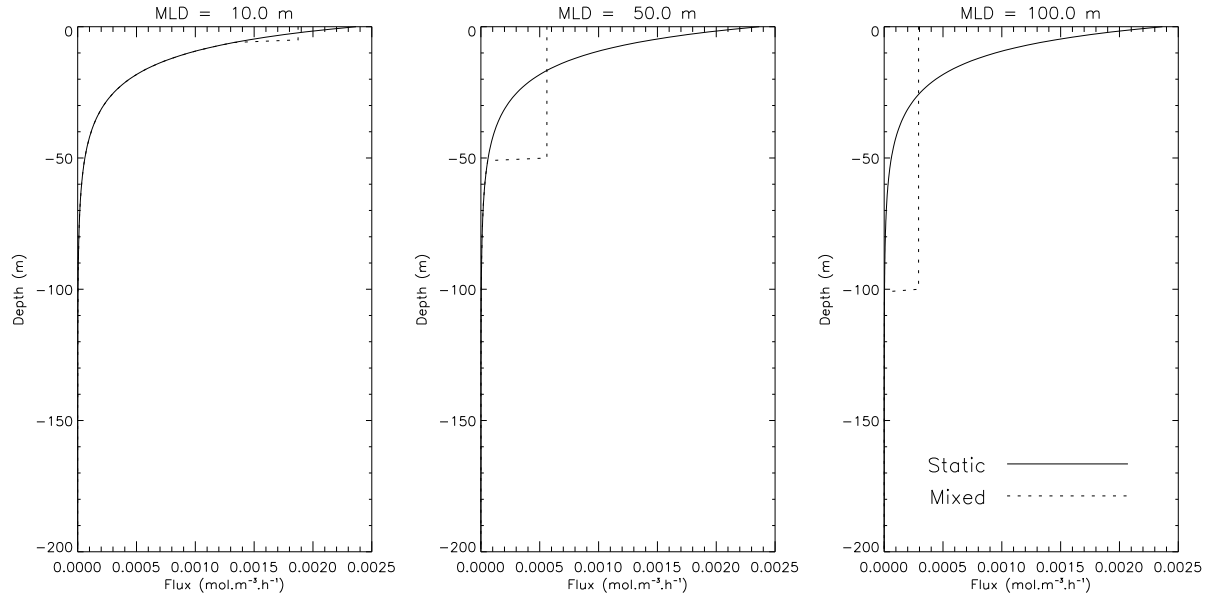

Figure 4.17: Vertical profiles of DIC fluxes (see eq. 2.19) for mixed and static conditions.

mixing simulations have been compared to those obtained with the classical "static" description of the light penetration within the water column (i.e. an exponential decrease of irradiance with depth from the surface to the bottom).

It appears that the presence of vertical mixing could induce an significant increase (up to 40%) of the water column daily DIC photoproduction with respect to static conditions (Figure 4.18). Simply, although mixing events lessen the maximal rates of DIC production, the water column PDIC is greater in mixed waters due to the presence of a significant DIC production even in the deep water for which the production levels are negligible when the water column is considered to be static. Further, the impact of vertical mixing is varying according to the ratio between the magnitude of the propagation of photosensitizing radiations in the water column (described by the 1% penetration depth for the UVA radiations, Z01UVA) and the amplitude of the MLD. Indeed, relative differences between static and mixed cases decrease with decreasing MLD/Z01UVA ratio (Figure 4.18). Therefore, if the stratification of the water column is located within the upper most productive part, mixing effect will be small ($< 10\%$ for MLD/ Z01UVA < 1). Conversely, mixing well below the productive zone would conduct to increase significantly water column DIC production since significant PDIC rates are distributed over a greater depth.

Independently of the MLD/ Z01UVA ratio, the location of the MLD itself might also be relevant for modulating the impact of vertical mixing. Indeed, considering a fixed MLD/ Z01UVA we observed that the more the stratification is located near the surface of the water column, (e.g. 10 m) the more the effects of mixing will be pronounced (Figure 4.18). This feature reflects the fact that the average level of photosensitizing irradiance to which CDOM is exposed within a thin ML is greater than for deeply mixed waters.

This simple approach is obviously based on many assumptions and the previous analysis underlines some of the needs to correct properly for vertical mixing effects in the context of a basin scale modelling:

- the consideration of the mean irradiance within the mixed layer can be representative if the

vertical velocity is sufficient enough to induce a homogeneous vertical distribution of the water constituents during the time scale (i.e. daily time steps) considered in the model.

- the vertical velocity is expected to change according to variation in the location of the MLD. Therefore, a simple average might not be relevant since it implicitly considers that the time needed to perform a complete vertical excursion from the surface to the bottom of the ML is equal for a MLD of 10 or 100 m, and that therefore the vertical velocity is inversely correlated to the MLD.

- the CDOM photolability is assumed to be constant with variations in the mixing regime. However, in the case of surface mixing conditions CDOM photolability is expected to be low and therefore the previous results might be greatly modulated. This feature should be ideally reflected in the AQY definition (Bélanger et al. 2006).

Therefore, the significance of this kind of approach, which considers a simple arithmetic mean, might be improved by calculating a weighted average taking into account changes in the mixing velocity, the MLD and the water optical quality. This could be done by confronting these results to those of a Lagrangian mixing model describing more precisely the hydrodynamical characteristics of the selected basins.

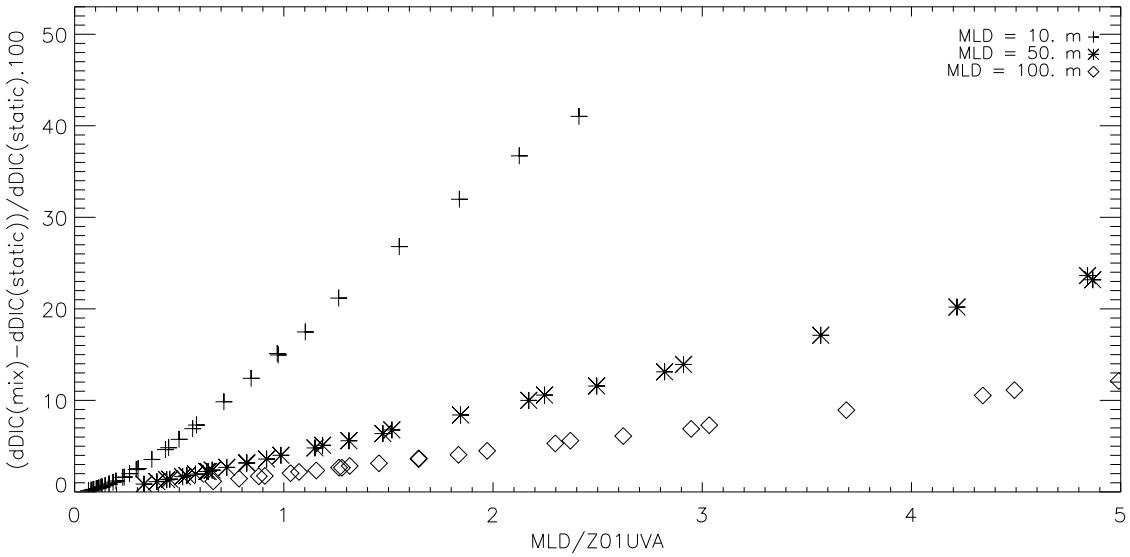

Figure 4.18: Dependence of the relative influence of vertical mixing (1 layer model) for the estimation of DIC water column daily integrated photoproduction on changes in the MLD/Z01UVA ratio, (dPDIC(mix)-dPDIC(static)/dPDIC(static) x 100).

4.6 Influence of the spectral and vertical resolution

In order to optimize the computational performance of the depth and spectrally resolved model which will be used for quantifying primary production (including UV inhibition) and/or DIC (and CO) photoproduction rates, it is useful to determine the relative impact of both spectral and vertical resolutions, which greatly modulate the computational time needed to derive large scale calculations, on the model outputs. For this purpose, several simulations have been performed by considering various spectral and temporal steps for the calculations (1, 2, 5, 10, 20 nm and 1, 2, 5, 10 m respectively). The quantification of the impact of the degradation of both the vertical and spectral resolutions has been performed by calculating the relative differences between the simulations performed at the highest resolution (1 m and 1 nm respectively) and the results of the other calculations. For this exercise, Uitz et al. (2006) profiles have been considered in order to take into account the heterogeneity of the biomass and CDOM vertical distribution.

From Figure 4.19 it appears that the degradation of the spectral resolution have a very restricted influence on the estimation of water column dPDIC and PP+UV since relative differences remain lower than 4% for the two processes.

Conversely, the degradation of the vertical resolution is particularly relevant since it might conduct to significant overestimations of both dPDIC and/or PP+UV production rates (Figures 4.20 and 4.21, respectively). The relative importance of the vertical resolution is however related to the water transparency and therefore to the thickness of the "productive" layer. Indeed, in the clearest waters the PP+UV estimations are only weakly affected by the choice of the vertical step (< 4 % for chl$a$ < 0.25 $mg.m^{-3}$) whereas differences can reach up to 40 % in the more turbid ecosystems (chl$a$ $= 3$ $mg.m^{-3}$). The same feature is observed for the DIC production estimations with differences ranging between ≈ 25 and 400 % for chl$a$ concentration varying from 0.03 and 3 $mg.m^{-3}$ respectively for a resolution of 20 m.

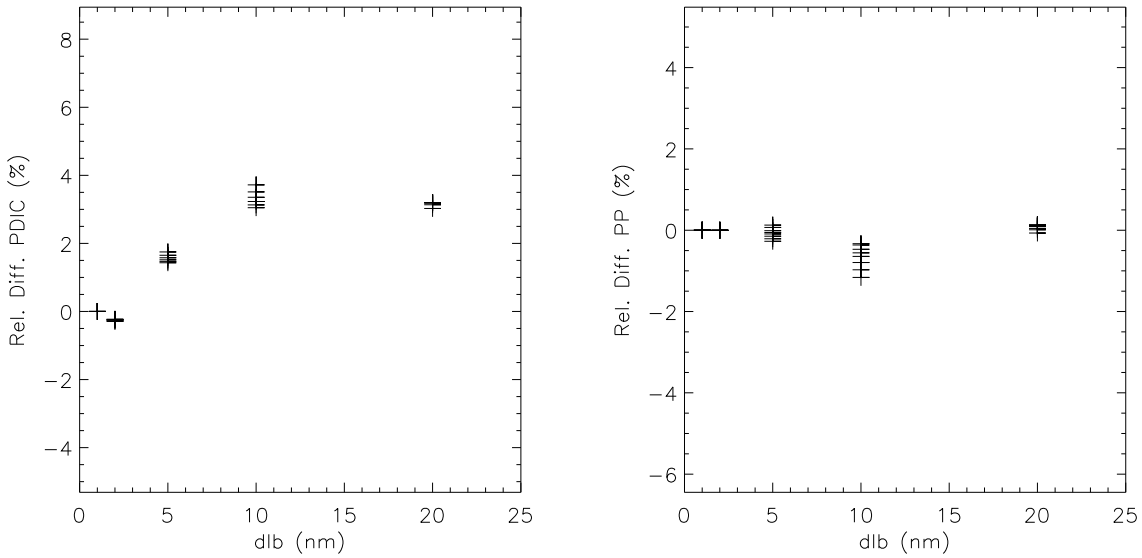

Figure 4.19: Influence of the degradation of the spectral resolution on the estimation of DIC and PP daily production (P(dλ)-P(1 nm))/P(1nm)*100.

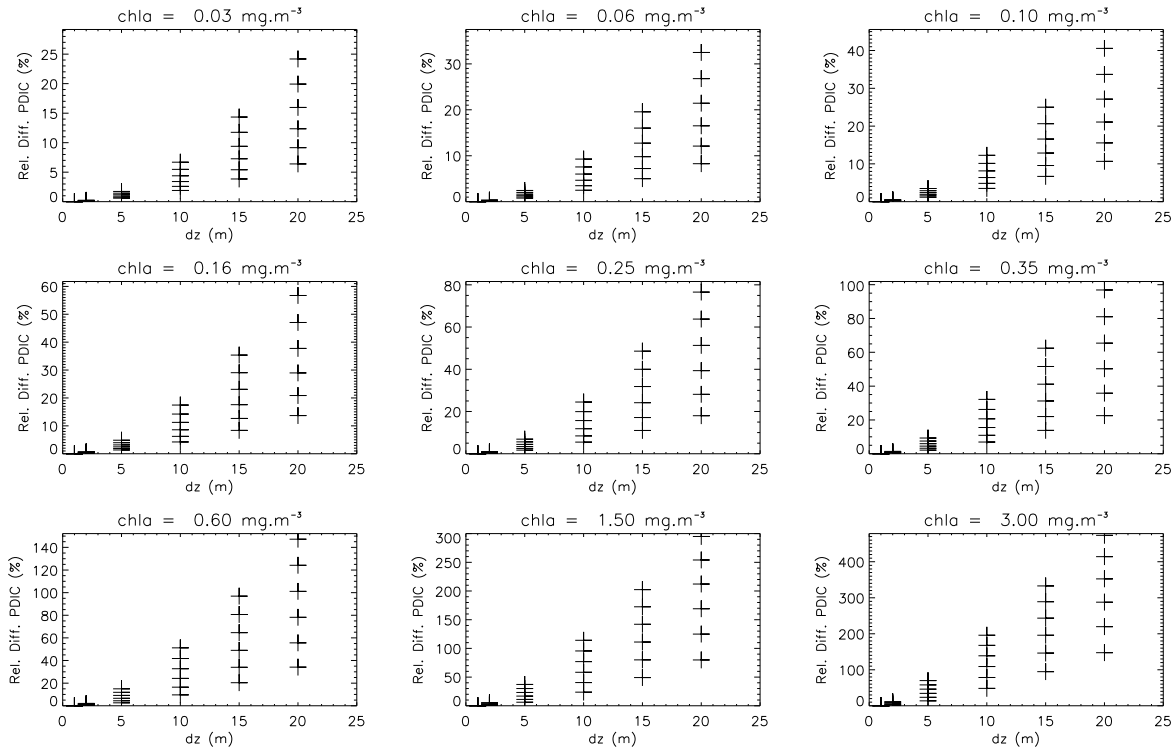

Figure 4.20: Influence of the degradation of the vertical resolution on the estimation of DIC daily production (PDIC(dz)-P(1 m))/P(dz)*100.

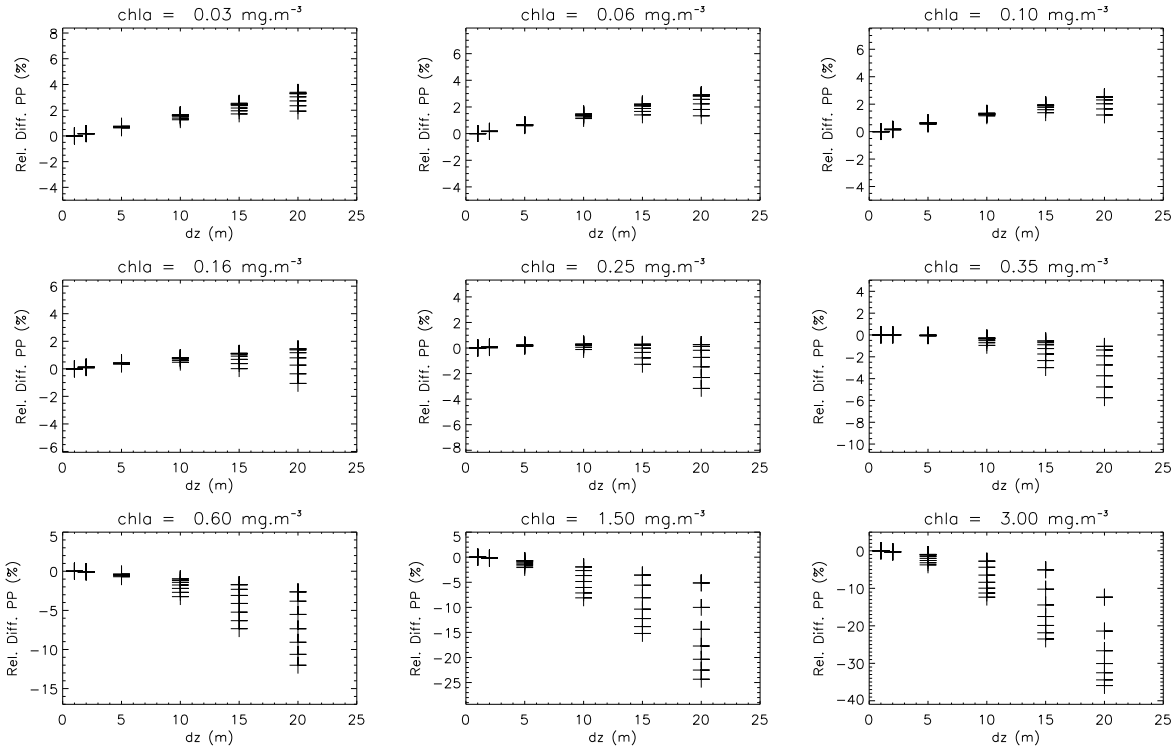

Figure 4.21: Influence of the degradation of the vertical resolution on the estimation of PP daily production (PP(dz)-P(1 m))/PP(dz)*100.

Summary

The choice of the parameterization needed for quantifying the selected photochemical or photobiological response according to changes in the amount of underwater irradiance (i.e. AQYs and BWFs) is obviously a key element to perform an accurate modelling. In particularly, the DIC photoproduction rates estimations strongly depend on the definition of the AQYs. Conversely, the estimations of CO production rates are in a broad agreement, reflecting the higher consistency of the AQYs for this photodependent process. This result obviously underlines the fundamental need to document extensively the variability of AQY for DIC photoproduction in various marine water types. Indeed, DIC photoproduction is certainly the photochemical process which is currently the less documented. Therefore, it appears necessary to better characterize the variations in the efficiency of UV photons for producing DIC according to changes in environmental conditions (e.g. water column mixing regime, temperature, water mass optical quality) but also in relation with variations in the CDOM origin and light history. Nevertheless, taking into account the variability in the AQY currently available in the literature, it appears necessary to distinguish at least, in a first approximation, the coastal waters from the open ocean for modelling application at basin scale (Johannessen and Miller 2001; Bélanger et al. 2006; White et al. 2006).

The description of the CDOM vertical profile is still problematic since no reliable global parameterization of CDOM vertical structure is currently available. However, it seems that the estimation of CDOM photoproduction will be only weakly affected by the consideration of a homogeneous description of the water column vertical structure. The latter feature is however not valid for the estimation of phytoplankton primary production which is significantly modulated by the chl*a* vertical structure.

The computational time needed to perform large scale calculation from a spectral and depth resolved model could be significantly reduced without modifying the accuracy of the model outputs by considering a relatively low spectral resolution (e.g. 20 nm). Conversely, the definition of the vertical steps for these calculations is more critical since it might induce severe biases in the estimation of both UV photochemical and photobiological effects. An good compromise between the need to optimize the computational performance of the model and the necessity to consider a relatively high vertical resolution could be to consider a vertical step varying with depth. Indeed, if a relatively high resolution is needed in the first meters of the water column, in particular for the modelling of DIC (or CO) production rates, a lower resolution could be reasonably considered to perform the calculations in the deep layer of the water column. Such an approach should however take into account variations in the water transparency and therefore in the thickness of the productive layer.

Further, the results of the sensitivity analyses can also serve to emphasize how environmental forcing can affect the marine primary production and/or CDOM photomineralization processes. For instance, it clearly appears that spatio-temporal variations in the water masses mixing regime would significantly modify both water column primary production and DIC photoproduction rates. On the contrary, changes in the atmospheric ozone amount, at least when considering short time scale estimations, would have a more restricted impact on these UV-dependent processes.

Chapter 5

Straightforward model for the estimation of UV inhibition of primary production estimation

In recent years, several straightforward methods have been proposed in order to reduce the computational time needed for the calculation of marine UV photochemical and photobiological effects at large scales (e.g. global) using for example a depth and/or spectrally resolved models:

- Weighted Transparency

  The concept of weighted transparency has been initially used to define an indicator of the effects of UVR in sub-arctic lakes through the description of the transmission of solar irradiance within the water column (Pienitz and Vincent 2000). Recently, this indicator has been shown to represent a potential effective tool for predicting phytoplankton primary production and UVR photoinhibition rates (Neale 2001; Lehmann et al. 2004).

  According to the recent works from Neale (2001), the rate of inhibition of photosynthesis induced by UVR can be related to the water column optical quality, through the calculation of the transparency for inhibiting irradiance (T_{PIR}, m) estimated using a formulation initially proposed by Pienitz and Vincent (2000) and modified by Cullen et al. (2001):

$$T_{PIR} = \sum_{290}^{395} \frac{1}{K_d(\lambda)} . \frac{\in(\lambda).E(\lambda,0)}{E^*_{inh}(0)} . \Delta\lambda \tag{5.1}$$

  In a similar manner, it is possible to define the transparency for PAR radiation which modulates the primary production rates (Pienitz and Vincent 2000): $T_{PAR} = 1/K_{PAR}$.

  Combining these parameters, Neale (2001) found a good correlation between the inhibition of water column production (Inh_z) and the product of the ratio between the transparencies for inhibiting irradiance and for PAR UV inhibition and PAR and surface inhibition (Inh_0):

$$Inh_z = Inh_0 . \frac{T_{PIR}}{T_{PAR}} \tag{5.2}$$

  More recently, Lehmann et al. (2004) have developed this approach on a synthetic dataset by defining a straightforward method for the assessment of the water column primary production

(with and without inhibition) as well as the relative rates of inhibition processes. For this purpose, the latter authors have defined two distinct weighted transparencies. The first one, $T^W_{PUR}(inm)$, corresponds to the transparency weighted for photosynthetically usable radiation (PUR):

$$T^W_{PUR} = \sum_{400}^{700} \frac{1}{K_d(\lambda)} . \frac{a_{ph}(\lambda)}{\bar{a}_{ph}} . \frac{E(0^-, \lambda)}{PAR(0^-)} . \Delta\lambda \tag{5.3}$$

where K_d is the diffuse attenuation coefficient (m^{-1}), $a_{ph}(\lambda)$ is the absorption coefficient of phytoplankton (m^{-1}), $\bar{a}_{ph}$ is the mean absorption of phytoplankton between 400 and 700 nm ($\bar{a}_{ph} = 1/301. \sum a_{ph}(\lambda)$), and $E(0^-, \lambda)$ and $PAR(0^-)$ are the surface spectral irradiance and integrated visible irradiance, respectively.

The second transparency parameter, $T^W_{PIR}(inm)$, corresponds to the weighted water transparency for photosynthesis-inhibiting radiations and which is equivalent to that proposed by Neale (2001):

$$T^W_{PIR} = \sum_{280}^{700} \frac{1}{K_d(\lambda)} . \in (\lambda) . E(0^-, \lambda) . \Delta\lambda \tag{5.4}$$

where $\in (\lambda)$ is the biological weighting function (BWF) describing the effectiveness of UVR for inhibiting primary production (in $(\mu\ molquanta.m^{-2}.s^{-1})^{-1}$).

T^W_{PIR} and T^W_{PUR} are then used to determine simple empirical parameterizations that predict the uninhibited (P^*_{opt}) and inhibited (P^*) phytoplankton primary production rates normalized by the product of biomass, and the maximum attainable rate of primary production per unit of biomass in the absence of photoinhibition (P^B_m, in $mgC[mg.chla]^{-1}.h^{-1}$, see equations 2.31, 2.32, 2.30). For a latitude of 45^oN at solar noon the obtained parameterizations are:

$$\begin{aligned} \int P^*_{opt} &= 2.91.(T^W_{PUR})^{1.09} \\ \int P^* &= 2.38.(T^W_{PUR})^{1.19}.(T^W_{PIR})^{-0.09} \\ \Delta P/P_{opt} &= 0.24.(T^W_{PUR})^{-1.08}.(T^W_{PIR})^{1.01} \end{aligned} \tag{5.5}$$

where $\Delta P/P_{opt} = 1 - \frac{\int P^*}{\int P^*_{opt}}$.

Similar relationships can be derived from our synthetic dataset, as illustrated by the good relationships obtained between T^W_{PUR} and normalized water column uninhibited P^*_{opt}, inhibited P^* primary production or between the T^W_{PUR}/T^W_{PIR} ratio and relative inhibition $\Delta P/P_{opt}$ rates (Figure 5.1). However, these relationships should account for a strong temporal dependence. For instance, T^W_{PUR} vs P^*_{opt} relationships vary strongly according to the hour of the day due to the fact that T^W_{PUR} is only weakly changing with time whereas P^*_{opt} increases with increasing irradiance, with the maximal production rates obtained at noon.

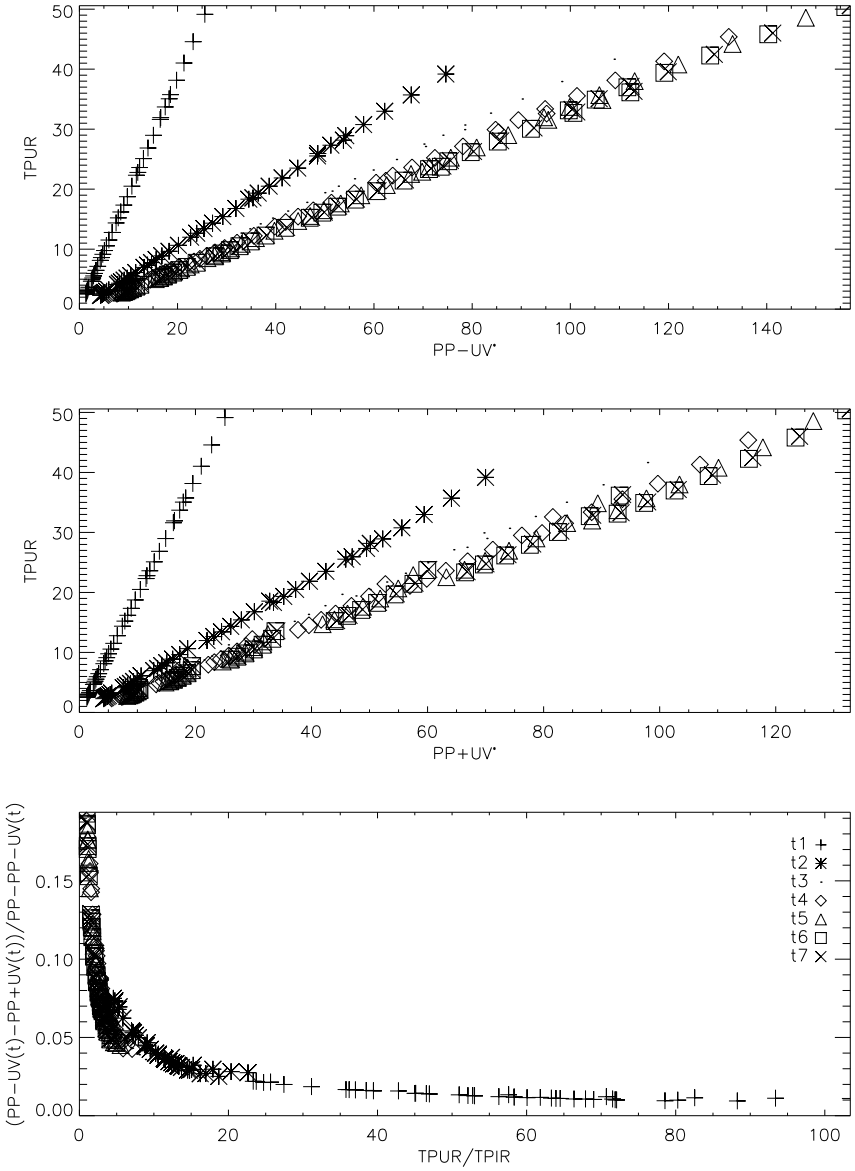

Figure 5.1: Relationship between TPUR and the inhibited and unhibited hourly production rates and between the PP inhibition rate and the TPIR/TPUR ratio considering the different time steps defined in the model from dawn to noon (t1 to t7).

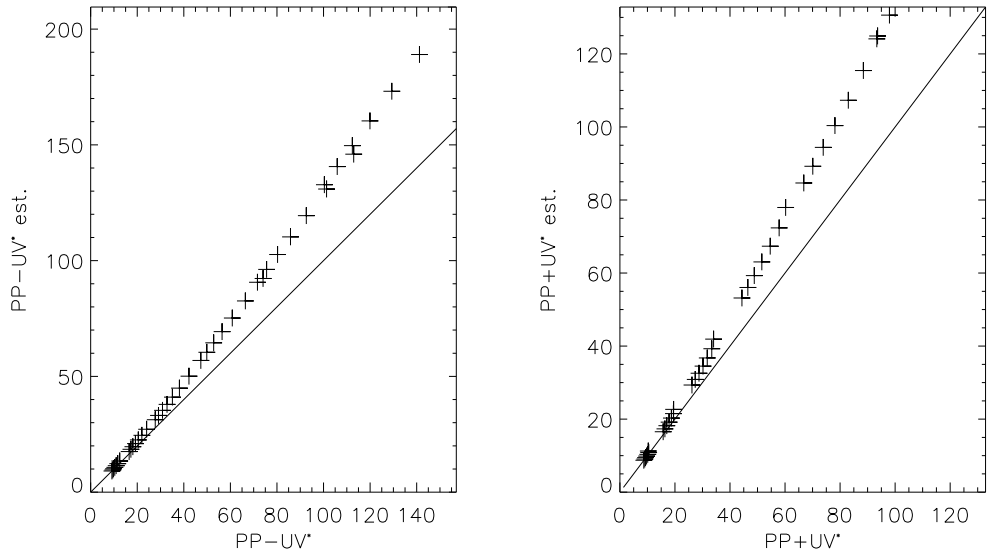

Figure 5.2: Comparison between the PP rate calculated and estimated from Lehmann et al. (2004) parameterization.

Further, the empirical functions used to predict P^*_{opt}, P^* rates are strongly constrained by the definition of the optical model used to construct the training dataset as underlined by the differences existing between the estimations of primary production rates obtained from Lehmann et al. (2004) parametrizations and those computed from our simulations with the same optical conditions (45^oN, at noon, Figure 5.2). This feature is further illustrated by the differences existing in the Zeu_{PUR} vs T^W_{PUR} relationships (Figure 5.4) considering our results and those from the latter authors.

Interestingly, a good agreement is found between our estimation of the relative inhibition of the water column and the results derived from the parameterization of Lehmann et al. (2004), at least if we restrict the comparison to the points corresponding to the same incident light conditions (at noon). This higher stability of the parameterization describing the relative inhibition rates might be explained by the fact that this parameter is not based on a single transparency but depends on the ratio between T^W_{PUR} and T^W_{PIR} as indicated by the values of the exponents in the equation 5.5 ($\approx$ 1 and -1 respectively). Conversely, the estimation of the uninhibited primary production rate is related to T^W_{PUR} only, while most of the variability in the inhibited primary production rate is also mainly explained by the T^W_{PUR} variability as indicated by the very low exponent for T^W_{PIR} (almost 0) in the equation 5.5.

As suggested by Lehmann et al. (2004) the water transparency approach could be used to predict any photobiological and/or photochemical effects of UVR for which spectral weighting functions exist. As a matter of fact, we applied the weighted transparency concept for estimating the DIC photochemical production rates. For this purpose, the corresponding water transparency (T^W_{DIC}) is defined by:

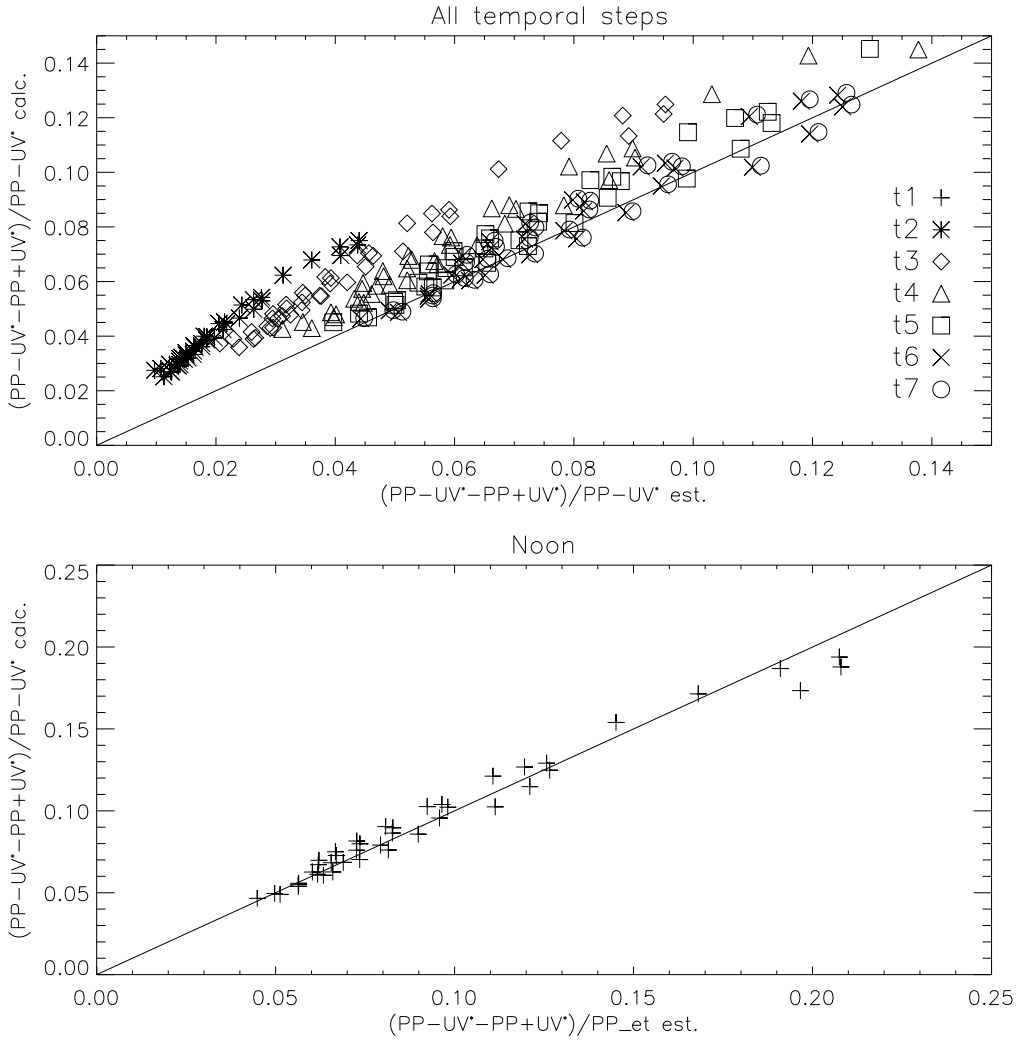

Figure 5.3: Comparison between the PP inhibition rate calculated and estimated from Lehmann et al. (2004) parameterization.

$$T^W_{DIC} = \sum_{\lambda min}^{\lambda max} \frac{1}{K_d(\lambda)} . AQY(\lambda) . E(0^-, \lambda) . \Delta\lambda \tag{5.6}$$

where $AQY(\lambda)$ is the quantum yield for the DIC production. In this example the AQY defined by Johannessen and Miller (2001) for oceanic waters has been considered. The spectral range of integration (from λmin to λmax) is defined by the experimental domain of application of the quantum yield (in this case from 280 to 480 nm). T^W_{DIC} values are then confronted to PDIC rates normalized by the CDOM absorption coefficient (at 412 nm).

Further, in the scope of the application of a photochemical model coupled to satellite remote sensing data, it could be interesting to relate the weighted DIC transparency to the DIC production of the water column at a single wavelength corresponding, in particular, to a SeaWiFS spectral band (e.g. 412 nm):

$$P^*_{DIC} = P_{DIC} / a_{CDOM}(412, 0^-) \tag{5.7}$$

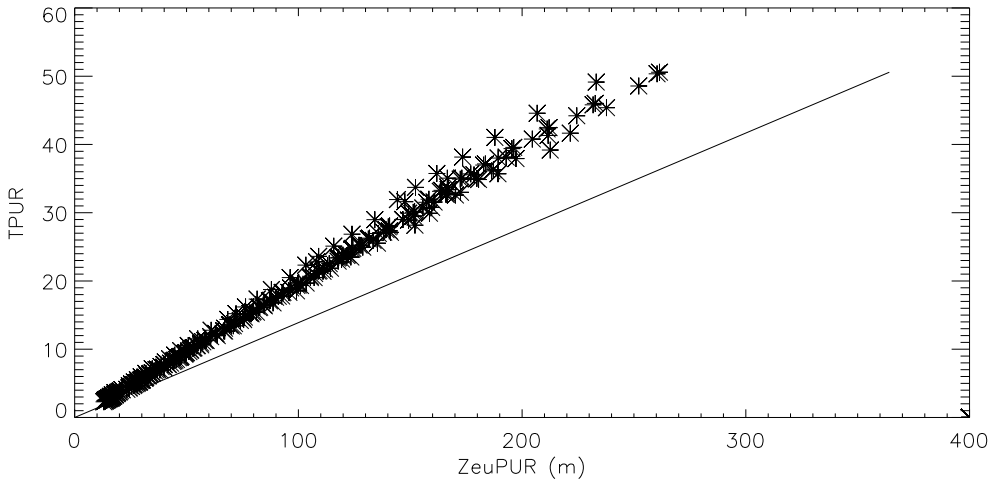

Figure 5.4: Relationship between ZeuPUR and the ZeuPAR/ZeuPUR ratio. The relationship defined by Lehman et al. (2004) is represented by the solid line.

$$T^W_{DIC}(412) = \frac{1}{K_d(412)}.AQY(412).E(0^-, 412) \tag{5.8}$$

A good agreement has been found between both T^W_{DIC} and $T^W_{DIC}(412)$ and P^*_{DIC} (Figure 5.5). This feature indicates that the use of the water transparency approach might provides satisfactory and rapid estimations of UV dependent photochemical processes.

- Fichot(2004) model

  Another straightforward approach has been recently proposed by Fichot (2004) for the estimation of CO production rates at global scale. This method aims to derive a single measure describing the rate of decrease of the CO photoproduction with depth from the surface rates.

  The general shape of CO (and/or DIC) daily production vertical profiles (Figure 3.8) seems to indicate that the production rates vertical decrease can be explained using a single exponential function. However, plotting the natural logarithm of DIC production profiles (Figure 5.6), it appears that the rate of the vertical decrease itself is also function of depth (Fichot 2004), as illustrated by the non-linearity of the curves in Figure 5.6. This feature, which occurs even for homogeneous very clear waters, is attributable to the variation of the relative contribution of each spectral domain to the total DIC (and CO) production rates with depth (see Figure 5.6). Based on these observations, Fichot (2004) proposed a relationship which takes into account this vertical dependence:

$$-ln\left(\frac{dPDIC(z)}{dPDIC(0^-)}\right) = \xi_{DIC}.z^2 + \Psi(0^-).z \tag{5.9}$$

  or

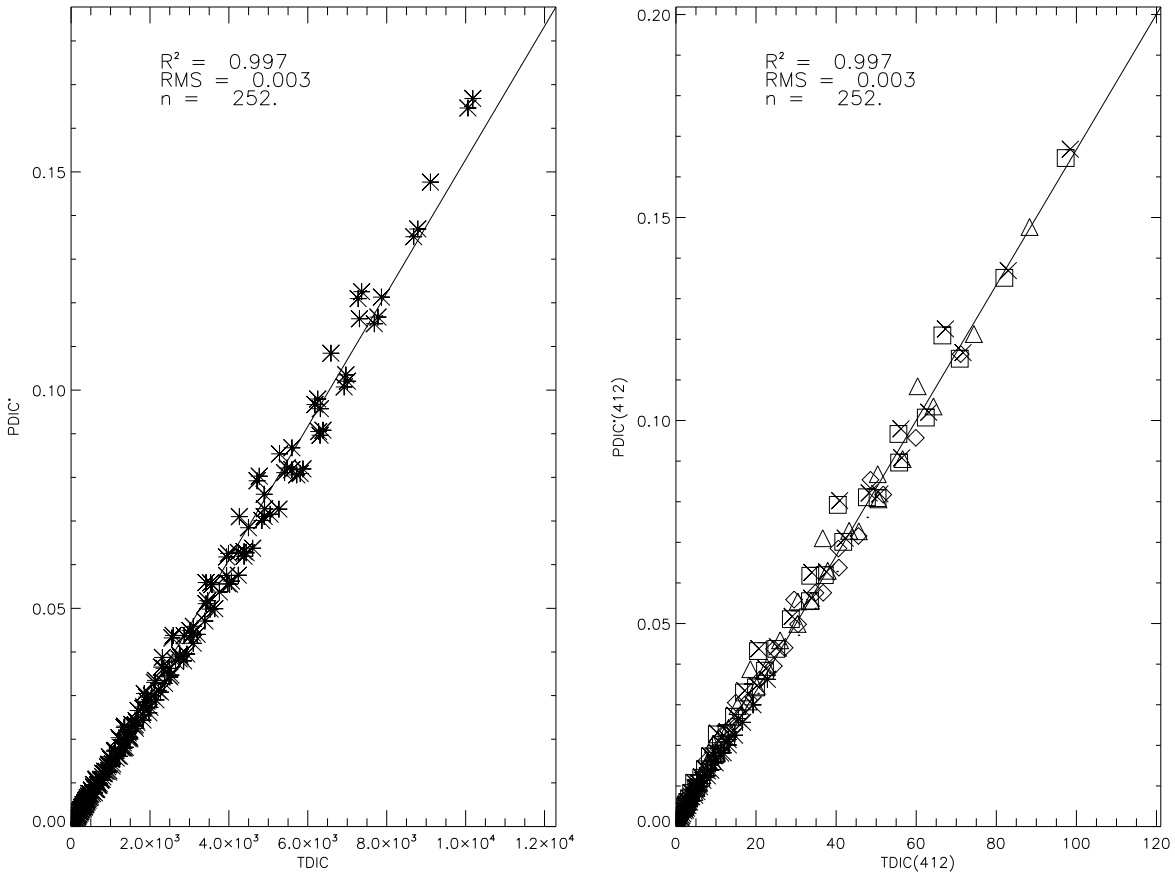

Figure 5.5: Relationships between $T^W_{DIC}(412)$ and $P^*_{DIC}(412)$ and between T^W_{DIC} and P^*_{DIC}.

$$dPDIC(z) = dPDIC(0^-).e^{-(\xi_{DIC}.z^2+\Psi(0^-).z)} \tag{5.10}$$

where ξ_{DIC} and $\Psi(0^-)$ are determined by a non-linear regression considering the ratio between the DIC production at a depth z vs the daily DIC production rate just below the surface of the sea $dPDIC(0^-)$.

The parameters of the regression ξ_{DIC} and $\Psi(0^-)$ vary according to the water mass loads in chl$a$ and CDOM (Figure 5.7 and 5.8), and thus according to the optical quality of the water body (Figure 5.9). As a matter of fact, Fichot (2004) demonstrated that ξ_{DIC} and $\Psi(0^-)$ can be well approximated from a single value of diffuse attenuation at 320 nm ($K_d(320)$, in m^{-1}). However, the use of a similar method for the retrieval of CO (or DIC) photoproduction rates is obviously constrained by the choice of the AQYs (Fichot 2004). In particularly, large variations in the spectral shape of the AQYs would be expected to have a strong influence on the final relationships (Figures 5.7 and 5.8).

Further, the performance of the parametrizations used for the description of DIC/CO production vertical profiles depends on the vertical layer considered in the regression analysis. Indeed, the consideration in the fit procedure of a very deep water column would induce a sharp decrease of the significance of the parameterization for the most productive surface layer by giving an important weight in the regression analysis to the deep (less productive) points (Figure 5.10).

Thus the application of this method should consider the variations in the thickness of the DIC "productive layer" by limiting, for example, the analysis to the UVA 1% penetration depth (Figure 5.10).

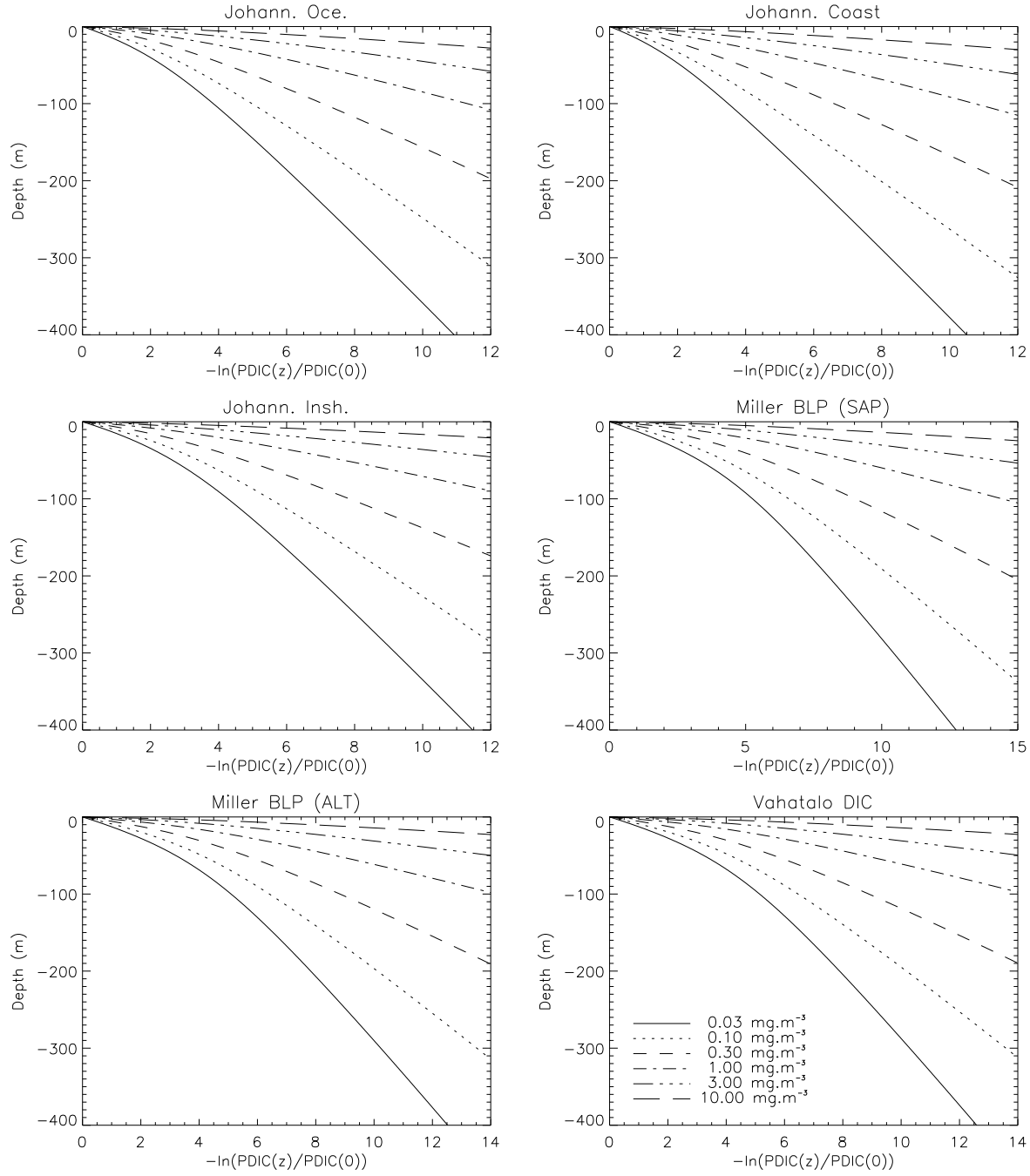

Figure 5.6: Decrease of the DIC production rates with depth for different water types and photomineralization models.

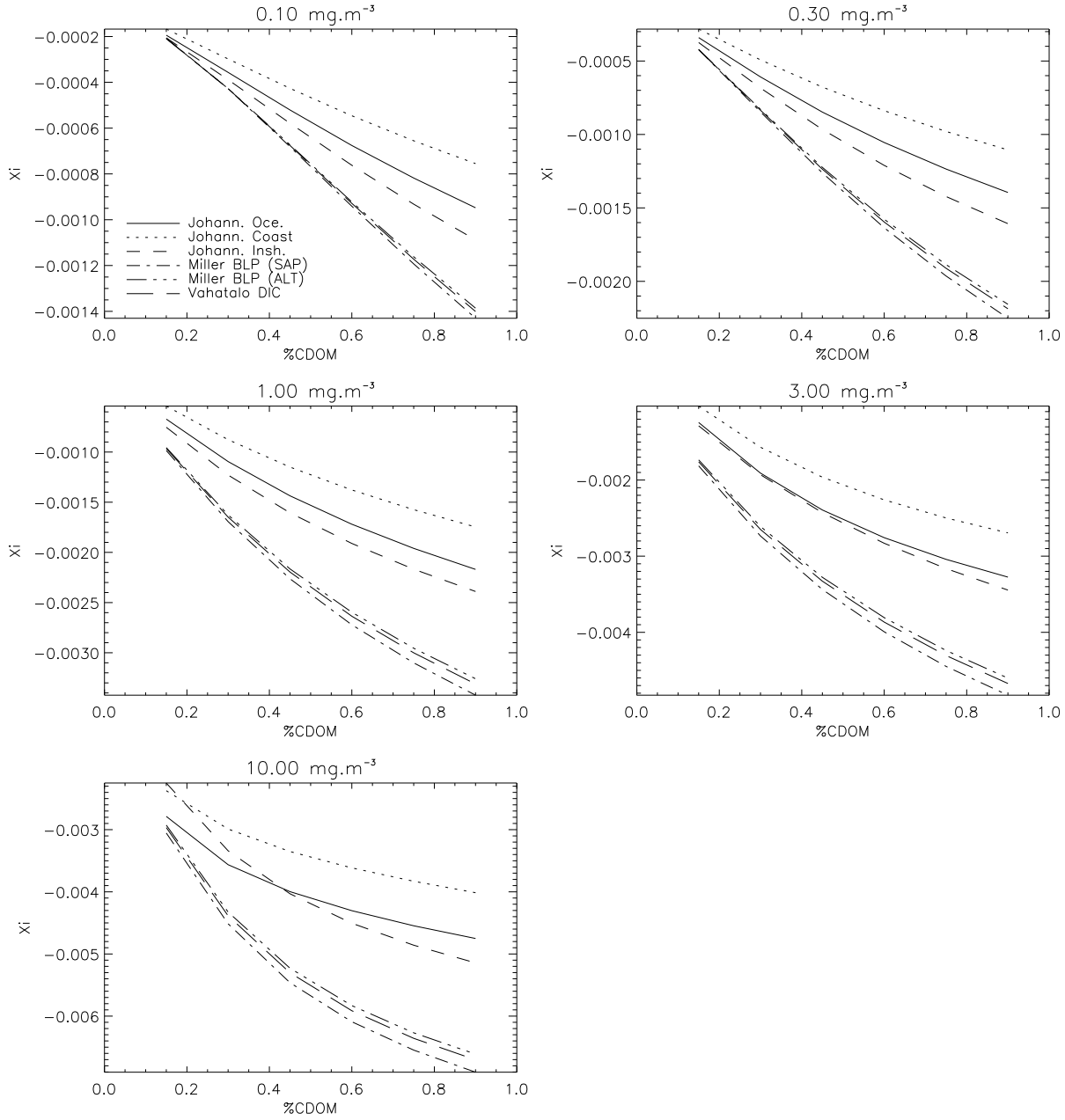

Figure 5.7: Dependence of ξ on model and water optical characteristics.

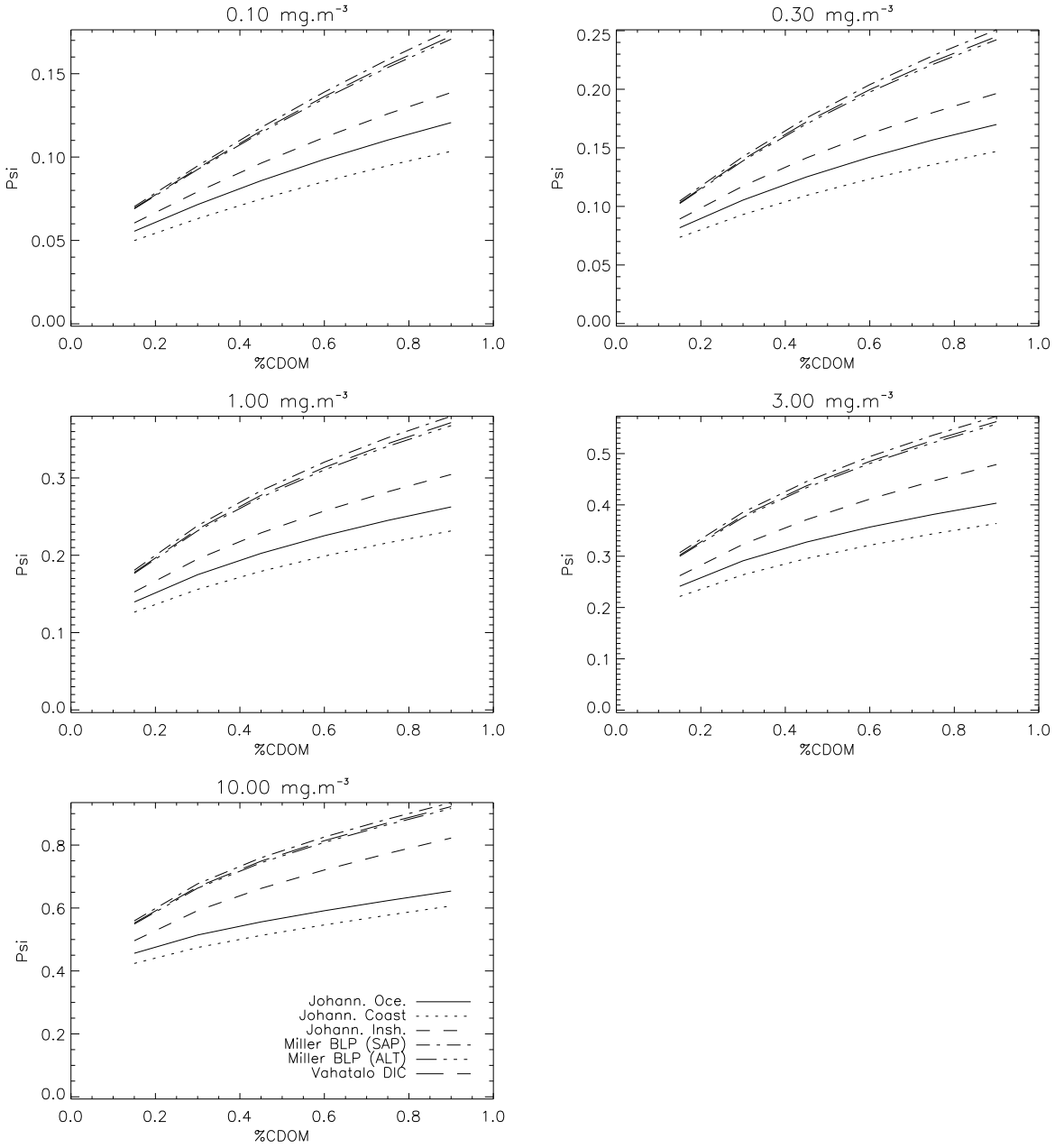

Figure 5.8: Dependence of Ψ on model and water optical characteristics.

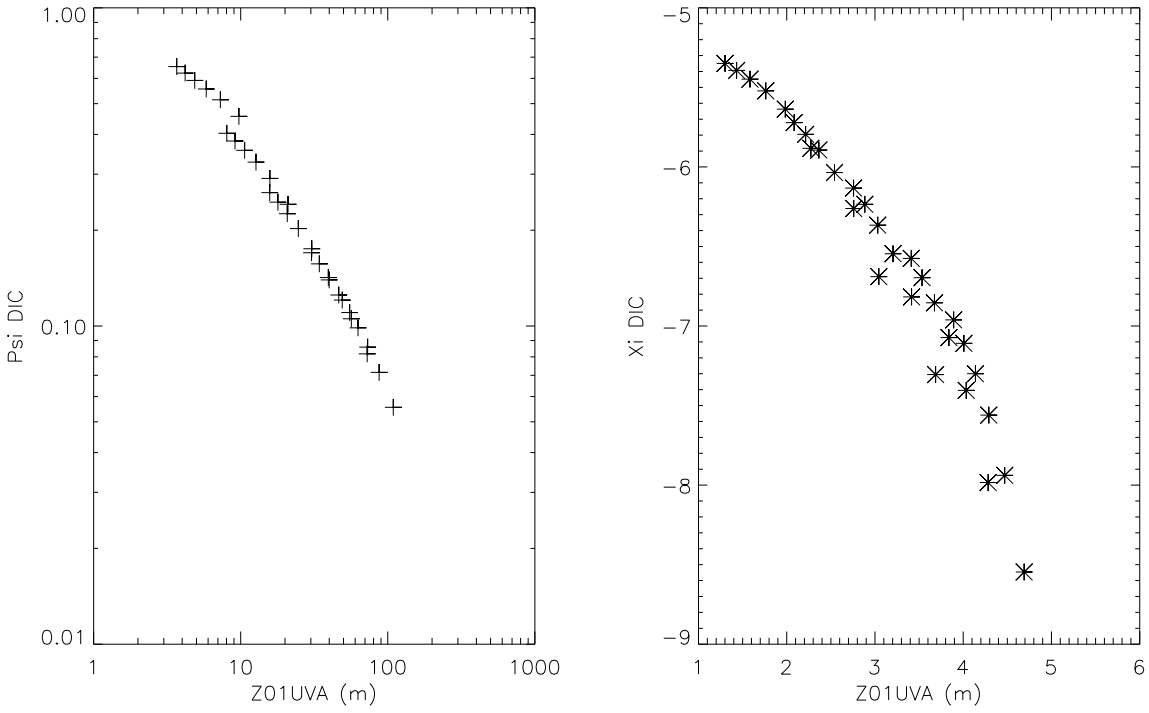

Figure 5.9: Relationship between Ψ and ξ and the 1% penetation depth of UVA radiation.

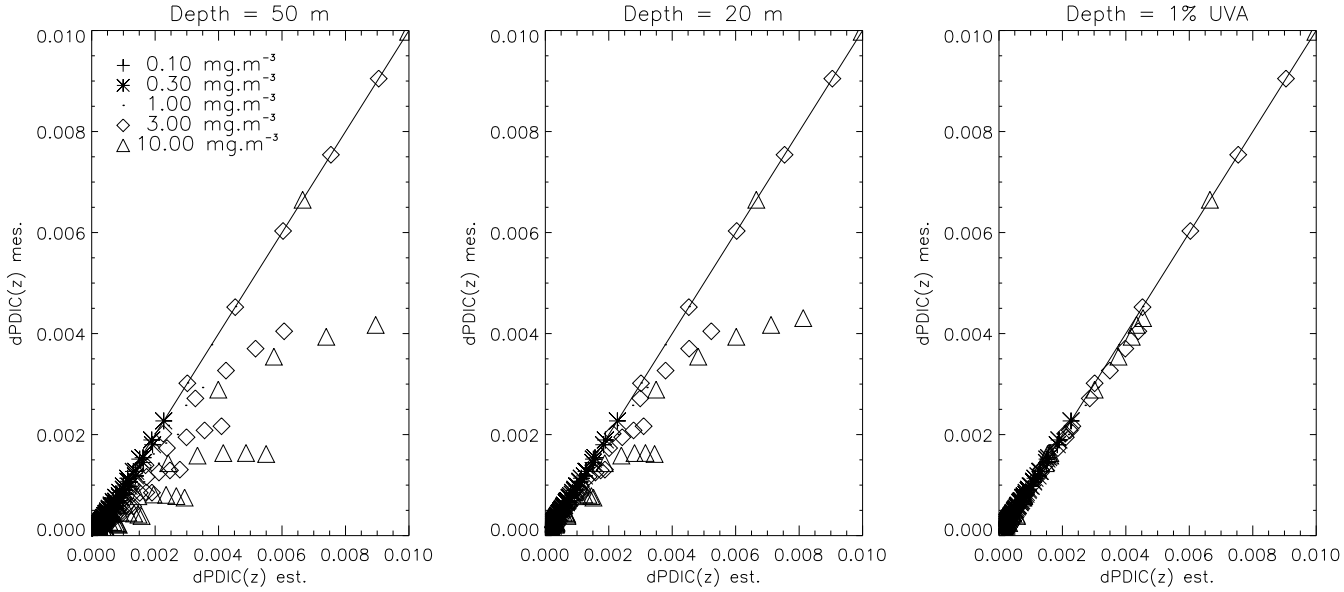

Figure 5.10: dPDIC(z) calculted vs dPDIC(z) estimated using Fichot (2004) parametrization applied to a water column layer of 20m, 50m or equal to the 1% UVA penetration depth.

Conclusions and future work

The objective of the research project is to derive, using the information provided by satellite remote sensing measurements, a distribution of visible and ultraviolet radiation in marine waters and to quantify, for selected basins, some of its biological and chemical impacts of relevance for the functioning of ecosystems and biogeochemical cycles.

In this context, the accurate assessment of CDOM distribution, and the understanding of the external factors driving its variability, are essential since this optically active component of seawater strongly influence the penetration of UVR in the water column that in turn is the central parameter of numerous UV-driven photochemical processes. Thus, the first objective of this report was to characterize, using a SeaWiFS archive recently produced for the period 1998-2004, the spatio-temporal variations of CDOM absorption coefficient (i.e. $a_{dg}(443)$) in the two test basins selected for this study: the Mediterranean Sea and subarctic Atlantic region. The variability existing in $a_{dg}(443)$ at both temporal and spatial scales can be related to the influence of various environmental forcings (hydrodynamics, water optical quality, incident irradiance) regulating the balance between photobleaching losses and CDOM sources (e.g. terrestrial and/or autochthonous). Moreover, the co-variation found in the two basins between $a_{dg}(443)$ and $a_{ph}(443)$ average values might indicate that CDOM is mainly originating from an *in situ* biological production. This result should be however characterized more precisely and further analyses will be undertaken on the satellite data archive by considering higher spatial and temporal resolutions. Moreover, it could be useful to evaluate the actual impact of photobleaching on CDOM turnover in the selected basins using, for instance, the model proposed by Del Vecchio and Blough (2002) which presents the advantage of considering explicitly both spectrally direct and indirect photobleaching processes. The relative contribution of the colored detrital material for the non-water absorption budget (i.e. the ratio $a_{dg}(443)$ / ($a_{dg}(443)$ + $a_{ph}(443)$) also vary spatially and seasonally. In general, the fact that in both the Mediterranean Sea and subarctic Atlantic region ($a_{dg}(443)$ / ($a_{dg}(443)$ + $a_{ph}(443)$) values are much greater than previously thought (more likely $\approx$ 60 % instead of 20 %, Prieur and Sathyendranath 1981; Morel 1991) is of a particular interest and will be considered for the definition of the ocean module of the model.

Furthermore, our results have provided clear evidence of the importance of both UV photochemical and photobiological effects for studying marine ecosystem functioning and biogeochemical cycle. In particular, the undersea UVR climate can dramatically influence the rate of carbon fixation by phytoplankton cells through photosynthesis by inducing a decrease of up to 25 % of the water column daily primary production. Conversely, the carbon released through photomineralization processes can represent a significant term in the global carbon cycle (Figure 5.11). At the global scale, annual DOC photomineralization processes (including CO and DIC photoproduction) are currently estimated to represent from 3% of the carbon fixed by primary production for the lowest estimates (Stubbins et al. 2006) to 10% (Mopper and Kieber 2000) or even 30% (Miller and Zepp 1995) for the highest estimates.

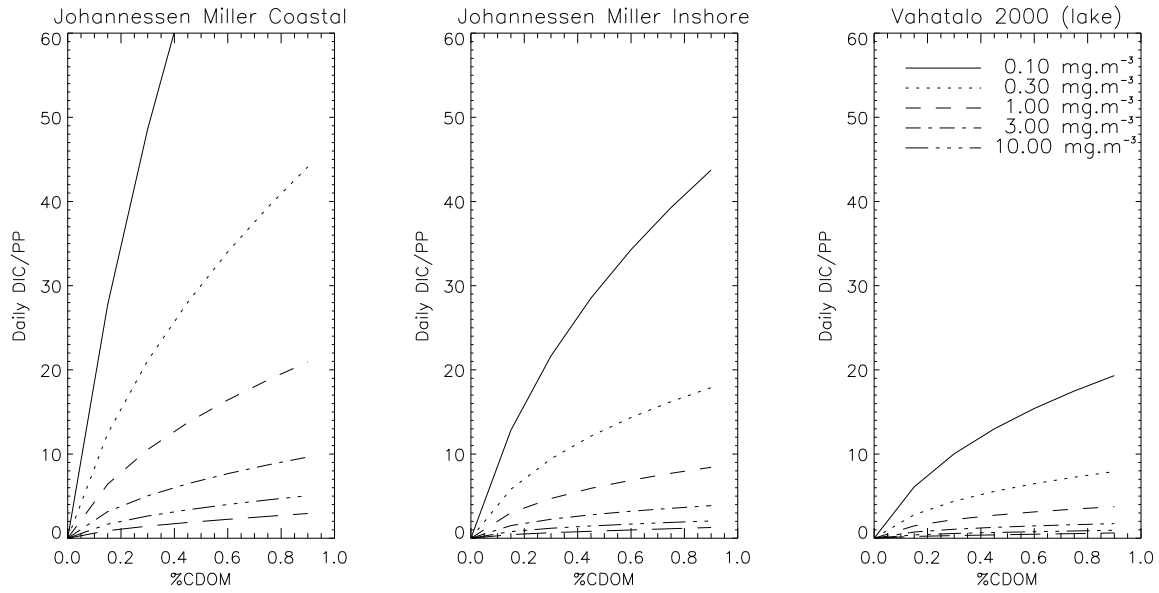

Figure 5.11: Comparison between the water column carbon fluxes from DIC photoproduction and primary production processes at the daily scale (in %).

In this report, we also underlined the main uncertainties related to the modelling of UV impacts on marine waters and therefore the current key aspects of the modelling efforts. The use of IOPs derived from satellite remote sensing techniques for modelling UV penetration depth and its selected impacts on marine ecosystems, entails a partition of the colored detrital matter absorption ($a_{dg}(\lambda) = a_{CDOM}(\lambda) + a_{NAP}(\lambda)$) leading to the determinatio of CDOM absorption . The vast majority of $a_{dg}(443)$ in the open ocean could be attributed to CDOM as already pointed out by previous studies at the global scale (e.g. Siegel et al. 2002, $\approx 81.7 \pm 13.7$ %). Our rough estimations of NAP contribution to $a_{dg}(443)$ are globally in agreement with the latter results. However, for the extremes cases NAP can account for 25% of $a_{dg}(443)$ in both selected basins. This would therefore lead to a significant overestimation of UV photomineralisation processes (e.g. approx 20% for a variation of CDOM percentage from 0.6 to 0.45 and a chl$a = 0.3\ mg.m^{-3}$ using Johannessen and Miller 2001, AQY for oceanic water). Note that some *in situ* measurements have indicated that the contribution of NAP for the $a_{dg}(443)$ coefficient can be substantially greater than the previous average value, representing up to 95 % of the colored detrital material in some coastal waters (see Bélanger et al. 2006 and references therein).

Diverse parameterizations have been recently developed in order to quantify the various effects of UVR on marine ecosystems, including its influence on bio-optical properties (i.e. CDOM photobleaching), photochemistry (i.e. DIC and CO photoproduction) and photobiology (primary production inhibition). All these functions (BWF and AQY), present a conservative pattern with photons from the shorter wavelengths having a greater efficiency for photosensitizing CDOM and/or for inhibiting photosynthesis than those at the longer wavelengths. However, the effective contribution of UVB, UVA and PAR radiations for these photo-dependent processes depend on the combination between photons efficiency and the water transparency for these radiations. As a matter of fact, UVA represents the main contributor to CDOM photomineralization processes. Conversely, the effective action of UVB is limited to the first meters of the water column, while a non negligible contribution of PAR irradiance for CDOM photo-oxidation processes has been identified. The latter feature underlines the importance of describing both UV and visible radiations with a common optical framework using the same forcing (the light field impinging on the ocean surface) and a common bio-optical model for the light propagation through the water column. The accurate description of how marine organisms and/or compounds respond to changes in the underwater light field (i.e. BWF and AQY) is obviously a crucial element for the quantification of the selected UV dependent processes. The choice of the AQY for DIC photoproduction rates seems to be particularly critical since the photon efficiency for producing DIC has been shown to vary widely according to CDOM origin and light history. However, the current scarcity of information on AQY variability according to changes in environmental forcing represents a major limitation for quantifying accurately this UV photochemical effect. Nevertheless, the actual knowledge on AQY for DIC production emphasizes the necessity to distinguish, in the context of modelling approaches, at least the coastal and oceanic waters since CDOM photolability for producing DIC shows clear discrepancies between these two marine domains.

Further, as already reported by numerous authors, the consideration of vertical mixing events represents a major challenge for deriving an accurate quantification of the UV impacts on marine ecosystems. Obviously, the ideal situation should be to develop a coupled physical-biological model allowing to reproduce precisely this environmental forcing. However, the current high uncertainties in AQY (including along the water column) need to be taken into account and reduced before the development of such a model is envisaged. A rough approximation could be to describe the DIC production within the mixed layer by its average value. However, instead of a simple arithmetic average it would be preferable to define a weighted mean taking into account the ratio between the UVA penetration depth and the MLD which seems to modulate the magnitude of the mixing effects.

However, the development of such parameterization would require additional knowledge on the MLD climatology and the vertical velocity at a regional scale.

Conversely, it seems that the current uncertainties on CDOM vertical distribution might be less limiting for the estimation of CDOM photomineralization processes, while the description of the water compounds (especially chl$a$) vertical structure is a key element for the estimation of the primary production rates. Moreover, abrupt changes in ozone concentration in the atmosphere would have only a restricted impact on the daily calculations.

Focusing on the optimization of the computational performance of the spectral and depth resolved model in the perspective of the estimation of UV photochemical and/or photobiological effects at large scale, we emphasized that a reasonable degradation of the spectral resolution could be envisaged with a limited impact on the model outputs. Conversely, the definition of the vertical resolution in the ocean module is critical since its degradation might induce severe biases in the calculations of the daily primary production and CDOM photomineralization rates. A practical approach could be to consider vertical steps varying with depth. Indeed, a high vertical resolution is needed for the description of the UV dependent processes in the first tens of meters of the water column while it is less so in the deep waters. The significant relationships found between the penetration depth and the thickness of the productive layer for DIC photomineralization processes (Z(90%)DIC) might be helpful to determine an appropriated decision criterion.

Finally, the various straightforward methods recently proposed in the literature to derive the UV impacts on marine waters could eventually represent an interesting alternative modelling approach. Indeed, coupling these models to satellite remote sensing information (e.g. $K_d(412)$) might provide rapid estimations of water column DIC photoproduction rates in particular. However, the robustness of these models should be examined more precisely considering larger changes in both atmospheric (i.e. cloudiness) and marine water characteristics.

List of Figures

List of Tables

References

Banaszak, A. and P. Neale (2001). Ultraviolet radiation sensitivity of photosynthesis in phytoplankton from an estuarine environment. *Limnol. Oceanogr., 46*, 592–603.

Barbieri, E., V. Villafañe, and E. Helbling (2002). Experimental assessment of UV effects upon temperate marine phytoplankton when exposed to variable radiation regimes. *Limnol. Oceanogr., 45*, 1648–1655.

Behrenfeld, M., J. Chapman, J. Hardy, and H. Lee (1993). Is there a common response to ultraviolet-B by marine phytoplankton ? *Mar. Ecol. Prog. Ser., 102*, 59–68.

Bélanger, S., M. Babin, H. Xie, N. Krotkov, P. Larouche, and F. Vincent (2006). CDOM photooxidation in the Arctic coastal waters: new approach using satellite informations and implications of climate change. In *Proc. Ocean Optics XVIII*, pp. Digital media.

Belzile, C., S. Demers, D. Lean, B. Mostajir, S. Roy, S. DeMora, D. Bird, M. Gosselin, J. Chanut, and M. Levasseur (1998). An experimental tool to study the effects of ultraviolet radiation on planktonic communities: a mesocosm approach. *Environ. Technol., 19*, 667–682.

Bertilsson, S. and L. Tranvik (2000). Photochemical transformation of Dissolved Organic Matter in Lakes. *Limnol. Oceanogr., 45*, 753–762.

Blough, N. and R. Del Vecchio (1995). Reactive oxygen species in natural waters. In C. Foote, J. Valentine, A. Greenberg, and L. J.F. (Eds.), *Active oxygen in chemistry*, pp. 280–333. Chapman and Hall, New York.

Boelen, P., M. de Boer, G. Kraay, M. Veldhuis, and A. Buma (2000). UVBR-induced DNA damage in natural marine picoplankton assemblages in the tropical Atlantic Ocean. *Mar. Ecol. Prog. Ser., 193*, 1–9.

Boss, E., M. Twardowski, and S. Herring (2001). Shape of the particulate beam attenuation spectrum and its inversion to obtain the shape of the particulate size distribution. *Appl. Opt., 40*, 4885–4893.

Boucher, N. and B. Prézelin (1996). An in situ biological weighting function for UV inhibition of phytoplankton carbon fixation in the Southern Ocean. *Mar. Ecol. Prog. Ser., 144*, 223–236.

Bouillon, R.-C. and W. Miller (2004). Determination of apparent quantum yield spectra of DMS photodegradation in an in situ iron-induced Northeast Pacific Ocean bloom. *Geophys. Res. Lett., 31*, L06310, 10.1029/2004GL019536.

Bricaud, A., A. Morel, M. Babin, K. Allali, and H. Claustre (1998). Variations of light absorption by suspended particles with chlorophyll *a* concentration in oceanic (case 1) waters: analysis and implications for bio-optical models. *J. Geophys. Res., 103*, 31033–31044.

Bushaw, K. L., R. G. Zepp, M. A. Tarr, D. Schulz-Jander, R. A. Bourbonniere, R. E. Hodson, W. L. Miller, D. A. Bronk, and M. A. Moran (1996). Photochemical release of biologically available nitrogen from dissolved organic matter. *Nature, 381*, 404–407.

Carder, K., F. Chen, Z. Lee, S. Hawes, and D. Kamykowski (1999). Semianalytic Moderate-Resolution Imaging Spectrometer algorithms for chlorophyll *a* and absorption with bio-optical domains based on nitrate-depletion temperatures. *J. Geophys. Res., 104*, 5403–5421.

Carder, K., R. Steward, G. Harvey, and P. Ortner (1989). Marine humic and fulvic acids: Their effect on remote sensing of ocean chlorophyll. *Limnol. Oceanogr., 34*, 68–81.

Charlson, R., J. Lovelock, M. Andreae, and S. Warren (1987). Oceanic phytoplankton, atmospheric sulphur, cloud albedo and climate. *Nature, 326*, 655–661.

Cullen, J., R. Davis, Y. Huot, and J. Lehmann (2001). Quantifying effects of ultraviolet radiation in surface waters. In *Ocean Optics: Remote sensing and underwater imaging*. Gilbert, G.D. and Frouin, R.J.

Cullen, J. and M. Lesser (1991). Inhibition of photosynthesis by ultraviolet radiation as a function of dose and dosage rate: Results for a marine diatom. *Mar. Biol., 111*, 183–190.

Cullen, J. and P. Neale (1997a). Biological weighting functions for describing the effects of ultraviolet radiation on aquatic sytems. In Häder, D.P. (Ed.), *The effects of ozone depletion on aquatic ecosystems*, Chapter 6, pp. 97–118. Environ. Intell. Unit, Academic Press and Landes, R.G. Company, Austin, TX.

Cullen, J. and P. Neale (1997b). Effects of ultraviolet radiation on shot-term photosynthesis of natural phytoplankton. *J. Photochem. Photobiol., 65*, 264–266.

Cullen, J., P. Neale, and M. Lesser (1992). Biological weighting function for the inhibition of phytoplankton photosynthesis by ultraviolet radiation. *Science, 258*, 646–650.

Del Vecchio, R. and N. Blough (2002). Photobleaching of chromophoric dissolved organic matter in natural waters: kinetics and modeling. *Mar. Chem., 78*, 231–253.

Del Vecchio, R. and N. Blough (2004). Spatial and Seasonal distribution of chromophoric dissolved organic matter and dissolved organic carbon in the Middle Atlantic Bight. *Mar. Chem., 89*, 169–187.

Donkor, V. and D. Häder (1996). Effects of ultraviolet irradiation on photosynthetic pigments in some filamentous cyanobacteria. *Aquat. Microb. Ecol. 11*, 143–149.

Farmer, D. and C. McNeil (1999). Photoadaptation in convective layer. *Deep-Sea Res., 46*, 2433–2446.

Fichot, C. (2004). *Marine Photochemistry from space*, pp. 217. Dalhousie University, Halifax, Nova Scotia, Canada: PhD Thesis.

Field, C., M. Behrenfeld, J. Randerson, and P. Falkowski (1998). Primary production of the biosphere: integrating terrestrial and oceanic components. *Science, 281*, 237–240.

Frenette, J.-J., S. Demers, L. Legendre, and J. Dodson (1993). Lack of agreement among models for estimating the photosynthetic parameters. *Limnol. Oceanogr., 38*, 679–687.

Furgal, J. and R. Smith (1997). Ultraviolet radiation and photosynthesis by Georgian Bay phytoplankton of varying nutrient and photoadaptative status. *Can. J. Fish. Aquat. Sci., 54*, 1659–1667.

Gallegos, C., T. Platt, W. Harrison, and B. Irwin (1998). Factors influencing photoreactions of dissolved organic matter in a coastal river of the southeastern United States. *Environ. Sci. Tech. 32*, 2940–2946.

Goldstone, J., R. Del Vecchio, N. Blough, and M. Voelker (2004). A multicomponent model of chromophoric dissolved organic matter photobleaching. *J. Photochem. Photobiol., 80*, 52–60.

Granéli, E., L. M., and L. Tranvik (1996). Photo-oxidative production of dissolved inorganic carbon in lakes of different humic content. *Limnol. Oceanogr., 41*, 698–706.

Häder, D., H. Kumar, R. Smith, and R. Worrest (1998). Effects on aquatic ecosystems. *J. Photochem. Photobiol. 46*, 53–68.

Han, B., M. Virtanen, J. Koponen, and M. Strakraba (2000). Effect of photoinhibition on algal photosynthesis: a dynamic model. *J. Plank. Res., 22*, 865–885.

Helbling, E., A. Buma, M. de Boer, and V. Villafañe (2001). In situ impact of solar ultraviolet radiation on photosynthesis and DNA in temperate marine phytoplankton. *Mar. Ecol. Prog. Ser., 211*, 43–49.

Helbling, E., V. Villafañe, and O. Holm-Hansen (1994). Effects of ultraviolet radiation on antarctic marine phytoplankton photosynthesis with particular attention to the influence of mixing. In C. Weiler and P. Penhale (Eds.), *Ultraviolet Radiation in Antarctica: Measurements and Biological Effects*, pp. 187–206. Antarctic Research Series.

Hernandom, M. and G. Ferreyra (2005). The effects of UV radiation on photosynthesis in a Antarctic diatom (*Thalassiosira sp.*): Does vertical mixing matter ? *J. Exp. Mar. Biol. Ecol., 325*, 35–45.

Herndl, G., G. Muller-Niklas, and J. Frick (1993). Major role of ultraviolet-B in controlling bacterioplankton growth in the surface layer of the ocean. *Nature, 361*, 717–719.

Højerslev, N. and E. Aas (1991). A relationship for the penetration of ultraviolet B radiation into the Norwegian Sea. *J. Geophys. Res., 96*, 17003–17005.

Hu, C., Z. Lee, F. Muller-Karger, K. Carder, and J. Walsh (2006). Ocean color reveals phase shift between marine plants and yellow sustance. *IEEE Geosci. and Remote. Sens. Lett., 3*, 262–266.

Jassby, A. and T. Platt (1976). The relationship between photosynthesis and light for natural assemblages of marine phytoplankton. *J. Mar. Res., 12*, 421–430.

Johannessen, S. C. and W. L. Miller (2001). Quantum yield for the photochemical production of dissolved inorganic carbon in seawater. *Mar. Chem., 76*, 271–283.

Kieber, D., J. McDaniel, and K. Mopper (1989). Photochemical source of biological substrates in sea water - Implications for carbon cycling. *Nature, 341*, 637–639.

Kieber, D., X. Zhou, and K. Mopper (1990). Formation of carbonyl compounds from UV-induced photdegradation of humic substances in natural waters: fate of riverine carbon in the sea. *Limnol. Oceanogr., 35*, 1503–1515.

Kirk, J. (1994). *Light and Photosynthesis in aquatic ecosystems 2nd Edition*, pp. 509. New York: Cambridge University Press.

Köhler, J., M. Schmitt, H. Krumbeck, M. Kapfer, E. Litchman, and P. Neale (2001). Effects of UV on carbon assimilation of phytoplankton in a mixed water column. *Aquat. sci., 63*, 414–422.

Kudela, R. (2000). A photochemical sink for dissolved organic carbon in the ocean. *PhD dissertation, Dalhousie University*.

Lee, Z., K. Carder, and R. Arnone (2002). Deriving inherent optical properties from water color: a multiband quasi-analytical algorithm for optically deep waters. *Appl. Opt., 41*, 5755–5772.

Lehmann, M., R. Davis, Y. Huot, and J. Cullen (2004). Spectrally weighted transparency in models of water-column photosynthesis and photoinhibition by ultraviolet radiation. *Mar. Ecol. Prog. Ser., 269*, 101–110.

Lesser, M., J. Cullen, and P. Neale (1994). Carbon uptake in a marine diatom during acute exposure to ultraviolet B radiation: relative importance of damage and repair. *J. Phycol., 30*, 183–192.

Lewis, M., E. Horne, J. Cullen, N. Oakey, and T. Platt (1984). Turbulent motions may control phytoplankton photosynthesis in the upper ocean. *Nature, 311*, 49–50.

Longhurst, A. (1995). Seasonal cycles of pelagic production and consumption. *Prog. Oceanogr., 36*, 77–167.

Mélin, F., J.-F. Berthon, and G. Zibordi (2007). Assessment of satelite ocean color products at a coastal site. *Remote Sens. Environ., Accepted*.

Mélin, F. and N. Hoepffner (2004). Global marine primary production: a satellite review. In *Publication EUR*, No 21084, pp. 1–210. JRC Report.

Mengelt, C. and B. Prézelin (2005). UVA enhancement of carbon fixation and resilience to UV inhibition in the genus Pseudo-nitzschia may provide a competitive advantage in the UV surface waters. *Mar. Ecol. Prog. Ser., 301*, 81–93.

Miller, W. and M. Moran (1997). Interaction of photochemical and microbial processes in the degradation of refractory dissolved organic matter from a coastal marine environment. *Limnol. Oceanogr., 42*, 1317–1324.

Miller, W., M. Moran, W. Sheldon, R. Zepp, and S. Opsahl (2002). Determination of apparent quantum yield spectra for the formation of biologically labile photoproducts. *Limnol. Oceanogr., 47*, 343–352.

Miller, W. and R. Zepp (1995). Photochemical production of dissolved inorganic carbon from terrestrial organic matter: Significance to the oceanic organic carbon cycle. *Geophys. Res. Lett., 22*, 417–420.

Moore, C., C. Farmer, and R. Zika (1993). Influence of the Orinoco River on hydrogen-peroxide distribution and production in the eastern Caribbean. *J. Geophys. Res., 98*, 2289–2298.

Mopper, K. and D. Kieber (2000). *Marine photochemistry and its impact on carbon cycling*. New York: Cambridge Environmental Chemistry Series vol. 10 Cambridge University Press.

Moran, M. and R. Zepp (1997). Role of photoreactions in the formation of biologically labile compounds from dissolved organic matter. *Limnol. Oceanogr., 42*, 1307–1316.

Morel, A. (1991). Light and marine photosynthesis: a spectral model with geochemical and climatological implications. *Prog. Oceanogr., 26*, 263–306.

Morel, A. and J.-F. Berthon (1989). Surface pigments, algal biomass profiles and potential production of the euphotic layer: Relationships reinvestigated in view of remote sensing applications. *Limnol. Oceanogr., 34*, 1545–1562.

Morris, D. and B. Hargreaves (1997). The role of photochemical degradation of dissolved organic carbon in regulating the UV transparency of three lakes on the Pocono Plateau. *Limnol. Oceanogr., 42*, 239–249.

Morrison, J. and N. Nelson (2004). Seasonal cycle of phytoplankton UV absorption at the Bermuda Atlantic Time-series Study (BATS) site. *Limnol. Oceanogr., 49*, 215–224.

Neale, P. (2000). Spectral weighting functions for quantifying effects of UV radiation in marine ecosystems. In deMora, S.J. and Demers, S. and Vernet, M. (Ed.), *The effects of UV radiation on marine ecosystems*, pp. 72–100. Cambridge Univ. Press.

Neale, P. (2001). Modeling the effects of ultraviolet radiation on estuarine phytoplankton production: impact of variations in exposure and sensitivity to inhibition. *J. Photochem. Photobiol. B, 62*, 1–38.

Neale, P., A. Banaszak, and C. Jarriel (1998a). Ultraviolet sunscreeens in Gymnodinium sanguineum (Dinophyceae): Mycosporine-like amino acids protect against inhibition of photosynthesis. *J.Phycol. 34*, 928–938.

Neale, P., J. Cullen, and R. Davis (1998b). Photoinhibition and the diurnal variation of phytoplankton photosynthesis. I. Development of a photosynthesis-irradiance model from studies of in situ responses. *Limnol. Oceanogr., 43(3)*, 433–448.

Neale, P., J. Fritz, and R. Davis (2001). Effects of UV on photosynthesis of Antarctic phytoplankton: models and their application to coastal and pelagic assemblages. *Rev. Chil. Hist. Nat., 74*, 1–16.

Neale, P. and D. Kieber (2000). Assessing biological and chemical effects of UV in the marine environment: Spectral weighting functions. In Hester, R. E. and Harrison, R. M. (Ed.), *Causes and Environmental Implications of Increased UV-B Radiation*, pp. 61–83. Issues in Environmental Science and Technology, Royal Society of Chemistry.

Nelson, N., D. Siegel, and A. Michaels (1998). Seasonal dynamics of colored dissolved material in the Sargasso Sea. *Deep-Sea Res., I, 45*, 931–957.

Oliver, R., J. Whittington, Z. Lorenz, and I. Webster (2003). The influence of vertical mixing on the photoinhibition of variable chlorophyll a fluorescence and its inclusion in a model of phytoplankton photosynthesis. *J. Plank. Res., 25-9*, 1107–1129.

Osburn, C., H. Zagarese, D. Morris, B. Hargreaves, and W. Cravero (2001). Calculation of spectral weighting functions for the solar photobleaching of chromophoric dissolved organic matter in temperate lakes. *Limnol. Oceanogr., 46(6)*, 1455–1467.

Oubelkheir, K., H. Claustre, M. Babin, and A. Sciandra (2005). The comparative bio-optical and biogeochemical properties of contrasted trophic regimes. *Limnol. Oceanogr., 50*, 1795–1809.

Pienitz, R. and W. Vincent (2000). Effect of climate change relative to ozone depletion on UV exposure in subarctic lakes. *Nature, 404*, 484–487.

Platt, T., C. Gallegos, and W. Harrison (1980). Photoinhibition of photosynthesis in natural assemblages of marine phytoplankton. *J. Mar. Res., 38*, 687–701.

Prezelin, B., N. Boucher, and R. Smith (1994). *Marine primary production under the influence of the Antarctic ozone hole: Icecolors'90*, pp. 159–186. Weiler, C.S. Penhale, P.A. Ultraviolet radiation and bilogical research in Antarctica.

Prieur, L. and S. Sathyendranath (1981). An optical classification of coastal and oceanic waters based on the specific absorption of phytoplankton pigments, dissolved organic matter, and other particulate materials. *Limnol. Oceanogr., 26*, 671–689.

Rhode, S., M. Pawlowski, and R. Tollrian (2001). The impact of ultraviolet radiation on the vertical distribution of zooplankton of the genus Daphnia. *Nature, 412*, 69–72.

Roy, S. (2000). Strategies for the minimisation of UV-induced damage. In deMora, S.J. and Demers, S. and Vernet, M. (Ed.), *The effects of UV radiation on marine ecosystems*, pp. 72–100. Cambridge Univ. Press.

Siegel, D., S. Maritorena, N. Nelson, M. J. Behrenfeld, and C. McClain (2005). Colored dissolved organic matter and its influence on the satellite-based characterisation of the ocean biosphere. *Geophys. Res. Lett., 32*, L20605:doi,10.1029/2005GL024310.

Siegel, D., S. Maritorena, N. Nelson, D. Hansell, and M. Lorenzi-Kayser (2002). Global distribution and dynamics of colored dissolved and detrital organic materials. *J. Geophys. Res., 107*, 3228, 10.1029/2001JC000965.

Simó, R. and C. Pedrós-Alió (1999). Role of vertical mixing in controlling the oceanic production of dimethyl sulphide. *Nature, 402*, 396–399.

Sinha, R. and D. Häder (2002). Life under solar UV radiation in aquatic organisms. *Adv. Space Res. 30*, 1547–1556.

Smith, E. (1936). Photosynthesis in relation to light and carbon dioxide. *Proc. Natl. Acad. Sci. U.S., 22*, 504–511.

Stubbins, A., G. Uher, C. Law, K. Mopper, C. Robinson, and R. Upstill-Goddard (2006). Open-ocean carbon monoxide photoproduction. *Deep-Sea Res. II, 53*, 1695–1705.

Toole, D. A., D. Kieber, R. Kiene, D. Siegel, and N. Nelson (2003). Photolysis and the dimethylsulfide (DMS) summer paradox in the Sargasso Sea. *Limnol. Oceanogr., 48*, 1088–1100.

Traykovski, L., W. Miller, and H. Sosik (2002). A new approach to evaluating spatial variability of photochemistry based on characterization of optical water types from satellites. In *Proc. Ocean Optics XVI*.

Twardowski, M. and P. Donaghay (2002). Photobleaching of aquatic dissolved organic materials: absorption removal, spectral alteration and their interrelationship. *J. Geophys. Res., 107*, 6.1–6.12.

Uitz, J., H. Claustre, A. Morel, and S. Hooker (2006). Vertical distribution of phytoplankton communities in open ocean: an assessment based on surface chlorophyll. *J. Geophys. Res., 111*, C08005, doi:10.1029/2005JC003207.

Vähätalo, A., M. Salkinoja-Salonen, P. Taalas, and K. Salonen (2000). Spectrum of the quantum yield for photochemical mineralization of dissolved organic carbon in a humic lake. *Limnol. Oceanogr., 45*, 664–676.

Vähätalo, A., K. Salonen, E. Saski, and M. Salkinoja-Salonen (2002). Bleaching of color of kraft pulp mill effluents and natural organic matter in lakes. *Can. J. Fish. Aquat. Sci., 59*, 808–818.

Vähätalo, A. and R. Wetzel (2004). Photochemical and microbial decomposition of chromophoric dissolved organic matter during long (months-years) exposures. *Mar. Chem., 89*, 313–326.

Vantrepotte, V. and F. Mélin (2006). UV penetration in the water column. In *Publication EUR*, No 22217, pp. 1–67. JRC Report.

Vasilkov, A., J. Herman, Z. Ahmad, M. Kahru, and B. Mitchell (2005). Assessment of the ultraviolet radiation field in ocean waters from space-based measurements and full radiative-transfer calculations. *Appl. Opt., 44*, 2863–2869.

Vasilkov, A., J. Herman, N. Krotkov, M. Kahru, B. Mitchell, and H. C. (2002). Problems in assessment of the ultraviolet penetration into natural waters from space-based measurements. *Opt. Eng. 41*, 3019–3027.

Vernet, M. (2000). Effects of UV radiation on the physiology and ecology of marine phytoplankton. In deMora, S.J. and Demers, S. and Vernet, M. (Ed.), *The effects of UV radiation on marine ecosystems*, pp. 237–278. Cambridge Univ. Press.

Vernet, M., E. Brody, O. Holm-Hansen, and B. Mitchell (1994). The response of Antarctic phytoplankton to ultraviolet light: absorption, photosynthesis and taxonomic composition. In

C. Weiler and P. Penhale (Eds.), *Ultraviolet Radiation in Antarctica: Measurements and Biological Effects*, pp. 143–158. Antarctic Research Series.

Vodacek, A., N. Blough, M. DeGrandpre, E. Peltzer, and R. Nelson (1997). Seasonal variations of CDOM and DOC in the Middle Atlantic Bight: Terrestrial inputs and photooxydation. *Limnol. Oceanogr., 42*, 674–686.

Webb, W., M. Newton, and D. Starr (1974). Carbon dioxide exchange of *Alnus rubra*: A mathematical model. *Oecologia, 17*, 281–291.

Weiss, P., S. Andrews, J. Johnson, and O. Zafiriou (1995). Photoproduction of carbonyl sulfide in South Pacific Ocean waters as a function of irradiance wavelength. *Geophys. Res. Lett., 22*, 215–218.

White, E., D. Kieber, and K. Mopper (2006). Photochemical mineralization of chromophoric dissolved organic matter in seawater. *Solas News 3*, 9.

Whitehead, R. and S. De Mora (2000). *Marine photochemistry and UV radiation*, pp. 37–60. The Royal Society of Chemistry.

Whitehead, R., S. De Mora, S. Demers, M. Gosselin, P. Monfort, and B. Mostajir (2000). Interactions of ultraviolet-B radiation, mixing, and biological activity on photobleaching of natural chromophoric dissolved organic matter: A mesocosm study. *Limnol. Oceanogr., 45(2)*, 278–291.

Wilhelm, S., M. Weinbauer, C. Suttle, and W. Jeffrey (1998). The role of sunlight in the removal and repair of viruses in the sea. *Limnol. Oceanogr., 43*, 586–592.

Williamson, C., P. Neale, G. Grad, H. De Lange, and B. Hargreaves (2001). Beneficial and detrimental effects of UV on aquatic organisms: Implications of spectral variation. *Ecol. Appl. 11*, 1843–1857.

Zafiriou, O., S. Andrews, and W. Wang (2003). Concordant estimates of oceanic carbon monoxide source and sink processes in the Pacific yield a balanced global "$blue - water$" CO budget. *Global Biogeochem. Cycles, 17*, 10.1029/2001GB001638.

Zepp, R. and M. Andreae (1994). Factors affecting the photochemical production of carbonyl sulfide in seawaters. *Geophys. Res. Lett., 21*, 2813–2816.

Zepp, R., T. Callaghan, and D. Erickson (1998). Effects of solar ultraviolet radiation on biogeochemical cycles. *J. Photochem. Photobiol. Sci. B., 46*, 69–82.

Zepp, R., B. Faust, and J. Hoigné (1992). Hydroxyl radical formation in aqueous reactions (pH 3-8) of iron(II) with hydrogen peroxide: the photo-Fenton reaction. *Environ. Sci. Technol., 26*, 313–319.

Zhang, Y., X. Huixiang, and C. Guohua (2006). Factors affecting the efficiency of carbon monoxide photoproduction in the St Lawrence estuarine system (Canada). *Environ. Sci. and Technol., xx*, xxx–xxx.

Ziolkowski, L. (2000). *Marine Photochemical production of carbon monoxide*, pp. 121. Dalhousie University, Halifax, Nova Scotia, Canada: M.Sc. Thesis.

European Commission

EUR 22720 EN – DG Joint Research Centre, Institute for the Environment and Sustainability
Title: Selected UV photochemical and photobiological impacts on marine ecosystems: general characteristics and sensitivity analyses
Authors: Vantrepotte, V. and Mélin, F.
Luxembourg: Office for Official Publications of the European Communities
2007 – 100 pp. – 21 x 29.7 cm
EUR - Scientific and Technical Research series; ISSN 1018-5593

Abstract

In the recent years, numerous efforts have been performed in order to characterize the impacts of UVR on marine photobiology and photochemistry. The quantification of these UV-dependent processes through modelling approaches requires (i) an accurate description of UV underwater light field (ii) an adapted parameterization of the response of marine water compounds and/or organisms to spatio-temporal changes in solar radiations. The spatial and temporal variability of the absorption coefficient of the colored detrital material, which is a key element for studying undersea UV climate, has been characterized in the two basins selected for this study (the Mediterranean Sea and the Norwegian Seas) using the SeaWiFS products archive recently achieved for the period 1998-2006. Moreover, the various models currently available for the description of selected optical (CDOM photobleaching), photochemical (CO and DIC production) and photobiological (primary production inhibition) effects of UVR on marine waters have been described. Further, the general characteristics of these UV-dependent processes have been presented focusing, in particularly, on their variability along the daily, vertical and spectral dimensions. Several sensitivity analyses have been performed in order to define the relative importance of the various inputs of the spectral and depth resolved model on the final estimations. Finally, some of the straightforward models recently proposed in order to estimate some of the UV impacts at large temporal and or spatial scales have been tested and their limits of application have been discussed.

EUROPEAN COMMISSION
DIRECTORATE-GENERAL
Joint Research Centre

The mission of the JRC is to provide customer-driven scientific and technical support for the conception, development, implementation and monitoring of EU policies. As a service of the European Commission, the JRC functions as a reference centre of science and technology for the Union. Close to the policy-making process, it serves the common interest of the Member States, while being independent of special interests, whether private or national.

Publications Office
Publications.eu.int